Francesco Visentin

The Development of a Flexible Sensor for Continuum Soft-Bodied Robots

Ph.D. Thesis

Università degli Studi di Verona
Dipartimento di Informatica

Advisor:
Prof. Paolo Fiorini

Series N°: **NOT YET ASSIGNED**

Università di Verona
Dipartimento di Informatica
Strada le Grazie 15, 37134 Verona
Italy

to my family and Laura,
who proved that love can overcome any distance.

Abstract

In this thesis, we investigate, develop, and verify an approach to sense soft and flexible materials based on the use of a tomographic technique known as Electrical Impedance Tomography. The technique has been already used in different application domains to sense rigid, or semi-rigid structures. In this work we wanted to expand its application to situations that involve deformable domains in which the the underlying geometry can change shape. The use of such capability can be beneficial in applications related to the fields of robotics, rehabilitation, costumer electronic devices, but also in the new field of *soft robotics*.

The technique used as transduction method allows to infer the internal structure of the domain under study by reconstructing its conductivity map. The use of EIT as sensing mechanism allows to reduce the number of rigid components in the systems, and enables the use of this sensing technique for large surfaces without the need of sensing based on "matrix" structures (e.g. two-dimensional capacitive or resistive sensors). By applying the technique to a material that changes its resistivity according to applied forces, it is possible to identify these changes and then localise the area where the force was applied.

In order to fully control all the parameters during the measurements, we developed a low-cost driving/measurement electronics and an inverse solver software. We then tested the system in both two– and three-dimensional scenarios. For the two-dimensional case, we used a conductive textile as domain under study and we evaluate the sensor capabilities to detect forces applied over a single point, over multiple points, and changes in the underlying geometry. For the three-dimensional case, we developed a silicon-rubber conductive substrate by creating a mixture of silicon rubber and dissolved carbon fibres. The resulting volume was than used to simulate the elongation and the bending of a soft robotic arm, and to prove the paradigm "the robot body is the sensor".

The main contribution of the work is to introduce Electrical Impedance Tomography to the field of deformable structure. The results are all promising, and open the way for the application of such sensors in different robotic contexts where there are strong requirements on the deformability and adaptability of the technology used to develop these robotic devices.

Contents

List of Tables

List of Figures

1

Introduction

Robots and robotic system represent one of the most relevant technological innovation of the current century, a revolution that is going to leave a deep impact on the society by changing it in different ways. The process started from the industrial domain in which robots were used to increase productivity, quality and repeatability of the manufactured objects. Then, thanks to the results in different research fields, robots started to extend their applications to other domains then the ones related to automation and made fast steps into our life by becoming more ubiquitous and present both in the workspace, and in other daily activities. As the process of integration continues, these devices provide innovation in the means of simplifying tasks, and substituting humans in dangerous or heavy situations. However, as the interaction space between human and robots becomes closer, the use of robots can lead to dangerous situations in which humans can be injured by the robot body—usually made of metals—as a consequence of miscalculation of the robot motion due to unpredictable changes in the working environment. As a consequence, additional precautions should be taken into account.

The investments in the robotic field lead to the development of many different kinds of robots: factory automation systems that weld and assemble car engines; medical devices that support surgeons in operations requiring high-precision manipulation; cars that drive automatically over long distances; vehicles for planetary exploration; service robots that help in daily tasks, and "companion robots" that assist or act as real partners for humans. These robots, mostly programmed to perform a single specific task, are commonly made of metal parts so that vibrations and deformations of the structure, together with the drivetrain, do not reduce the accuracy of the movement. To move such robots powerful electrical or hydraulic motor are connected to each joint, encoders are used to estimate the robot position, and sensors (e.g. force sensors, and cameras) are used to gather information about the surroundings. While these solutions allow the robots to perform tasks in a fast, precise, strong, and repetitive way, they also make them bulkier and difficult to be moved outside of their confined, and well structured environment. As these robots are moving out from the cages where they used to work in, they must become less rigid in movements, less specialised, and able to perform in environment subjected to the uncertainty while ensuring a safety.

In fact, unlike industrial environments, spaces shared with humans are typically unstructured, which means that events that happen in the surroundings can be unpredictable also because of the humans presence. Solutions as the approaches used in traditional industrial, where the control of robot end-effectors is achieved by embedding prior knowledge about the object that has to be handled and the environment into the robot's control algorithm, can not be applied in similar cases. Instead, perception need to be added to the robot's control strategies. Additionally, since robots interact directly with with humans, these must be adequately soft and lightweight in order to prevent injuries during contacts and collisions. Features such as compliance matching and biocompatibility are especially important for applications in nursing and elderly care that require carrying, lifting, and other forms of intimate contact. With conventional machines and rigid robots, safe and comfortable human-machine interaction is possible but requires precision sensing, fine motor control, and advanced feedback systems.

Robots, however, have not to be made necessarily of rigid metal components. This has been proven by the emerging community that takes the name of *soft robotics* [111]. The main idea takes its inspiration from the fact that soft elements are ubiquitous in biological systems. They have optimised their configuration for specific tasks according to the habitat they occupy. They are multifunctional and did not evolved for only one specific functionality. This is possible by one of the key feature of biological systems: compliance. It allows them to adapt their motion according to the environmental contingencies while maintaining robustness in the control of the task they are performing (e.g. running on unstable terrain). By studying how animals use soft elements to move in complex, unpredictable environments we can acquire insights for emerging robotic applications that can revolutionise the role of robots in the fields of healthcare, search and rescue, and cooperating human assistance. Looking at biology for inspiration is not novel for the robotic community. In fact, for more than 40 years [9, 61, 110, 133] many researchers have been motivated to build better robots by adopting some of the working principles of animals. Biological inspiration can be drawn from many aspects of animals, including their behavioural strategies, the physical structure of their bodies, and the organisation of their nervous systems. Among these aspects one that raised a lot of interest in recent years is about exploiting the softness of the biological system to endow robots with capabilities that are not based on the control system but in the properties and morphology of their bodies.

Soft robotics is already making an impact on the robotic community in many different ways. Advantages include safety features such as not having sharp edges and the ability to handle objects of different shapes and sizes. The softness gives even more flexibility than what metallic systems would have. The use of soft deformable and variable stiffness materials in robotics represents an emerging way to build new classes of robotic systems that are expected to interact more safely with the natural, unstructured, environment and with humans, and that better deal with uncertain and dynamic tasks (i.e. grasping and manipulation of unknown objects, locomotion on rough terrains, physical contacts with human bodies, etc.). In addition, because they are composed of materials that match the compliance of biological elements, soft robots are mechanically biocompatible and capable of life-like functionalities. These features will potentially lead to many of promising new

	Strenghts	**Weakness**
Hard Robots	High accuracy in the movements, and repeatability. Can handle heavy loads.	Fixed working space. Heavy body. Not safe for human interaction. Work well in structured environment.
Soft Robots	High dexterity. Can manipulate delicate objects and adapt to their size. Adaptable to the environment. Save interaction.	Low accuracy and repeatability of the task. Difficulties in control. Reproducibility of the device not always achievable.

Table 1.1: Comparison between hard– and soft-type robots.

technologies, from soft wearable robots for human motor assistance and biologically inspired field robots for autonomous exploration to soft and lightweight cooperative robots that safely interact with people. A new generation of soft robots could not only do the same jobs with less complex control built into their software programs, but will also operate more safely around humans. However, introducing softness into the mechanics involves design and control issues that differ completely from those used in conventional hard robotic systems. In application domains such as medical and personal co-robotics, soft machines allow a safe and bio-mechanically compatible interaction with humans. Following the new paradigm, in the last years different robots have been been developed. In contrast to conventional machines and robots, these robots contain few or no rigid parts and are instead composed of fluids, gels, soft polymers, and other easily deformable elements. As a field of academic research, soft robotics is highly interdisciplinary and introduces several challenges that demand further scientific exploration. In Table 1.1 the advantages and disadvantages of hard and soft robotics are summarised.

1.1 The Rise of Soft Robotics

Soft robotics—as the branch of bio-inspired research field in which robots are not only performing more natural motion but also made of soft and deformable materials—is a young, promising, and growing research field. The need for soft robots emerged in robotics to face the problem of unstructured environments, and in artificial intelligence to provide an embodiment to implement the morphological computation paradigm which is based on the the adaptability of body and its interaction with the environment.

Using soft materials for building robots poses new technological challenges: the technologies for actuating soft materials, for embedding sensors into soft robot parts, for controlling soft robots are among the main difficulties. Though still in its early stages of development, soft robotics is finding its way in a variety of applications, where safe contact is the main issue, in the biomedical field, as well as in exploration tasks and in the manufacturing industry.

Soft robotics is not just a new direction of technological development. "The use of soft materials in robotics is going to unhinge its fundamentals, as most of the methods for analysis no longer stand" [81]. In fact, common techniques for

kinematic and dynamic modelling in robotics cannot be used alone and must be integrated with techniques for modelling continuum structures. Even the control of the robot should be reconsidered, not only for the lack of adequate methods, but also for the increased role of the interaction with environment. As a consequence, a novel set of design and control principles that can act as a bridge between these two different approaches has to be developed. By considering all these factors, soft robotics is the broad term that represents a novel approach to robotics and artificial intelligence and has the potential to produce a new generation of robots, in support of humans in our natural environments.

The state of the art in soft robotics is increasingly rich, not only considering the robotic field alone. Following this new paradigm, several types of soft biomimetic robots have been developed so far. These devices can execute tasks, with some intrinsic limitation due to their deformable structures, in a similar way to their rigid counterparts. As an example, a simple pneumatically-powered actuator composed only by soft elastometers can perform, in a open loop configuration, the function of a complex arrangement of mechanical components, electric motors and feedback sensors [65, 75]. Beside this, they can exhibit other valuable properties. Soft grippers [19, 65] can handle fragile and uneven objects by deforming their body and clutching around them. They can show different locomotion behaviors such as swimming [72, 139], crawling [125, 126], jumping [128, 137], and walking [91, 103, 113, 140] adapting their gait to different leg configurations and to the underlying terrain. Due to their soft structure soft robots can easily squeeze to pass through gaps and small holes [124] or beneath obstacles [65], and then recover their initial shape and functionalities. Others can use attached micro-fluidic layers in order to be easily spotted, e.g. in a rescue mission, or to camouflage with the surroundings [99]. The paradigm of soft materials guides researchers towards building inherently compliant machines that exhibit passive dynamics. This is an important feature since it allows performing more natural movements rather than robot-like ones. It has the potential to lead to robots that are more adaptable, capable, and safer than the existing ones. In addition, their soft structure can absorb energy in case of an impact or adapt to meet the contact with an uneven object. This makes them more suitable for human interaction as they pose minimal injury risk in assistance applications such as helping elder or disable people [90, 120].

Although soft robotic seems to provide distinct benefits to the robotic community, as mentioned above, there are enormous challenges and unique problems to overcome in order to fully exploit their potential. For example, it is quite clear that it is not possible to use standard materials and manufacturing processese to build such robots. They require a change in the way we think about traditional fabrication methods used in assembling electromechanical tools and devices. As a result of these needs, new methods have been proposed and various materials have been tested [26, 38, 39, 161]. Furthermore, the use of such materials implies the introduction of additional complexity into the system and in its control. Modelling the kinematics and dynamics of a fully deformable system is not always straightforward since it exhibits non-linear behaviour and a high strain under normal situations. Different solutions have been proposed [97, 141, 149] to tackle this problem but they address only specific condition and are not generalisable. Moreover, sensors and actuators have to be embedded into the system during the fabrication

process making them part of the reinforcement structure. This dual functionality prevents the use of many traditional rigid actuators and sensors since their bulky structure can limit the flexibility of the system. Actuators made from unconventional materials, such as shape memory alloys, piezoelectrical crystals, and micro-chemical actuators can be adopted and used with such robots.

While many different actuators have been efficiently applied to soft robots, more effort should be devoted to address their control challenges. Due to the lack of dedicated technologies for soft robot control, and the fact that it is not trivial to equip soft robots with sensors, sensorimotor control is normally missing in the soft robotics literature [81]. Additionally, there are limited choices of commercially available sensors which can be embedded into soft robots, and once embedded their power and signal cabling can reduce, or nullify, the flexibility of the soft device. An other problem that should be considered is the fact that soft robots contains infinite degrees of freedom (DoF) and it is impossible to capture all the DoF into correspondingly actuators and sensors. This prevent the adoption of traditional kinematic and dynamic control strategies used in rigid-structures. In fact, soft materials exhibit both elastic and viscous responses, and therefore the effects of applied forces propagate in the soft structure in an unpredictable manner. Additionally, even though machine learning techniques to track the varying dynamics of the robot and the environment have shown promising results, these are tractable only in specified applications but can be challenging to extend these to general-purpose platforms.

1.2 Aim of this Work

As mentioned earlier, one of the most challenging topics within the soft robotics domain is providing sensing capability to the soft device. Considering the literature on the topic, as it will be shown in following chapters, while sensory-motor control and exteroceptive sensing is well identified, closing the loop for motor control and the related proprioception has been investigated less due to the complexity in being able to discriminate between the sensor response due to external forces/toques and the one given by the deformation of the soft structure. By looking at the state of the art, very few dedicated technologies have been developed and are currently in use on such devices. Some have been developed with the new generation of robots in mind, and as a consequence exploit the properties of the soft materials. Others, instead, have been borrowed from different domains and then adapted to the novel field (e.g. by embedding them into soft material) with the expected consequences (i.e. stiffening of the structure). In fact, the compliance and morphology of soft robots precludes the use of many conventional sensors including encoders, metal or semi-conductor strain gauges, or inertial measurement units (IMUs). Although flexible-bending sensors based on piezoelectric polymers are available as commercial products, these may not be appropriate due to the need for all elements of the system to be both bendable and stretchable.

Obtaining kinematic configuration information of soft bodied robots is one of the current challenges in the field. The traditional approach, because of to the high number of passive DoFs and its continuously deformable segmented body, results

to be less effective. For this reason there is the need for new sensing techniques. The basis of proprioceptive sensors for a soft robot is usually either non-contact sensors or very low modulus elastomers combined with liquid-phase materials. Because soft robots are actuated by generating curvatures, proprioception relies on curvature sensors. Alternatively, exteroceptive sensing may be used to measure the curvature of a soft robot's body segments in real time. To expand the applications of soft robotics, compatible chemical and biological sensors may be used to sense environmental signals. Such sensors may be more compatible with soft robots than the optical and audio recorders typically used in robotics.

Starting from the current state of the art, this research is motivated by the following research questions

- How is it possible to provide sensing solution to soft robots without adding too many stiff components to its structure?
- What is the best sensing capability for a soft robot?
- Which is the information we can acquire from these sensor?
- Can we obtain proprioception information from such sensor?

Among the various approaches that can be used in such contexts, we found very promising the tomographic technique known as Electrical Impedance Tomography (EIT) [109]. In this technique, a small current is injected into a conductive domain, and electric potentials are then measured around the boundaries in order to infer the internal structure of the domain. Approaches that use this technique are not new, and they have been used in different application domains, spanning from geophysical inspection [76, 98] to biomedical measurements [12, 41], and recently, robotic applications [74, 100]. In all of these applications, EIT has been used to localise areas of inhomogeneity within the domain caused by the presence of elements that change the domain conductivity. If applied to a stretchable conductive substrate—as in [32, 130, 131, 157, 158]—the technique can be used to develop a flexible sensor with arbitrary size and shape that does not suffer from the presence of wires within the sensing area. Even if it sounds promising, the technique has some drawbacks, especially related to spatial resolution.

By exploiting this sensing technique, the aim of this dissertation is to investigate and present a low-cost, small in size sensor that is able to adapt to different surfaces and still provide information even when deformed. Following the bio-inspired paradigm, the idea of using the body of the device as a unique sensing unit (similar to many biological systems that have distributed dedicated sensors) has been explored. The main idea is the whole body is a sensor, so we can achieve distributed sensing without the need of many localised sensing unit. By exploit the robot body as sensor we can overcome some of the limitations currently present in the literature and thus provide the initial step in the development of dedicated technology for sensorimotor control of soft robots.

1.3 Main Contribution

The use of EIT in robotic applications, as mentioned earlier, has already produced interesting results but only when applied to rigid or semi-rigid domains. In this

work, our main intent is to extend the application range of EIT to domains that can deform, and use such technique to detect and monitor changes that not only occur over the surface but also within the body of the device. The returned information can be used as metrics to measure the deformation of the structure as consequence of an applied force, together with data related to the force itself. In order to achieve such goal, we need to develop a system that consists of the following components:

- A current injection/potential measurement system used to acquire data,
- an image reconstruction software,
- and a conductive domain used for sensing

Our main contribution is, starting from the current state of the art, the development of a simpler and effective sensor that can be used in novel research areas where simplicity in the hardware architecture and deformability of the device are the key points. The sensor we developed is small in size, so the circuitry and the cable assemble that compose the whole electronics do not interfere with the morphological changes of the device where it is embedded, and modular to adapt to different situations. As this thesis will show, a thorough study of EIT has been carried out, and the results presented can have a positive impact in the field of soft robotics, and in others where EIT can provide solutions to current problems.

In this thesis, we analyse the the interdisciplinary nature of the field, and we address all the aspects related to developed hardware (electronics and sensor), and software have been practically realised. The developed system has been tested to demonstrate its working capabilities both in generic situation, and in possible practical cases. In these experiments we showed that the sensor is able to detect single, and multiple events when forces are applied independently and simultaneously, to identify changes in curvature and the presence of external events, and to maintain its sensing capabilities even when subjected to large deformations. Additionally, the use of EIT as transduction technique allows to reduce the number of rigid components in the systems, and enables the use of this sensing technique for large surfaces without the need of sensing based on “matrix” structures.

1.4 Thesis Outline

The research presented in this thesis is organised in nine chapters. After the introduction to the research field and the problem treated in this dissertation presented in this chapter, chapter 2 introduces the state of the art of sensors used in the soft robotic domain. Chapter 3 presents the main core of this thesis by providing the basis of the imaging reconstruction algorithms, together with details about the mathematical model used to solve an EIT problem. The measurement system, which consists of a driving and readout electronics, and a MATLAB® based control software, will be presented and discussed in chapter 4. In the same chapter we will be also introduce and discuss the methodology used for the development of the structures used as sensing layers. Chapter 5 will introduce a series of preliminary experiments used to characterise the textile-based conductive domain used in later applications. These applications are introduced and discussed in chapter 6. Results of the experiments carried out on the developed continuum soft-bodied

sensor, instead, will be presented in chapter 7. Finally, a general discussion on the results is presented in chapter 8 followed by conclusions and a consideration about future work presented in chapter 9.

Various parts of this thesis have been published or are in the process of publication. The background information about EIT in chapters 3 and 4, along with preliminary results of the deformable sensitive fabric sensor in chapter 5, have been published in a conference paper and then extended into one journal publication. The results presented in chapter 6 have been published in three different conference papers.

2

Toward the Development of a Dedicated Sensor for Soft Robots

Sensing is one of the fundamental property a system must posses to detect events or changes in its configuration or in the surroundings. This information is then used to plan novel sequences of actions to complete the assigned task while adapting to those changes. The problem of providing sensing capabilities to robots and robotic systems has been studied extensively in the last years, and now many solutions are available for the community. While these can be directly applied in the classical, rigid-link robot case, if soft robots are considered, the use of the available sensors require further adaptation due to the complications that arrise when rigid components are embedded into the soft structure of the robot. In fact, one of the most challenging topics in this field is related to the development of dedicated sensors that can be easily embedded into the robot' structure without limiting its deformability, and that remain usable even when it is subjected to large deformations.

In this chapter, we will introduce some of the most interesting examples of sensors that have been adapted or developed for the soft robotic domain. We are mainly focusing on those presented in the last 10 years, but we will not consider chemical sensors even though they are promising for future applications [155].

2.1 Sensors for Soft Robots

Sensors can be classified according to different parameters. Depending on the location where they are placed over a robot body, the sensing capability can be classified as extrinsic or intrinsic. Intrinsic sensors, used to replicate the kinaesthetic sensing of biological systems, are usually placed within the structure of the robotic system and the acquired data is in the form of magnitude of applied force or torque. Extrinsic sensors or tactile sensors, instead, are placed as contact interfaces and are used to capture local information provided by the interaction with the surrounding environment. The extrinsic sensors can be further divided accordingly on the resolution they can achieve and the application domain. Another classification can be based on the mechanical properties of the sensors: they can be labeled as rigid, flexible, compliant, stretchable, and so on. An additional

classification can be made with regards to the physical nature of the transduction method.

Change of capacitance, resistance, optical distribution, electrical charge can be used in a sensing system, and they are referred as transduction. With the change of the transduction method, the type of sensors varies. In the following sections, a survey on the different types of transduction methods will be given. Despite the efforts made to prove the effectiveness of different types of transduction principles, various issue have strongly limited the development of embedded systems. Advantages and disadvantages of each sensor type are summarised in Table 2.1.

Despite the advancements in the sensor development, in the literature only few studies address the complete integration of soft sensors within soft-bodied robotic systems. Among the main reasons why it has not been done, there is the commercial availability of sensors for a precise mechanical design and are specialised for a particular platform and its tasks. As any robotic system, in order to reach their full functionality soft robots require tailor-made solutions. As a consequence, a dedicated technology is needed. The lack of dedicated sensors for soft robots is also motivated by the fact that miniaturisation and the hardness brought by the embedded cables still represent a limitation to the design of small sized embedded sensors. Additionally, most of the proposed solutions share a common

Type	**Advantages**	**Disadvantages**
External sensors [59, 94]	Many commercial solutions exist, simple to manufacture, high precision	Work in structured environment, not applicable in avery domain
Piezoresistive sensors [37, 48]	Different commercial solutions exist,easy to manufacture, can be flexible.	Non-linear response, temperature and moistness dependence, fatigue, permanent deformation, hysteresis.
Capacitive [143, 152]	A number of commercial solutions, can be flexible, may have higher bandwidth than piezoresistive.	Susceptibility to electromagnetic noise, sensitivity to temperature, non-linear response, hysteresis.
Piezoelectric sensor [23, 156]	Very high bandwidth.	Temperature dependence, dynamic sensing only.
Quantum tunnelling composite [64]	Linear response, higher dynamic range (w.r.t. capacitive and piezoresistive).	More complex for manufacturing (w.r.t. capacitive and piezoresistive).
Optical sensors [85, 96]	High spatial resolution, high sensitivity, repeatability, immunity to EM noise.	Bulky, high-power consumption, high computational costs.
Sensors based on barometric measurements [27]	High bandwidth, high sensitivity, temperature and moistness independence.	Low spatial resolution.
Structure borne sound sensors [15]	High bandwidth.	Dynamic sensing only.

Table 2.1: Comparison between the different methods used in the development of sensors.

disadvantages: the sensor's readings are relative to a specific area of the device. This, by itself, is not a limit—in fact, most of the commercially available sensors have the same characteristic—but in the case of soft robotics it can be an issue during the design and development process. In fact, the sensor position should be known in advance and if a wider or different region should be sampled it would require a re-design and re-development of the robot to house the additional cables and electronic circuits. In addition, the presence of additional stiff components can compromise or worst nullify the advantages obtained by the use of the soft materials.

2.2 Shape Estimation

In order to reconstruct the shape configuration of the robot, it is important to be able to retrieve the position of all of its components, and then derive the robot overall configuration. The usual approach of applying an encoder to each joint of the robot is not possible when soft robots are considered. In fact, these robots are usually treated as continuum structures and thus considered to have infinite degrees of freedom (DoF - the number of parameters in a system that may vary independently). As a consequence, it is not possible to deploy a sensor and thus track the position of each of the DoF of the robot. The state of the art contains different methods to track portion of the body and then reconstruct its overall structure.

2.2.1 External Sensor

Different approaches have been used to address this problem using both internal or external sensors. External sensing is based on the use of fiducial markers and external cameras. In an early soft robotics work by Hannan et al. [59], the 2D curvature of a 32 DoF elephant trunk-like continuum actuator is obtained by using a high speed camera. The image processing returns the curvature of each section and thus the full system configuration can be obtained. Similarly, in Marchese et al. [94], camera and markers are used to closed-loop position control of a highly compliant planar continuum manipulator made almost entirely of soft silicone rubber. The position of the end-point is derived by computing the curvature of each body segment. Additional information about the 3D shape of a soft interface can be achieved with the use of a depth sensor, e.g. the Microsoft Kinect. Stanley at al. [136] developed a haptic jamming tactile display that can change its shape and mechanical properties simultaneously by adjusting the pressure inside the individual cells. Even if promising, such controlling architecture is not suitable for every situation, since it is not portable and difficult to use when the robot has to move in confined spaces.

To enable the use of soft robots in real applications, it is important to progress towards alternatives that imply a more "on-board approach". This can be done by using different transduction methods that allow the miniaturisation of the sensing components.

2.2.2 Optical Sensors

Light Emitting Diode (LED) and photodiodes can be used to measure deflection angles when correctly placed within a deformable structure as in [36]. The deflection angle between the two planes can be extracted from the LED light intensity detected by the photodiode due to the bell-shaped angular intensity profile of the emitted light. The main advantage of this system is that the components are not in physical contact with the deflection region as in the case of strain gauges and similar sensing methods. The sensors have a high resolution—it can discriminate angles with 1 degree of resolution—but all the tests have been performed in system not made of soft materials. This may reduce the accuracy of the measurements due to the different propagation angle of the light when it interacts with the interface between two media.

The problem has been addressed by Yoshikai et al [159] who developed different soft sensors to be used in a humanoid robot. Among these, a soft multi-axis deformation sensor is proposed. It uses 3 infrared LEDs that are placed at the bottom of the sensor, and light-receiving elements mounted on the surfaces facing the LEDs. The whole rigid part is then molded into a urethane cube. Sensitivity and detected forces of the sensor unit can be adjusted to some extent by changing the property of the urethane foam. In the developed prototype, the sensor can detect applied forces with range from 0 to about 1.4 kgf with a linear approximation. By arranging different units of this sensor it is possible to create a soft substrate that can be used as artificial skin. To improve tactile sensing an additional sensor element has been developed using a pair of IMUs and a force sensor sandwiched within a soft urethane foam. The sensors can provide different spatial information on how the external shape of the structure changes according to the applied forces, but the main challenge is in the information processing of the enormous amount of tactile sensor information provided by each sensor. A simpler approach that uses optical fibres as sensors to detect deflection angles is presented in [42]. The sensors consist of a IR LED and four surface-mount IR phototransistor devices placed at the end of four optic fibres. By combining the output of the four sensors, it is possible to detect changes in the device shape. An interesting approach that uses optical sensing to measure bending curvature in a soft manipulator is presented in [123]. The method is based on light intensity modulation and uses light reflectivity to determine the relative position in several channels that run the length of the robot. The use of such technology allows the development of a low cost and is temperature independent sensor.

A different approach to measure shear stresses is presented in [96]. In the paper, a very thin and flexible ($40\mu m$) sensor foil is described. This bases its sensing on the coupling change of optical power between a laser and photodiode chip that were separated by a deformable sensing layer. The small package and the capabilities of the sensor to capture μm-scale shear stress allow it to be used in applications where conformable and unobtrusive sensors are desirable.

2.2.3 Strain Gauges

Strain gauges are among the most used sensing technologies to retrieve information about shape changes. The working principle is simple, as the sensor increase its

length, its cross section is reduced and thus the resistivity changes. With a proper characterisation of this variation in the measurements, it is possible to obtain insight about the change that is occurring. The measures are purely one-dimensional, thus if more complex deformations occur, must be arranged to arrange multiple sensors along the different axis.

One of the early works related to the development of soft sensors for soft actuators is presented in [156]. In the paper a flexible displacement sensor is presented that can keep the compliance of a soft actuator. The sensor consists in a structure that contains non-conductive polymer within two layers of piezoelectric polymer. By detecting the changes in the piezoelectric polymer it is possible to retrieve information about the displacement. In order to capture all the 3D motion of the soft actuator (i.e. bending along any direction, and elongation), 3 sensors have been mounted on the surface of the actuator. The sensor shows a linear relationship between its output values and the measured ones, but also shows a large hysteresis due to the viscoelasticity of the material used to make the soft actuator. A different approach has been used by Lee et al. [82] who developed a printable skin adhesive stretch sensor used to measure rotation angle of a multi-axis joint. The sensor has not been used directly on a soft robot, instead it was applied over a human shoulder and could estimate its rotation angles. Lo et al. [87] embedded different strain gauges in a custom-made deformable display to create a deformable user interfaces. Position and direction of the strain gauges can be arranged in different configurations in order to better capture the deformation of the thin device. A similar approach has been presented in [115] where a set of 16 strain gauges have been embedded into a thin layer and its complex 3D surface shape has been reconstructed.

2.2.4 Capacitive Sensors

Capacitive sensors typically consist of a dielectric layer sandwiched between two conductive layers, whose thickness changes in response to an applied deformation. To date, capacitive sensors have primarily been used in pressure, tactile, or shear sensing. In [45] Frutiger et al. present a textile-mounted, capacitive soft strain sensor fibres for detecting elongation strains. Each fibre consists of four concentric, alternating layers of an ionically conductive fluid and a silicone elastomer that serve as the conductor and dielectric, respectively. The so developed sensor has been tested to capture the gate cycle of human walking at different speed. Despite the noise in the captured data, the sensors show different behaviours with the increase of the walking speed. An interesting result that takes inspiration from the biological domain is presented by Lucarotti et al. in [88]. The sensors are developed with a bottom-up approach trying to mimic the compress/stretch behaviour of the cells that make up the soft roots of plants. The sensing system consists in two capacitive sensing elements placed at its opposite walls of a cylindrical flexible and soft body. To model the strain induced by a bending stimulus, the main hypothesis is that, when the system is mechanically stressed, the capacitive sensing element is subjected to the same deformation of the body surface, since it conforms to the structure. Such deformation results in a change both in the thickness of the dielectric layer and in the sensing area, with a consequent variation in the

capacitance value. By comparing the capacitance at both sensing units it is possible to retrieve the bending direction and its intensity. Follmer et al. [43] propose a shape-sensing jamming user interface based on capacitive sensors. Using rows of transmitting electrodes in a rigid back, and columns of receiving electrodes in a flexible skin, it is possible to sense the jammable volume's shape through time-division-multiplexing for each of the intersections in the sensing matrix.

2.2.5 Resistive Sensors

The piezoresistive effect is a physical process during which electrical resistance changes when the material is mechanically deformed. By correctly placing these sensors inside a robotic structure, it is possible to capture changes in its shape. An example that uses resistive textile for the sensorisation of continuum soft robots is presented by Cianchetti et al. in [28]. The idea is to use stretch sensors to reconstruct the spatial configuration of a robotic structure: differential measurements on strain values can be used to derive local curvatures. Multiple pieces of Electrolycra has been attached to a conical piece of silicone and data acquisition in rest and deformed state. Even if tests show interesting results, the method suffers from the need of a high number of cable to acquire the measurements from each sensing unit.

Sensing through structure is a simple, scalable approach to designing and integrating sensors into soft objects. Slyper et al. [134] presents a method for designing and constructing rugged and soft multi-point sensors by reducing applied interaction into structural units of deformation. These atomic sensing structures make up a sensing vocabulary, to be used as building blocks when a sensor is designed. Sensing is obtain using a resistor network (stranded 32-gauge wire was connected to a copper polyester conductive fabric) to minimise wiring and thus allow complete deformability of the structure. The sensing capabilities are strictly related to the design and the atomic units used.

Recently, the most accepted method to develop sensors that can retrieve changes in shape (of the sensing unit) are based on the use of conductive liquids (e.g. eGaIn) that fill complex micro-channels. The sensing transduction method is based on the change of resistivity of the conductive liquid when it is compressed. By changing the design of the micro-channel is possible to obtain different types of measurements—i.e. force, bending—while keeping the soft matter device free of wires within the sensing area. Despite this, the methods suffer by two main drawbacks: measurements suffer from significant hysteresis due to the movement of the liquid within the empty portion of the micro-channels, and the fragility of the micro-channels after repetitive application of forces. An early prototype of the use of such technology can be found in Park et al. [104, 106, 108] where a highly compliant artificial skin sensor that consists of multilayered micro-channels filled with a conductive liquid is presented. The sensors has been initially proposed to measure normal forces, but later [104, 105, 107] has been used to measure the 3D orientation of the foot in a orthotic device. By layering different micro-channel structure is possible to obtain a multi-modal sensor capable of detecting strain and contact pressure simultaneously. The sensor shows linearity in strain sensing and nonlinearity in pressure sensing. However, the sensor signal is repeatable in both

strain and pressure responses. Similar results have been presented in [78, 79, 93] where the same principle has been used to develop a curvature sensor to measure fingers's displacement using a smart glove and a tactile touch sensor.

2.2.6 Camera-based Sensor

Cameras can be used not only as external sensors, but also as internal ones in combination with micro-patterns or fixed markers. An example of deformation tracking using this approach can be found in [63]. Hristu et al. developed a deformable tactile sensors that consist of a membrane—filled with fluid-like clear gel—on which a grid of dots is drawn at precisely computed locations. An optical fibre provides illumination on the interior part of the membrane, while a camera is used to capture the images of the grid of dots under deformation. The use of the gel allows local deformations to be distributed throughout the enclosed volume allowing the membrane to wrap around the object of contact. Differences in the dots pattern between a reference image—taken when no force is acting over the membrane—and a deformed one are used to reconstruct the 3D shape of the membrane and thus obtain the location of the contact point. The system can determine deformation depth for small deformations, and very precise curvature measurements.

2.2.7 Electroactive Polymers

Electroactive Polymers (EAPs) are structures that can convert chemical energy directly into mechanical energy. They take advantage of certain material property that enable them to contract, expand and bend reversibly when placed under a large voltage [8]. Generally, EAP can be divided into two major groups based on their activation mechanism including: ionic EAP and electronic EAP [95]. Ionic polymer-metal composites (IPMC), a class of ionic EAP, have particular properties that can be exploited to realise sensing devices. By mechanical bending the material, it is possible to change the distribution of the charges. The output voltage is proportional to the volume deformation and its rapidity. Using the voltage information provided, it is possible to develop mechanical and velocity sensors. One of the most problematic limitations is the dependence on a solvent in order to function. Typically, water is used as the solvent, but because water will quickly evaporate in air, the applications for these devices are quite limited.

Due to their compliance, and the possibility to use them both as actuators and sensors, IPMCs have been used in different soft robotics application. An example can be found in [16] where an integrated motion sensor-actuator system is presented. Similarly Kamamichi et al. [73] design a integrated system to control in position the IPMC actuator to generate the propulsive motion of a snake-like swimming robot. The idea has been further extended and used in [24] with the development of a model for sensor's response to rotary joint motion to be used to recognise the movement of a human finger joint.

2.2.8 Other Sensing Method

Single points of curvature can also be measured by the use of backscatter of RFID sensors [55]. Backscatter RFID in sensor networks relies on the radio communication between an RFID reader, acting as the control unit, and a multitude of passive or semi-passive RFID transponders, acting as sensor nodes. The transducer's impedance changes (both magnitude and phase) as a function of bending. Consequently, the RFID reader can wirelessly detect the sensor data without the need of additional circuitry on the backscatter sensor. Different prototypes have been tested and despite the fact the resonant frequencies differed because of manufacturing variances, they show the same resonant frequency trend when subjected to bending. Tests with multiple tags have not been performed, but ideally the presence of multiple closely-placed transducers can create problems in the data collections since the receiver can not discriminate between the different tags. A similar approach has been used also by Becker et al. in [13] where a RFID backscatter sensor has been used to measure displacement—between one and five millimetres—of a human finger from a reference position. Measurements showed good agreement between the wirelessly estimated transducer input impedance and ground-truth measurements for most displacements.

Reconfigurable sensor networks can be used to retrieve shape information in devices with different shapes. An example of these systems is provided in [34] where the SensorTape is introduced. It consists of a modular and dense sensor network in the form factor of a tape that incorporate IMUs and proximity sensors controlled by independent microcontrollers. A master node controls all the slave nodes and is used to communicate with a computer. The sensor network is able to perform deformation-self sensing by mapping the orientation data from IMUs to a kinematic chain model and deformations of 3D surface. The results show accurate and repeatable measurements in various application scenarios. Instead of using IMUs, Chien et al. [25] use a dense linear array of strain gauges. The developed sensor can be easily embedded into different devices and track their shape deformation. In its current implementation FlexiBend can only effectively detects shapes in 2D. Despite this, it can also sense 3D gestures on deformable fabrications such as twisting, stretching, and bending the spiral model.

2.3 Force Sensing

In the soft robotic case, there is an increasing interest in the development of deformable touch interfaces that also can perform similarly to the human skin. Tactile sensing is fundamental to capture external information, such as collisions, and plan safe motions to avoid damage. In addition, by knowing the location and intensity of the pressure point, it is possible to obtain information of deformation produced by the applied force. At its current stage, the development of dedicated technology suffers from scalability issues. Most of the proposed solutions are commonly based on the "matrix" approach where the sensing area is filled with wires over which capacitive, or resistive measurements are carried out. Even if the results are very promising when applied to small areas, when extended to larger surfaces there is a reduction in the resolution and an increase of rigid components that reduce the

deformability of the sensor. Additionally, the control architecture becomes more complex and the sampling time increases.

2.3.1 Resistive Sensing

Cheng et al. introduce in [23] a novel design of a highly twistable tactile sensing array that uses spiral electrodes as sensing electrodes and scanning traces. The proposed skin can conform to complex surfaces without damaging the metal interconnects on the sensing array. The results provided show a good stability of the measurements in a wide range of applied pressures. Ventrelli et al. [146] present a novel tactile skin-like sensor with the capability of detecting at the same time external mechanical stimuli like pressure and shear strain and which possesses some of the intrinsic properties of human skin, like extensibility, flexibility and compliance. The sensor is resistive based and integrates two sensing parts built by means of electrically conductive polymer composites and elastic metallic thin films. The sensor can detect two types of mechanical stimuli, i.e. pressure and shear strain, simultaneously and in a decoupled way.

Rendl et al. [114] present a pressure-sensing input device that is based on a ferroelectric material. It is structured as a sadndwich four layers that can be printed easily on any material. The sensor is embedded into a thin deformable (bendable not stretchable) foil. The two layers of electrodes are forming a capacitor. Charge changes in the ferroelectric sensor layer cause measurable voltage potentials between the electrodes. Every pressure-change on a sensor spot generates a change in the measured voltage. If no further pressure-change occurs, the voltage discharges through internal resistance of the piezoelectric film and the input resistance of the measurement circuit. The sensor is a bendable sensor technology, meaning that the sensor can be mounted on different curved surfaces. The bending radius depends on the size and the distance of the printed piezoelectric spots.

Resistive fabrics can be an alternative candidate for the development of wide area tactile sensing. In [14] Bhattacharjee et al. present a sensor used to sense across articulated joints, which requires sensing across a surface whose geometry varies over time. The sensors is made up of multiple units consisting of five layers of fabric. The layer in the middle is resistive fabric, which is sandwiched between two layers of conductive fabric. The resistance between the two electrodes made of conductive fabric decreases given an applied force that compresses the layers. Wired connections are made for each electrodes using a grid-based wiring. A combination of conductive textile and silicone rubber has been used in [80] to create a flexible and stretchable multi-touch sensor.

As for the case of shape estimation, resistive sensing based on conductive fluids are very promising in soft robotics. Vogt et al. [147] extend the previous work with a novel micro-channel design that allows multi-axis force sensing. The sensor is composed of three main components: a highly deformable base elastomer material, conductive micro-fluidic channels, and a force transmission element. Depending on the magnitude and the direction of an applied force, the different micro-structure change resistivity. When a normal force is applied to the surface, the force is distributed uniformly compresses all channels, resulting in increased electrical resistance in the three channels. The addition of more channels can in-

crease the sensor accuracy at the expense of spatial complexity. A similar sensor structure and operation principle is presented in [119].

A similar sensor has been developed by Tseng et al. [142]. The sensor mimics the human slow-adapting mechanoreceptor. The tactile signal is detected as the impedance change resulting predominantly from the resistance variance and is measured across the electrode pair. The sensor design contains a micro-fluidic channel with a hemispherical reservoir containing the electrolyte solution and a pair of sensing electrodes. Force exerted on the surface of the sensor will cause an indentation in the reservoir, and this deflection will push the electrolyte into the channel. The greater the depth of the indentation, the greater the volume of fluid ejected into the fluid channels and the greater the coverage of the electrodes by the electrolyte. This results in a change of impedance between the electrode pairs. An alternating current voltage is applied and impedance changes are detected by the measurement of voltage across the electrodes. The sensor has a basic slow-adapting behaviour and is capable of static pressure sensing.

2.3.2 Capacitive Sensing

A simple but robust, low-cost, low-noise capacitive force sensing array is presented in [144]. This highly scalable design provides excellent noise immunity, low-hysteresis, and has the potential to be made flexible and formable. Noise immunity is accomplished through the use of shielding and local sensor processing. A small and low-cost multivibrator circuit is replicated locally at each taxel, minimising stray capacitance and noise coupling. Wire count is minimised through serial or row-column addressing schemes, and the use of an open-drain output on each taxel allows hundreds of sensors to require only a single output wire. Despite the promising properties, only a 4x4 array has been implemented and tested, and no experiment has been conducted using soft material.

Another approach to develop a force sensor is presented in [160] where a soft piezoelectric tactile sensor array is proposed for measuring three-axis dynamic contact force distribution. The array consists of six tactile units arranged as a matrix, in which each unit consists of a sandwiched structure of electrodes and insulation layers. A truncated pyramid bump is located above the four piezoelectric capacitors to improve force transmission. A three-axis contact force transmitted from the top of the bump will lead to the four piezoelectric capacitors underneath undergoing different charge changes, from which the normal and shear components of the force can be calculated. The tactile units show good sensitivity and work with good linearity, relatively low coupling effect, high repeatability, and acceptable frequency response.

As for the resistive case, also capacitive sensor can be created with the use of conductive liquids. Roberts et al. [116] develop a sensor composed of a sheet of elastomer that is embedded with fluidic parallel-plate capacitors. When the elastomer is pressed or sheared, the electrodes of the embedded capacitors come closer together or slide past each other, respectively, leading to a change in capacitance. Four different areas are created and by combining the measurements of each of those, it is possible to distinguish between press, and shear moments in the along the two directions. Similarly Li et al. [86] developed a highly-deformable tactile

sensing arrays. The structure is made with two microchannel planes dividing the device into three layers. The device is reversibly stretchable up to a maximum of 460%, and it is able to reversibly compress up to 10 MPa.

There are some limitation when capacitive sensing is applied as transduction method to large area. For example, when a wider area has to be sensed, the use of a matrix based sensing technique suffer from high delay time in the detection due to the need to scan repetitively the multiple rows and columns that form the matrix. However, it is possible to find in literature different works that provide solutions to this problem. Maiolino et al. [92] extend the capacitive sensing to large surfaces and use thermal compensation in order to stabilise the pressure measurements. The sensing system is composed of multiple units with a triangular shape. Several triangles can be interconnected to form a mesh of sensors to cover the desired area. The use of a triangular shape allows a flexible adaptation also to curved surfaces. Instead of using silicone as dielectric, 3D fabric is used. Another approach is presented in [84] where Leigh et al. propose a novel method to overcome the issue related to the time delay in measurements. They employed simultaneous orthogonal signals to reach an high scan rate with low latency. A different "orthogonal" signal is transmitted onto each of the surface's rows. When a row and column are touched simultaneously, a small amount of the signal that is present on the row is coupled into the corresponding column. A receiver, attached to each column, is designed to receive any of the transmitted signals, or an arbitrary combination of them, and to individually measure the quantity of each of the orthogonal transmitted signals that is present on that column. Once the signal has been received and analysed, it is possible to calculate their strengths and thus create a map that interpolates the different extracted values and shows the location of the contact points. Hoshi et al. in [62] also tackle the problem related to the development of wide area tactile sensors. They proposed a skin consisting of two components. One is a sensor element which detects a contact area in addition to a contact force. The other component is a sensor/communication chip. The chips are arranged at the boundaries of the elements, and the chips measure the capacitances between the conductive layers and send signals through the same conductive layers. Each unit is connected to a close one following a specific path in order to reduce the number of cables within the sensing layer. A last example of large area sensing is proposed by Lee et al. [83] who introduced a modular expandable capacitive tactile sensor. Each sensor module can be connected through interconnection lines to form an extended sensor skin for large-area deployment. A sensor module consists of 16x16 tactile cells. Among the possible transduction mechanism, they chose a capacitive sensing mechanism because it is less susceptible to noise and immune to temperature change. Measurements work as normal matrix based sampling. The fabricated tactile sensor module shows good flexibility and captures distinctive tactile images.

2.3.3 Optical Sensing

Ohmura et al in [102] present the design of a conformable tactile sensor skin. The skin is organised as a network of self-contained modules consisting of tiny pressure-sensitive elements which communicate through a serial bus. By adding or removing

modules it is possible to adjust the area covered by the skin as well as the number of tactile elements. The tactile sensing element consists of a IR photo-reflector covered by urethane foam. The foam provides mechanical compliance, protective covering, and insulation from external light sources. In [30], Cirillo et al. propose a sensorized flexible skin based on the use of IR LED and photo-diodes. The skin, composed by 36 elements, has been applied over a rigid robot and is able to detect the position of the contact point and the three components of the applied force with high repeatability and accuracy.

A different approach than using LEDs and photo-diodes consists of the using of internal cameras and optical patterns. Cramphorn et al. [33] apply the method for active touch with a biomimetic tactile sensor, which combines tactile perception with control of sensor location. Images are acquired and each pin is identified based on its proximity to a default set of pin positions recorded in a reference position when not in contact with any surface. Location perception of the optical pattern is finer than the sensor resolution, leading to super-resolved tactile manipulation along a complex trajectory. The system has been tested while the sensor gradually rolled the test object with a small lateral displacement. Similar results has also been presented in [68] by Ito et al. Photo interrupters has been used also in [101] for the development of a three-axis force sensor. The sensors has been integrated in a deformable robot arm to measure external interacting forces and torques.

An interesting use of IR LEDs and photo-receiver is presented in [85] where an array of these sensors is molded at the boundary of a deformable planar PDMS smart skin. The light signal is converted to electrical signal through an electronic system and an algorithm running on a computer reconstructs the pressure map. The intensity of an electromagnetic wave traveling in a waveguide is modulated by mechanical deformations of the waveguide itself. From the intensity measured at the boundaries of the waveguide, it is possible to reconstruct the location and entity of mechanical deformations, by solving an inverse problem by a process that is similar to tomographic backprojection. The losses of electromagnetic intensity caused by the changes in curvature can be expected to be non-linear, similarly to what is observed when deforming optical fibres.

An early approach similar to the later, is presented by Rothmaier et al. [117]. The paper reports of the development of a pressure sensitive sensor based on flexible optical fibres technology. The fibres, made by a deformable polymer, are braided according to different schemes but for each of them a LED and a photo-receiver are placed at opposite sides of each fibre. Location and strength of the applied force can be obtained by measuring the changes in the signal strength at every row and column and then intersect them. The sensor has been tested under different circumstances and proved to be reliable.

2.3.4 Other Sensing Method

Barometric sensors are very reliable in measuring changes in the atmospherical pressure. In these sensors are over-molded with deformable material, it is possible to obtain touch/force measurements from the collected pressure data. An example of this application cam be found in Chuah et al. [27] where a 2-by-3 array of barometric pressure sensors is presented. Measurements have been improved compared

by previous works by the use of Least Squares Artificial Neural Network. The use of this approach could have broader implications in greatly reducing the amount of time needed to train an estimator for tactile sensor arrays where the number of sensor elements are large.

An alternative technique used to perform measurements over large area is the use of Time Domain Reflectometry (TDR). The technique originally used in diagnosing cable faults, can also locate where a cable is being touched. TDR touch sensing relies on detecting capacitance changes caused by conductive objects near the wire pair. In [153] Wimmer et al. explore how to extend time domain reflectometry in order to touch-enable thin, modular, and deformable surfaces and devices using single-wire TDR. The technique is promising and offers different advantages as compliancy, simplicity in the development, and scalability. However, the presence of a long metal wire can create antenna effects and thus make the sensor very susceptible to radio interference. In addition, high spatial resolution TDR systems are still bulky and expensive. A possible alternative that overcome these limitation is the use of optical TDR.

2.4 Electrical Impedance Tomography

An alternative to common approaches for tactile sensing is the use of tomographic techniques, such as Electrical Impedance Tomography (EIT), as transduction method. EIT is a tomographic technique that allows to infer the conductivity distribution within a domain by solving an inverse problem. The idea of combining conductive substrate and EIT to develop a pressure sensor was first introduced by Fulton and Fulton et al. in [46]. Even though the technology was ready, the experimental trials failed in the identification of a suitable material to be used as conductive substrate. The idea was then reconsidered years later by Nagakubo et al [5, 100]. The approach allowed to overcome the problem of having a large number of wires within the sensing area and to estimate the location of an applied force over the sensor. Since most of the sensing area contains no wiring, it is possible for the sensor to be made extremely deformable. Also by using a conductive material capable of transforming deformations into changes of resistance distribution, deformations over the material can be measured. Such a deformable tactile sensor is also very useful for safe human robot interactions, implementation to joint surfaces, implementation to complex three-dimensional curved surfaces and detecting richer and more sophisticated tactile stimuli. Following the same approach, different EIT-based sensors have been developed [32, 130, 131, 157, 158] but it has always been applied to rigid and well defined structures. The method, however has many advantages when compared to other transduction methods that can be exploited and used in the field of soft robotics.

2.5 Summary and Conclusions

Even if the problem of providing sensing capabilities to robots and robotic systems has been already studied in deep in the last years, when a soft bodied robot are

considered, the use of the available technologies requires further adaptation. In this chapter a series of technologies adapted or developed ad hoc for the soft robotic domain have been presented. These have been classified according to their application—such as shape estimation, and force sensing—and by the transduction method used. A generalisable solution is not yet available, and most of the reviewed approaches share a common limitation related to the need of rigid components placed within the sensing area that stiffen it.

Electrical impedance tomography (EIT) is a non-invasive technique that reconstructs the internal characteristics of an electrically conducting body by using measurements made on its boundary. When it is applied to sensitive substrates it is possible to create large-scale flexible sensors that do not require wires within its sensing area. Like other available technologies EIT has some drawbacks, one of which is its low spatial resolution. By considering the current range of application for soft robots, it has been hypothesised that using EIT as transduction mechanism can provide the underlying sensing technology required to equip soft robots with non-intrusive sensing. The following chapter describes the mathematical background of EIT in detail, and the requirements used in the development of the technology used in this work.

3

Electrical Impedance Tomography

3.1 Introduction

Electrical Impedance Tomography (EIT) is a relatively new medical imaging technique [109] that provides information of the internal structure of a conductive body as an image obtained from current-voltage measurements made at the boundary of the body [18]. Specifically, when the conductivity in a region of the body changes the current distribution within the body also changes. EIT can be used to quantify these changes. If the body if made of a thin, flexible and stretchable material that can change its local conductivity as a consequence of the applied force (in the form of applied force or stretch), EIT can be used as transduction mechanism to be used in artificial skin sensitive to touch.

The application of EIT as sensitive skin was previously described by Kato et al. [74] and Nagakubo et al. [100] and Alirezaei et al. [5]. In these papers, the conductive domain was a rubberised fabric that responded to applied pressure with local changes in resistivity. By applying EIT, changes in resistance could be identified. These artificial skins have been proven to be effective in identify the pressure locations when applied over rigid structures.

From the mathematical point of view, the EIT reconstruction problem is an ill-posed non-linear inverse problem, in which the main complication is that the reconstructed image is not necessarily a unique and stable solution: small changes in the data can cause large changes in the reconstruction. As a common approach to solve this ill-posed problem, regularisation is used.

The remainder of this chapter presents the mathematical theory behind the EIT problem and describes how it is used to create a flexible and stretchable artificial sensitive sensor for a soft robot. Section 3.2 gives a general overview of EIT. Section 3.3 introduces the mathematical model used in the forward EIT problem and the numerical approximation based on the use of the finite element method. In section 3.4 the inverse solution, Jacobian calculation, regularisation and image reconstruction are discussed. Data acquisition hardware, reconstruction software, and other design and implementation considerations are presented in section 3.5. Conclusions and discussion will be summarised at the end of the chapter

3.2 Background of EIT

The use of EIT as imaging technique to infer the internal structure of a conductive domain was introduced by Henderson and Webster [60]. In their pioneering work, a rectangular array of electrodes was used to produce an image of the tissue contained in the chest area. The same approach has been used by Lytle and Dines [89] in the field of geophysical imaging. Since then, different groups have developed their own EIT system and reconstruction software and focused their research on a variety of topics. From the initial areas of interest, this imaging technique has been used in different applications ranging from biomedical analysis [1, 11, 18, 44, 109, 129], geophysical exploration [76], industrial applications [58, 69], and most recently as sensitive skin for robotic systems [5, 74, 100].

In a typical EIT application, one or more arrays of electrodes are equally placed at the boundaries of a conductive body. At every step of the measurement process, among these electrodes, two are selected to be used to inject electrical current into the domain (driving electrodes), while all the others (measurement electrodes) are used to acquire the electric potentials—generally measured with respect to a common ground—which is generated at the boundaries of the domain. Local variations in the internal conductivity or permittivity of the body alter the distribution of the current inside the body, and produce changes of potential at the boundaries. By applying an imaging technique and scanning around various driving electrode pairs, it is possible to calculate an approximated resistivity distribution inside the body through inverse solution of Maxwell's equations.

Compared to other tomography methods, EIT suffers from severe limitations that may prevent its adoption for routine medical diagnosis. For example, EIT is not suitable for anatomical imaging in the way that Magnetic Resonance Imaging (MRI) or Computed Tomography (CT) are, due to its large variability of images between subjects. Also, its low spatial resolution and susceptibility to noise and electrode errors makes the matter even worse. However, EIT does show promise as a diagnostic tool for medical clinicians. It has the advantage of a low cost and simple implementation when compared to other imaging technique such as MRI, CT. or even Positron Emission Tomography (PET).

The earliest method for EIT reconstruction was back-projection [10, 11]. Each measurement may be assumed as similar to x-ray beam that represents the impedance of a volume contained between the recording and drive electrodes. However, differently from X-rays, this is not a neatly defined beam, but a diffuse volume which has graded edges. The change in impedance recorded with each electrode combination is then back-projected and overlapped to produce a blurred reconstructed image, which can then be sharpened by using filters. Since the method was very successful for the simple case, a number of deterministic algorithms based on a sensitivity matrix were introduced. This matrix is a linearised map from the resistivity of each voxel in the subject, and hence, images, to the recorded voltage measurements.

Despite the use of more powerful tools to reconstruct the EIT image, the problem remains difficult to solve. One of the main issues is related to the non-local property of conductivity imaging. It means that to find the conductivity image one must solve a system of simultaneous equations relating every voxel to every mea-

surement. Non-locality in itself is not the main complication, in fact, the problem is ill-posed. According to Hadamard [56] a problem is well-posed if

1. for all admissible data, a solution exists,
2. for all admissible data, the solution is unique, and
3. the solution depends continuously on the data.

The problem of recovering an unknown conductivity from boundary data is severely ill-posed, and it is the third criterion which provide the main issue. This means that for any given measurement precision, there are arbitrary large changes in the conductivity distribution witch are undetectable by the boundary voltage at that precision. A partial solution can be provided by considering additional information about the conductivity distribution—such as smoothness—and thus constrain the solution with a nearby well-posed problem.

3.3 Forward Problem

Most EIT systems use constant current sources and measure voltage differences between pairs of electrodes. To obtain an image with good spatial resolution, a number of such measurements are required. This can be obtained by applying different current distributions to the body, and repeating the measurements by changing the electrodes' configuration. From the measurements, an image reconstruction technique generates the tomographic image. Mathematically, the known quantities are the voltages and currents at certain points in the domain; the unknown is the resistivity within the domain. In order to solve with respect to the unknowns, a forward problem has to be solved. The starting point for EIT is Maxwell's equations for electromagnetics [109]. For a conductive domain Ω with a known conductivity σ, enclosed in a boundary $\partial\Omega$, the forward problem is to find the potentials at the boundary of the domain due to a given current injected through the boundary. Maxwell's equations in non-homogeneous medium can be written in in their time-harmonic representation as

$$\nabla \times \mathbf{E} = -j\omega\mathbf{B} \tag{3.1}$$
$$\nabla \times \mathbf{H} = \mathbf{J} + j\omega\mathbf{D} \tag{3.2}$$
$$\nabla \cdot \mathbf{D} = \rho \tag{3.3}$$
$$\nabla \cdot \mathbf{B} = 0, \tag{3.4}$$

where $\mathbf{E}$ is the electric field, $\mathbf{B}$ is the magnetic induction, $\mathbf{H}$ is the magnetic field intensity, $\mathbf{D}$ is the electric displacement, $\mathbf{J}$ is the electric current density, and ρ is the total charge density.

Although in a typical EIT application driving currents are time-harmonic alternating current signals (AC), it is possible to use direct current (DC). This choice, in addition to simplifying the hardware needed in the measurements, allows to make two mathematical simplifications [109,112,145]. The first is to assume static conditions and thus neglect the effects of magnetic induction. The second is to neglect capacitive effects. In addition, although conductivity and permittivity could

be combined as a complex admittivity ($\gamma = \sigma + i\omega\epsilon$), only conductivity is relevant with DC excitation.

Following such simplifications, Maxwell's Equations (3.1) and (3.2) become

$$\nabla \times \mathbf{E} = 0 \tag{3.5}$$

$$\nabla \times \mathbf{H} = \mathbf{J}. \tag{3.6}$$

If the current density is considered divided into two components $\mathbf{J} = \mathbf{J}_o + \mathbf{J}_s$, where $\mathbf{J}_o = \sigma\mathbf{E}$ is the Ohmic current, and $\mathbf{J}_s$ are the current sources, then equation (3.6) can be re-written as

$$\nabla \times \mathbf{H} = \sigma\mathbf{E} + \mathbf{J}_s. \tag{3.7}$$

In the absence of internal current sources ($\mathbf{J}_s = 0$ inside the domain), and considering that when the curl of the electric field vanishes ($\nabla \times \mathbf{E} = 0$) the electric potential u is a scalar whose negative gradient equals the electric field, then Maxwell's equations for electrostatics in a linear isotropic medium with static conditions are

$$\mathbf{E} = -\nabla u \tag{3.8}$$

$$\nabla \times \mathbf{H} = \sigma\mathbf{E}. \tag{3.9}$$

Then, if the divergence theorem is applied to both sides of equation (3.9)

$$\nabla \cdot (\nabla \times \mathbf{H}) = \nabla \cdot \sigma\mathbf{E}. \tag{3.10}$$

Since the divergence of the curl of any vector field ($\nabla \cdot (\nabla \times \mathbf{H})$) is identical to zero, then

$$0 = \nabla \cdot \sigma\mathbf{E}. \tag{3.11}$$

and substituting equation (3.8) into (3.11), the Laplacian elliptic partial differential equation is obtained

$$0 = \sigma\nabla^2 u \quad \text{in } \Omega. \tag{3.12}$$

The equation (3.12) describes the steady-state conductivity distribution in the absence of current sources and sinks within the domain Ω. In a practical EIT application, current is injected through electrodes attached to the boundary of the domain, as shown in Figure 3.1. Assuming that there are no current sources inside the domain ($\mathbf{J}_s = 0$) and no electric fields outside the domain, then

$$-\sigma\mathbf{E} \cdot \mathbf{n}|_{inside} = -\mathbf{J}_s \cdot \mathbf{n}|_{outside} \tag{3.13}$$

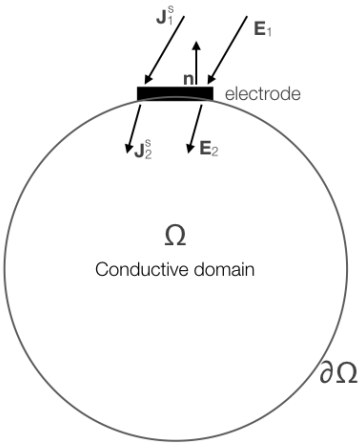

Fig. 3.1: EIT boundary conditions: $\mathbf{J}_1^s$ and $\mathbf{J}_2^s$ are respectively the current source densities outside and inside the domain; $\mathbf{E}_1$ and $\mathbf{E}_2$ are the corresponding electric fields. Adapted from [145].

holds, where $\mathbf{n}$ is the unit normal to the boundary. By applying the Neumann boundary condition to the Laplacian equation (3.12) we obtain

$$-\sigma \frac{\partial u}{\partial \mathbf{n}} = -\mathbf{J}_s \cdot \mathbf{n} \equiv j \quad \text{on } \partial\Omega. \tag{3.14}$$

where j is the inward-pointing normal component of the injected current density $\mathbf{J}_s$ on the boundary. For the remainder of this thesis j will be referred to as the injected current.

To complete the mathematical model, it is necessary to determine an appropriate electrode model that takes into account the effects of current injection and potential measurement through electrodes.

Electrode Model

The simplest EIT model is the *continuum model* [22]. This model assumes that the injected current j is a continuous function, without any discrete electrodes present on the boundary. The continuum model considers the Laplacian (3.12) and the boundary condition (3.18), together with a conservation of charge condition

$$\int_{\partial\Omega} j = 0 \text{ and } \int_{\partial\Omega} u = 0, \tag{3.15}$$

which amounts to choosing a voltage reference.

However, in a real application the current is injected through a discrete number N of electrodes attached to the boundary. This case is considered in the *gap model* [145] where the total injected current j is assumed as follows

$$j = \frac{I_i}{|e_i|} \text{ on } e_i,\ i = 1, 2, \ldots, N \tag{3.16}$$

within the electrode and zero elsewhere. I_i is the current injected at the i-th electrode, and $|e_i|$ is the electrode contact length.

By considering that the voltage potential V_i measured across the i-th electrode is constant, and by changing the boundary condition (3.12) into the following

$$\int_{e_i} \sigma \frac{\partial u}{\partial \mathbf{n}} ds = I_i \text{ on } e_i,\ i = 1, 2, \ldots, N \tag{3.17}$$

where the current density over the electrode surface s is required to be equal to the current I_i, it is possible to obtain a different electrode model that is known as the *shunt model* [22, 145].

The combination of the *gap model*, and the *Shaunt model* produce the *complete electrode model* [22, 145] that considers the existence of a discrete number of electrodes of finite size, the shunting effect of a conductive electrode, and the potential drop due to the electrode's contact impedance z_i. The model is defined by the equation (3.12) together with the boundary conditions expressed in equation (3.16), (3.17), and the following conditions:

$$u + z_i \sigma \frac{\partial u}{\partial \mathbf{n}} = V_i \text{ on } e_i,\ i = 1, 2, \ldots, N \tag{3.18}$$

$$\sigma \frac{\partial u}{\partial \mathbf{n}} = 0 \text{ in the gap between electrodes.} \tag{3.19}$$

To ensure the uniqueness of the solution the conservation of charge theorem must also hold

$$\int_{\partial \Omega} j = 0 \ \Rightarrow \ \sum_{i=1}^{N} I_i = 0, \tag{3.20}$$

together with a choice of a ground or reference voltage

$$\int_{\partial \Omega} u = 0 \ \Rightarrow \ \sum_{i=1}^{N} V_i = 0. \tag{3.21}$$

3.3.1 Numerical Approximation

A common approach to solve systems of partial differential equations is the Finite Element Method (FEM) [132]. It is a numerical analysis technique for obtaining approximate solutions to a wide variety of engineering problems. Due to its ability to model arbitrary geometries and various boundary conditions, the FEM is the most common method currently used for the numerical solution of EIT

problems [10]. The FEM first discretises the medium under analysis into a finite number of elements collectively called a finite element mesh. Within each element, the field variable is approximated by simple functions that are defined only within the individual element. The approximating functions (sometimes called interpolation or shape functions) are defined in terms of the values of the field variables at specified points on the element called nodes. It can be seen as a reduction of a continuum problem of infinite dimension to a discrete problem of finite dimension in which the nodal values of the field and the interpolation functions for the elements completely define the behaviour of the field variable within the elements and the individual elements collectively define the behaviour of the field over the entire medium.

Our starting point is to approximate the domain Ω as union of a finite number of elements Ω_k, which for simplicity we will take to be simplices. In two dimensions a simplex is a triangle and in three dimensions a tetrahedron. A collection of such simplices is called a finite element mesh, and we will suppose that there are K simplices (or elements) with M vertices (or nodes). The potential can be approximated by using the generated mesh and a series of functions, which are linear on each simplex, and continuous across the faces. The discrete approximation u_h can be written as

$$u_h = \sum_{i=0}^{N} u_i \phi_i, \tag{3.22}$$

where ϕ_i are a set of functions that are one on vertex i and zeros at the other vertices. These have an additional property that are completely determined by their values at the vertices. For simplicity, only the two-dimensional case will be expressed in the following formulation. It is possible to easily extend the analysis also to the three-dimensional case. The FEM procedure starts by combining the Laplacian (3.12) equation in its weak form

$$\int\int_{\Omega} \sigma \nabla \phi_i \cdot \nabla u_h \; dx \; dy = 0 \;\; \mathrm{i} = 1, \ldots, \mathrm{M}, \tag{3.23}$$

by applying Green's second identity the equation becomes

$$\int\int_{\Omega} \sigma \nabla \phi_i \cdot \nabla u_h \; dx \; dy = \int_{\partial\Omega} \sigma \phi_i \nabla u_h \cdot \mathbf{n} \; ds, \tag{3.24}$$

where $\nabla u_h \cdot \mathbf{n}$ is the directional derivate of u_h pointing in the direction of the outward normal $\mathbf{n}$.

By re-writing the boundary condition (3.18) as

$$\sigma \nabla u_h \cdot \mathbf{n} = \frac{1}{z_i}(V_i - u_h) \tag{3.25}$$

and incorporating it into equation (3.24) gives

$$\int\int_{\Omega} \sigma \nabla \phi_i \cdot \nabla u_h \; dx \; dy = \sum_{l=1}^{L} \int_{e_l} \frac{1}{z_l}(V_l - u_h)\phi_i \; ds. \tag{3.26}$$

Then, by substituting the Galerking formulation u_h into each element in the finite element model we obtain

$$\sum_{i=1}^{N} \left\{ \left(\int\int_{\Omega} \sigma \nabla \phi_i \cdot \nabla \phi_j \; dx \; dy + \sum_{l=1}^{L} \int_{e_l} \frac{1}{z_l} \phi_i \phi_j \; ds \right) \right\} u_i - \sum_{l=1}^{L} \left\{ \int_{e_l} \frac{1}{z_l} \phi_i \; ds \right\} V_l = 0 \tag{3.27}$$

for $\phi|_{i,j=1,\ldots,N}$. If $\mathbf{U}$ are the potentials at the nodes and $\mathbf{V}$ are the potentials measured at the electrodes, then

$$(\mathbf{A}_M + \mathbf{A}_Z)\mathbf{U} - \mathbf{A}_V \mathbf{V} = 0 \; dx \; dy \tag{3.28}$$

where

$$A_{M(y,j)} = \int\int_{\Omega} \sigma \nabla \phi_i \cdot \phi_j \; dx \; dy \tag{3.29}$$

$$A_{Z(y,j)} = \sum_{l=1}^{L} \int_{e_l} \frac{1}{z_l} \phi_i \phi_j \; ds \tag{3.30}$$

$$A_{V(y,j)} = -\frac{1}{z_l} \int_{e_l} \phi_i \; ds. \tag{3.31}$$

To impose the boundary condition (3.17), at least one element of the mesh should share a face with an electrode. Then, by combining Equations (3.17) and (3.25)

$$I_l = \int_{e_l} \frac{1}{z_l}(V_i - u_h) ds, \tag{3.32}$$

substituting U_h from equation (3.22), and assuming z_l is constant for every electrode e_l we obtain

$$I_l = \frac{1}{z_l}|e_l|V_l - \sum_{i=1}^{N} (\int_{e_l} \frac{1}{z_l} \phi_i \; ds) u_i, \tag{3.33}$$

where $|e_l|$ is the size (length in two-dimension, and area in three-dimensional case) of the l-th electrode. The equation shows that the current I_l is partially dissipated as power across the electrode's contact impedance, while the remaining current generates the potential in the conductive domain.

Rearranging the finite element system of equations into a matrix representation [50, 132] yields

$$\begin{bmatrix} \mathbf{A}_M + \mathbf{A}_Z & \mathbf{A}_V \\ \mathbf{A}_V^T & \mathbf{A}_D \end{bmatrix} \begin{bmatrix} \mathbf{U} \\ \mathbf{V} \end{bmatrix} = \begin{bmatrix} 0 \\ \mathbf{I} \end{bmatrix} \tag{3.34}$$

where $\mathbf{A}_M$ is a NxN symmetric matrix from the Laplacian (3.12) without the boundary conditions, while $\mathbf{A}_Z$, $\mathbf{A}_V$, and $\mathbf{A}_D$ contain the electrode model. $\mathbf{A}_D$ is diagonal matrix with its non-null elements equal to $\frac{|e_l|}{z_l}$.

To complete the system, the forward model must include a set of current injection patterns such that the current injected at the boundary electrodes equals the current sunk out. Although the number of current patters does not have to match the number of boundary electrodes, this is a common approach and it will be followed in this work.

3.3.2 Forward Solution

Given the discrete FEM approximation of the EIT problem for a known conductivity distribution within the domain and a current injection pattern, the resulting boundary potentials can be calculated as the solution of a well-posed, forward problem having a unique solution. The matrix form of the problem (3.34) can be expressed in a compact form as

$$\mathbf{Y} = \mathbf{Q}\mathbf{A}^{-1} \tag{3.35}$$

where $\mathbf{A}$ is symmetric admittance matrix (first element of Equation 3.34), $\mathbf{Y}$ is the vector of potentials $[\mathbf{U}\ V]^T$ and $\mathbf{Q} = [0\ \mathbf{I}]^T$.

Since the forward problem involves matrices that are square, symmetric, full rank, and well-conditioned for inversion, a stable and unique least-square solution exists. For small two-dimensional problems a standard approach to solve the linear system can be used. The most common approaches are the QR factorisation, the LU factorisation or the Cholesky factorisation. For large, three-dimensional systems, a direct solution might be computationally expensive and iterative methods have been introduced to solve the system efficiently. Some examples of the these methods include the conjugate and pre-conjugate gradient methods. These are adequate because for real application only an approximation set by the error estimate in the measurement is required.

3.4 Inverse Problem

The EIT reconstruction problem consists of finding the conductivity distribution within a conductive domain when a set of currents and the resulting potentials are known. Mathematically, this is an ill-posed, non-linear, inverse problem in which the main complications are: the reconstruction image is not necessarily a unique solution, and small changes in the boundary data can result in large changes in the reconstructed image.

A number of different method exist for solving inverse problem but, to some extent, they all follow the same basic approach: if the problem is non-linear, then linearise it; if it it ill-posed, then use regularisation to find a nearby well-posed problem; if the approximation is not accurate, then use an iterative approach to solve it. These methods can be divided in two groups: static imaging and dynamic imaging.

In static imaging [154], the absolute values of the conductivity distribution inside the domain are reconstructed by using an iterative method. Dynamic imaging [1] is a fast non-iterative method to reconstruct only dynamic time-varying distribution of conductivity changes. Although the reconstruction produced by static imaging has the potential to be more accurate in distinguishing internal structures, for the application presented in this work only the conductivity changes are required and the ability to perform reconstructions in real time was set as a high priority. For these reasons, dynamic imaging was used.

The main idea behind dynamic imaging is to first calculate an initial set of potentials $\mathbf{V}$ on the boundary of an homogeneous domain with known conductivity σ_0. The discrete model is then replaced with an approximated linearised version that is used to compute only the conductivity difference $\Delta\sigma$ from the homogeneous case. Then, after calculating the Jacobian $\mathbf{J}$ between changes in boundary potential and internal conductivity, the discrete form of the linearised problem becomes

$$\Delta\mathbf{V} \approx \mathbf{J}\Delta\sigma + \mathbf{n}, \tag{3.36}$$

where $\Delta\mathbf{V}$ is the difference in potential between two measurements, and $\mathbf{n}$ is a vector of measurement noise. The time-varying distribution of conductivity changes can be evaluated by taking two different sets of potential measurements ($\mathbf{V}_1$ and $\mathbf{V}_2$) at two different time intervals and computing the difference $\Delta\mathbf{V}$ and $\Delta\sigma$. Since only conductivity changes are calculated, the method is fast and also reduces possible problems related to electrode positioning and unknown contact impedance.

3.4.1 Jacobian Calculation

The Jacobian matrix is the derivative of the non-linear function that maps perturbations in the internal conductivity domain to changes of the potential on the boundary. It can be calculated directly by perturbing each of the K elements in the FEM mesh by $\Delta\sigma$, and then by solving the forward problem (3.35) to calculate changes of potential $\Delta\mathbf{V}$ at the electrodes. A differential approximation for $\mathbf{J}$ is obtained by dividing $\Delta\mathbf{V}$ by $\Delta\sigma$ to give

$$J_{i,j} \approx \frac{\partial V_i}{\partial \sigma_j}; \quad i = 1 \dots M; \quad j = 1 \dots K, \tag{3.37}$$

where M is the number of potential measurements on the boundary. A direct calculation, however, is computationally expensive. For this reason, in this work the Jacobian is computed only once, off-line, for the computation of the linearised form of the inverse problem (3.36).

Due to the small amount of current passing through most of the elements, many values of the Jacobian matrix will have values close to zero. Dividing by such small values causes numerical instability in the solution. This ill-conditions the problem but it is still possible to proceed with its resolution by applying regularisation.

3.4.2 Regularisation

Regularisation refers to the process of introducing additional information in order to solve an ill-posed problem by replacing it with a nearly well-posed problem. Regularisation involves a trade-off between the exact but unstable solutions, and a more approximate stable solution controlled by imposing certain prior distributions on model parameters. In EIT the additional information is the assumption that the change in conductivity $\Delta\sigma$ varies slowly or it is discontinuous.

Conventional regularisation methods include Tikhonov regularisation and approaches based on singular value decomposition (SVD) [109,145]. Although SVD is an important tool for understanding the ill-conditioning of matrices—a large value of the condition number indicates the ill-conditioning of the matrix—Tikhonov regularisation is more commonly accepted because its computation is simpler and more efficient.

The main idea of Tikhonov regularisation is to solve the ill-posed problem is the following;

$$\Delta\sigma = \mathbf{J}^{-1}\Delta\mathbf{V}, \tag{3.38}$$

by minimising the least-square function

$$\min_{\Delta\sigma}\{||\mathbf{J}\Delta\sigma - \Delta\mathbf{V}||^2 + \alpha^2||\mathbf{R}(\sigma_0 - \sigma_r)||^2\}, \tag{3.39}$$

where α is a scalar hyper-parameter that controls the amount of regularisation, $\mathbf{R}$ is a regularisation matrix that controls the smoothness of the solution, and σ_r is the initial reference conductivity, which is not necessarily the same as σ_0. The regularisation matrix is usually assumed to be equal to the identity matrix $\mathbf{I}$. This allows the penalty term $\alpha^2||\mathbf{R}(\sigma_0-\sigma_r)||^2$ to prevent extreme values of conductivity, but it does not enforce any smoothness or impose any constraint to the solutions. In the EIT imaging problem, it is commonly assumed that the conductivity in each element of the FEM mesh is constant and of similar value to nearby elements. To ensure such property a different regularisation matrix should be used such as:

- *Gaussian-type prior* [1, 51]: an approach that penalises components with high spatial frequency in the reconstructed image by assuming higher correlation between neighbouring elements and a gradually diminishing correlation with increased distance.
- *Laplacian-type prior* [4]: that uses a discrete approximation of the Laplacian edge filter. This is a second-order filter that models inter-element correlations, penalises high spatial frequencies (edges), and smooths the solution.

- *Newton's one-step error reconstructor* (NOSER) *prior* [21]: an algorithm that utilises the first step of the Newton-Raphson method for non-linear equations with assumed homogeneous conductivity. When combined with the Tikhonov regularisation, it can be seen as a smoothing approach in which the regularisation matrix is scaled by the sensitivity of each element.

The formal solution to the problem (3.39) as given by Lionheart et al. [109] is

$$\Delta\sigma = (\mathbf{J}^T\mathbf{J} + \alpha^2\mathbf{Q})^{-1}(\mathbf{J}^T\Delta\mathbf{V} + \alpha^2\mathbf{Q}(\sigma_r - \sigma_0)), \tag{3.40}$$

where $\mathbf{Q} = \mathbf{R}^T\mathbf{R}$. An alternative solution incorporates a weighting matrix $\mathbf{W}$ to model the noise variance between the potential measurements and then overcomes noise in the potential measurements produced by faulty electrodes. The full solution takes the form [1, 52, 145]

$$\Delta\sigma = (\mathbf{J}^T\mathbf{W}\mathbf{J} + \alpha^2\mathbf{Q})^{-1}(\mathbf{W}\mathbf{J}^T\Delta\mathbf{V} + \alpha^2\mathbf{Q}(\sigma_r - \sigma_0)) \tag{3.41}$$

In the work presented here, it will be assumed that full data sets are available and all measurements have equal noise variance. The generalised Tikhonov regularisation (3.40) will therefore be used. In addition, since only the changes in conductivity will be measured, it can also be assumed that $\sigma_r = \sigma_0$. Then, for a fixed initial conductivity σ_0, the Jacobian $\mathbf{J}$ and $(\mathbf{J}^T\mathbf{J} + \alpha^2\mathbf{Q})\mathbf{J}^T$ can be precomputed off-line, improving the speed in the inverse resolution.

3.5 Data acquisition

Since the introduction of the first system, EIT instrumentation has continued to evolve following the advances in analogue and digital electronics. While there are many different EIT system designs, in general they consist in one or more current sources, a mechanism for generating current patterns, a data acquisition unit, and software for inverse problem solution and image reconstruction. Figure 3.2 presents a block diagram of a typical EIT system. Iit is possible to inject voltage and measure current, but most systems apply currents and measure voltages because the effects of contact impedance that exist between the electrodes and the conductive domain are significantly reduced by the large input impedance of the voltmeters as compared to the low impedance of the ammeters.

The remaining of this chapter will introduce the current injection and potential measurements patterns used in a typical EIT system. Detail of the implementation on the single components developed in this work will be given in the next chapter.

3.5.1 Current Sources

In a classical EIT system, sinusoidal AC signals at low frequency are injected into the studied domain. Using such method allows to cancel long-term polarisation of the electrodes, and allows to acquire both the capacitive and resistive components

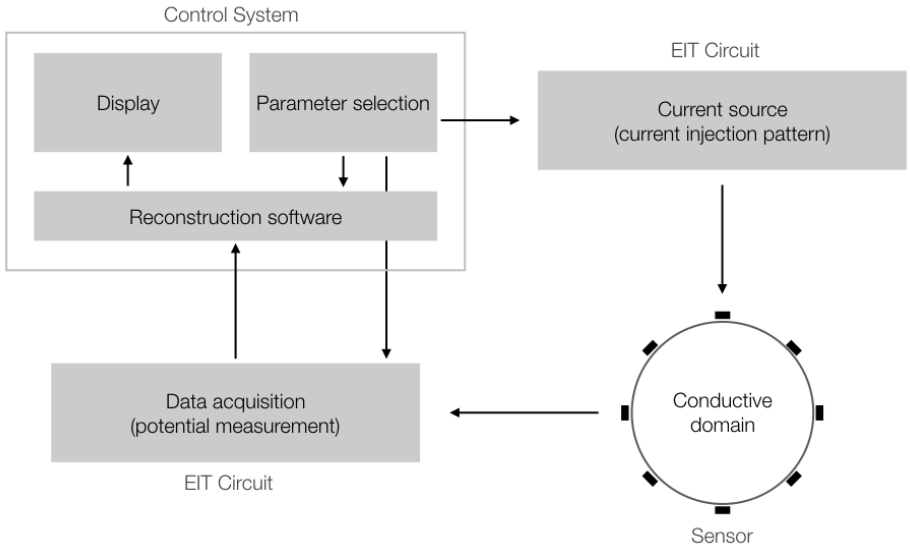

Fig. 3.2: Schematic representation the EIT system.

during the measurements. This information is valuable when the domain under study is the human body. However, the use of AC signals requires additional hardware that is used to synchronise the detection circuit with the waveform generator, and a series of low-pass filters or other processing techniques to condition the signal and obtain a clear measurement. This not only complicates the hardware design, but requires also more power to run, and affects the real-time performance of the whole system.

A different approach has been presented by Cillers et al. [29] where instead of using AC signals, bi-directional DC current pulses are used as excitation technique. Here, the current to the driving electrodes is kept constant during each half cycle. As a consequence, the driving current is a square wave, and potential measurements can be taken during the constant flat part of the cycle once static electromagnetic conditions have been achieved. The use of DC current is desirable for robotic application because it allows the implementation in battery-powered hardware. Although the bi-directional excitation approach is preferred to eliminate the effect of long-term polarisation of the electrodes, the use of non-bi-directional DC currents was previously demonstrated by Nagakubo et al. [100] and Alirezaei et al. [5] and it will be used for all the experiments presented with the next chapters.

3.5.2 Current Injection and Potential Measurement

Many different strategies for current injection and potential measurement can be used in EIT. In general, drive patterns can be divided into two groups according to the number of current sources used: *bipolar* (single-source) and *optimal* (multi-source) patterns.

Bipolar patterns are those in which a single current source and sink are used for current injection through a single pair of electrodes, while potential measurements are taken at the remaining electrodes pairs. The bipolar drive pattern most commonly used is the *adjacent* method [17,18,129,145] in which the current is injected through a pair of neighbour electrodes that are systematically rotated through all the possible combination. At each step, the resulting potential is measured at all the remaining electrodes using the same strategy. Figure 3.3 shows the first two steps of the driving pattern. As this method is symmetrical–there is complete and symmetrical interchange of current injection and potential measurement and the reciprocity principle holds. This principle [47] states that the potential measured by a pair of electrodes when the current is injected by a different pair is identical to the potential when the current injection and the potential measurement pairs are inverted. Other bipolar patterns, are the *polar* [6, 129, 145] method in which the electrode carrying the current source and sink—driving electrodes–are opposite each other, the *cross* pattern [6,129] in which the driving electrodes are placed on orthogonal lines, and a variation of the polar—the *pseudo-polar* [129]—in which the current sink electrode is located exactly one electrode before the electrode opposite to the source.

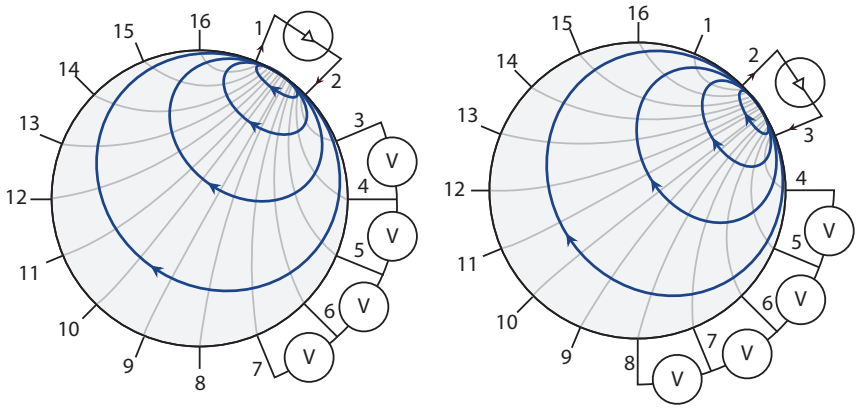

Fig. 3.3: Example of bipolar adjacent pattern. Two electrodes are selected as the driving ones, while all the others are used to measure the electric potentials generated between adjacent pairs. The injection and measurement pattern is than switched by changing the driving electrodes until a full cycle is completed. Electric potentials measured at the driving electrodes are commonly not taken in order to ensure stability in the acquired data. In the image, dark-grey lines indicate isopotential areas, while the current flow is shown in blue.

Optimal patterns [35, 71] are those patterns based on the concept of distinguishability [67], which states that optimal current patterns are obtained by maximising the difference between potential measurements at the boundary of the conductive domain resulting from two pre-determined conductivity distributions. The problem of optimising the drive patterns in EIT was first considered in the computation of the optimal placing of a pair of point drive electrodes on a disk to

maximise the voltage differences between the measurement of a homogeneous background and an offset circular anomaly. These patterns work under the assumption that multiple current sources are simultaneously used for current injection while potential measurements are taken at all boundary electrodes. Even if optimal patterns have the potential to produce more accurate image reconstructions—*trigonometric* current pattern [31, 49] are the best in distinguishing a central circular inhomogeneity inside a circular homogenous domain—they also need as many independent AC current sources as there are electrodes. In addition, optimal patterns are less tolerant to errors such as electrode location, contact impedance and incorrect forward model [77], although these can be averted with difference imaging. For these reasons, only bipolar patterns are considered for the research described in this thesis.

3.6 Summary and Conclusions

This chapter presented the mathematical background of Electrical Impedance Tomography, an imaging technique used to estimate the internal conductivity distribution of an electrically conductive body by taking measurements at its boundary. The mathematical formulation with the complete electrode model was introduced and used for the numerical approximation of the forward problem using the finite element method. Inverse solution and image reconstruction were performed to solve the linearised EIT problem using dynamic imaging, a non-iterative method to reconstruct only the dynamic time-varying distribution of conductivity changes that is needed for the application considered in this thesis.

The following chapter will present the implementation of the hardware and software implemented, and the methods that were used to evaluate them.

4

Skin Fabrication & Hardware

4.1 Introduction

In this chapter the mathematical description presented in the previous chapters will be converted into guidelines and requirements for the development of the experimental hardware and software used in this research. For each developed component both the descriptive requirements that it has to satisfy, and the implementation will be presented.

Since the early stage of this work, it has been decided to develop all the required components in-house. This was not due of a lack of off-the-shelves technologies, but to have the full control each phase of the data acquisition and image processing. In addition, this allowed us to develop a more compact system than the one currently available on the market.

In addition to the developed EIT hardware, in this chapter we will also describe the conductive domain used in the experiments. This consists of two different structures: an artificial skin that has been used to test the feasibility and capability of the system under different scenarios; and a conductive silicon-based material that can be used in the development of a soft deformable robot having embedded sensing capabilities. by exploiting the paradigm "the robot body is the sensor" and by applying EIT as transduction method, it is possible to overcome the current limitations related to the embedding of sensors within the soft device and thus obtain a shape-independent sensorized structure.

4.2 Hardware requirements

In the following section, the main requirements for the development of the portable EIT system will be provided. These can be organised into two main groups: one related to the requirements for the current source, and the second that summarises the requirements for the current injection and potential measurement system. Most of the decisions made during the development were done in order to simplify the hardware design, and thus reduce its space needs, to develop a prototype that can be compatible in size and weight with a soft robot.

4.2.1 Current Sources

Most of the current sources used in EIT systems are more appropriately called voltage-to-current converters, since they produce an output current that is proportional to an input voltage. Ideally, a current source should have an infinite output shunt impedance resulting in the current delivered to the load being independent of the load voltage. However, real sources have a finite impedance that is affected by the presence of the load. For this reason, the current source in an EIT system must be able to deliver current with a desired precision over a specified frequency range to load impedances within an expected range of values. While a higher level of precision is generally desired, current accuracy is also important. Higher accuracy can be obtained through current source calibration, where the current source is calibrated to deliver an accurate current to a test load having an impedance that is within the range of expected load impedances.

4.2.2 Current Injection and Potential Measurement

The hardware implemented to manage the driving patterns has to satisfy, the requirements defined as follows

- Bipolar current patterns are preferred over optimal patterns to simplify hardware implementation and to reduce cost and power consumption. A single current source multiplexed over multiple channels can be used with bipolar patterns.
- Non bi-directional DC current sources will be adopted in accordance to the specifications presented in section 3.5.1. Potential measurements will be taken after static electromagnetic conditions have been achieved.
- For bipolar patterns, potential measurements will be taken at all electrodes. To achieve a constant dynamic range in the data, potential measurements from the driving electrode–current source and sink–are not acquired.
- Although in all the experiments the *adjacent* pattern will be used, the ability to change between different bipolar patterns is desirable to give flexibility within the experimental EIT system.f

4.3 Hardware for a Portable EIT System

Starting from these requirements, in this research we designed and developed a simplified version of a commercial EIT system to be used as the main component of our sensing system. The main focus was placed on developing a low-cost, adaptable system that is able to perform measurements by applying different patterns, and powered by a DC current source. The use of DC current simplifies the hardware requirements, and allow the use of the developed hardware even in battery-driven applications. The electronic system is composed of two independent printed circuit board (PCB): a voltage to current generator, and a driving/read-out circuit. Figure 4.1 shows a schematic representation of the driving and readout electronics for a given channel.

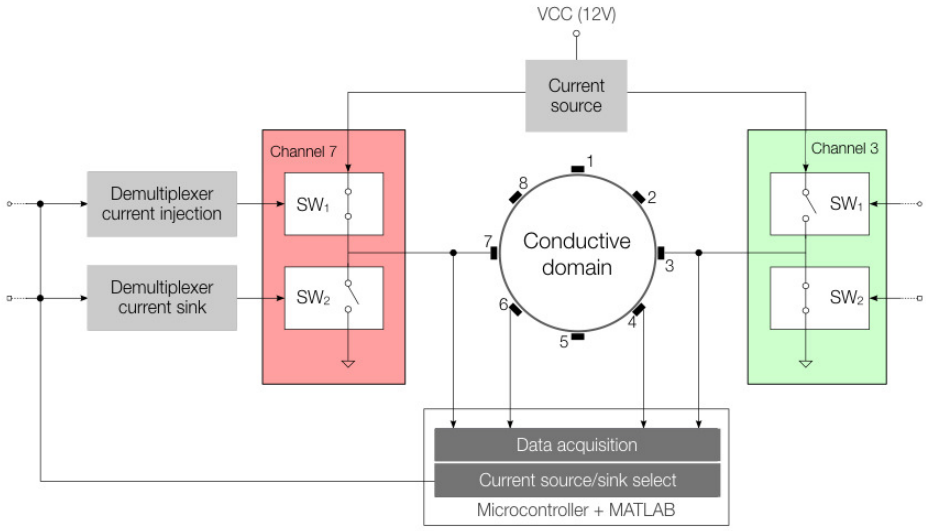

Fig. 4.1: Schematic representation of the EIT system. In this configuration: channel 7 is connected to the current source, channel 3 to the ground, and channels 4 and 6 are used to measure the voltage potential generated at the boundary. For simplicity in the representation only few electrodes are connected.

The current generator, is implemented by a voltage regulator (Texas Instruments LM317) set up as precision current-limiter circuit. The output current value is controlled by a variable resistor, and it can be adjusted linearly by changing the resistor value. In order to provide a constant current supply on varying load, a voltage source of 12 V is used as input to the voltage regulator. The electrical current is then multiplexed across the different channels by the driving/read-out electronics. Each channel in the driving/read-out electronics is designed to operate at three independent stages. To provide such capability we implemented it as a half H-bridge where an n-MOSFET (International Rectifier IRLML6344TR) and a p-MOSFET (International Rectifier IRLML9301TR) act as two independent switches connected to the same path. In such configuration, the p-MOSFET is connected to the positive source, while the n-MOSFET to the ground. By opportunely turning on and off the single switch, it is possible to set each channel to act as current source, current sink, or setting it to its high-impedance state in which the channel can be used to measure the voltage. As initial choice, the control of the driving/read-out electronics was performed directly by the microcontroller. In order to reduce the number of wires, and add modularity to the system, we moved to an integrated solution that uses two independent de-multiplexer (Texas Instruments CD74HC237M). To capture the smaller voltage variations, we added to each channel an amplification stage. It consists of a low power, general-purpose instrumentation amplifier (Texas Instruments INA118) with variable gain. The output of this initial stage is referred to ground. The signal then passes trough two subsequent op-amp (Texas Instruments OPA827, and TLV2371 respectively)

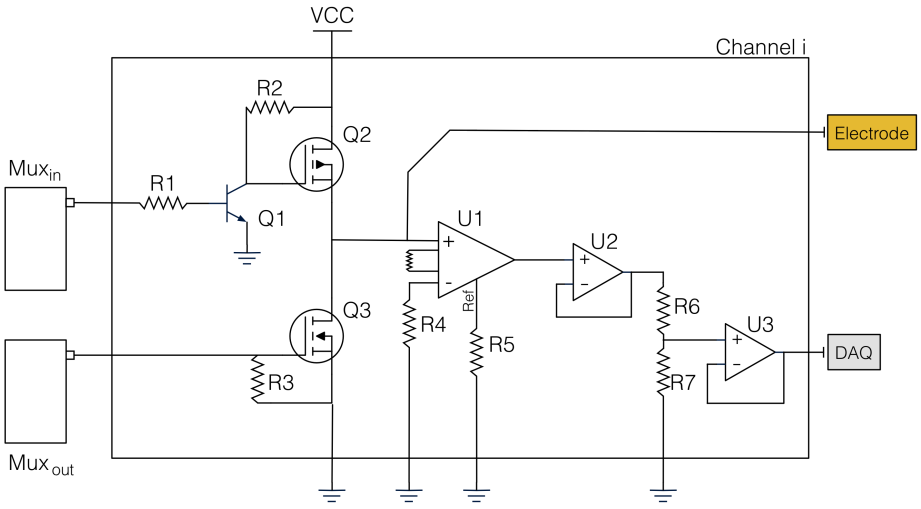

Fig. 4.2: Schematic overview of the driving and readout electronics. The image depicts the configuration for a generic channel and its components. By using this configuration, a single channel can be set as: (i) current source; (ii) current sink (ground electrode); or (iii) used to measure the electric potentials with respect to an external common ground. The process is controlled by the two independent de-multiplexers connected at each channel. DAQ: data acquisition board. In the figure, Q1 is the NPN transistor, Q2 and Q3 respectively the P-MOSFET and N-MOSTEF, U1 is the INA118, U2 is the OPA827, and U3 is the TLV2371.

both configured in a non-inverting gain configuration. Figure 4.2 shows the structure of a single channel.

The driving/read-out electronics used in this design has 8 independent channels. Although, the system has been designed to be modular to easily adapt its use to different requirements. Each channel is connected to the domain under study by a single-ended cable that has at its extremes an alligator clip. The acquired signal is routed toward an analogue pin of the micro-controller (Atmel ATmega2560). Since each channel is measured independently, it is possible to perform any possible pattern combinations either at run-time or in post-processing. It is worth to mention that in the current version of the acquisition system no further signal processing, e.g noise filtering, or signal conditioning, is performed. Figure 4.3 shows an overview of the developed electronics connected to an Arduino Mega2560.

A full set of potential measurements is obtained using bipolar drive patterns. In this technique two boundary electrodes are initially used for current injection while potential measurements are taken from all the remaining boundary electrodes. The electrode pair used for current injection is then systematically rotated through all electrode pairs while additional potential measurements are acquired at each current injection step. The frequency of data acquisition is configured through the ATmega2560 micro-controller at around 10 kHz. To guarantee static electromagnetic conditions, a suitable experimentally defined short delay ($\tau \approx 2$

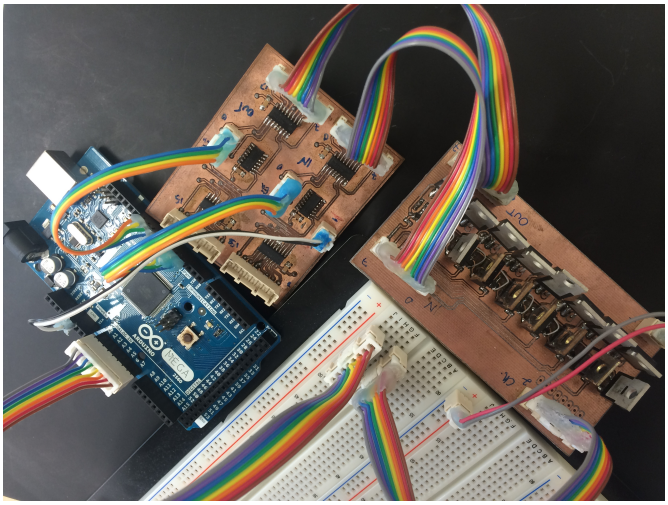

Fig. 4.3: Developed EIT driving/read-out electronics connected to the microcontroller board.

ms) is added after each current injection step. To improve signal-to-noise-ratio, an oversampling technique is implemented by acquiring multiple potential measurements from all boundary electrodes and averaging before switching to a new pair of current-injecting electrodes.

4.4 Reconstruction Software

A user interface for experimental control and for the real-time inverse solution and image reconstruction was written in Matlab®. Although Electrical Impedance Tomography and Diffuse Optical Tomography Reconstruction Software (EIDORS) [4] was used for the initial testing, most of the experimental software was designed and implemented by the author. This provided better control of the software and all desired changes that were required for this application.

Figure 4.4 shows a flow chart of the software implemented. From that, it is possible to notice that the user interface is used to configure all parameters and control of data acquisition and real-time visualisation. Some of the main properties of the software package are the following:

- The *geometry* of the domain can be selected among a predefined set of shapes.
- *Electrodes* can be up to sixteen in accordance with the hardware design.
- *Mesh size* used in the solving the inverse problem can be changed to control the number of elements of the FEM and thus adjust its resolution.
- The initial homogeneous *resistivity* of the domain. It is required for modelling and solving the forward problem.

- The contact *impedance* can be set to improve the accuracy of the model. However, since difference imaging is used, only an approximated value is required. In fact, any error in the inverse solution is cancelled out.
- *Injection*, and *measurement* patterns can be chosen, and can be further added by the user. Additionally, the *algorithm* for the inverse solution, and the prior regularisation prior can be selected accordingly a predefined set.
- The value *alpha* of the hyperparameter that control the smoothness of the regularisation.

Once the parameters are set, the algorithms proceed to creating the forward model. Once the model is set, the Jacobian $\mathbf{J}$ and $(\mathbf{J}^T\mathbf{J} + \alpha^2\mathbf{Q})^{-1}\mathbf{J}^T$ in Equation 3.40 can be computed from the assumed homogeneous conductivity distribution. All quantities, at this point, can be calculated off-line increasing the speed of the inverse resolution.

In this work, difference imaging has been used. This technique requires the acquisition of two sets of potentials, $\mathbf{V}_1$ and $\mathbf{V}_2$, taken at two different times. The difference in the potentials, $\Delta\mathbf{V}$, is then used to calculate the changes in conductivity, $\Delta\sigma$, inside the conductivity domain. A first set of potential $\mathbf{V}_1$ is acquired and stored as an initial reference. Then, the inverse solution is computed inside an infinite loop that constantly updates $\mathbf{V}_2$ with the acquired measurements and computes the inverse solution. Within the same loop it is possible to display the reconstructed conductivity, and to store the acquired data for later off-line processing. For display purposes only, a two-dimensional circular averaging filter was used after image reconstruction to reduce the stepwise changes caused by the FEM approximation.

The image reconstruction rate is affected by the complexity of the inverse solution, which depends linearly on the number of elements in the Jacobian matrix $\mathbf{J}$. Any dynamic contact that contains frequency components exceeding one half of the reconstruction frequency would not be accurately determinate by the system, according to the Nyquist sampling theorem.

4.4.1 Metrics for Reconstruction Evaluation

Assessing the quality of a reconstructed image in EIT is difficult. In fact, EIT imaging performance depends strongly on the reconstruction algorithm and its parameters. To minimise bias when investigating driving patterns and verify that improvements to the EIT reconstruction are available, several commonly used regularisation methods and hyperparameter values were compared. Several metrics [1, 3, 151] have been used to measure the quality of the reconstructed images. In this work three metrics—in addition to the *maximum intensity value*—previously used in medical imaging are considered.

Maximum Intensity

This metric is calculated as the value of maximum intensity of conductivity change in the reconstructed image. A constant intensity change, due to the same stimulus at any position across the conductive domain is the desired behaviour to achieve.

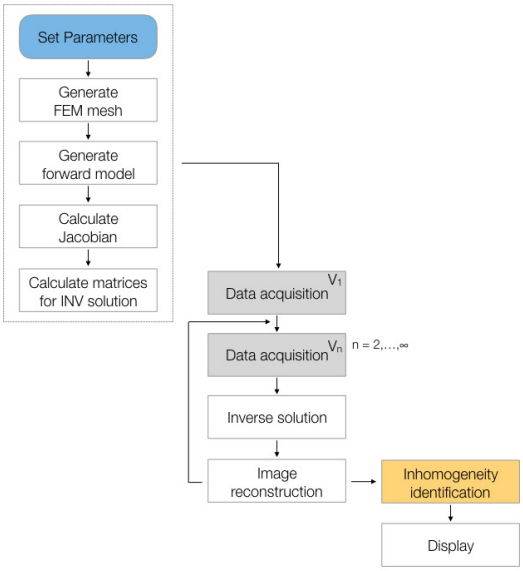

Fig. 4.4: Flow chart of the experimental EIT software. Data acquisition stage (grey boxes) is described in detail in Figure 4.5

Spatial Resolution at 50% of Image Amplitude

This value (RES_{50}) is calculated by evaluating the ratio between the number of elements in the reconstructed image having value at least 50% of the maximum amplitude, and the total number of elements in the mesh.

$$RES_{50} = \left(1 - \sqrt{\frac{\text{Elements over } 50\% - 1}{\text{Total Elements}}}\right) \tag{4.1}$$

The metric is similar to the ones proposed in Adler and Guardo [1] and Wheeler et al. [151]. As the spatial resolution increases, so does the capability of the system to discriminate between two different stimuli rather than to mis-reconstruct them as one.

The relatively low resolution of the EIT-based imaging, as compared to other technologies, also affects its capability to discriminate between stimuli and makes it not suitable for applications where high spatial resolution is required. In a soft robot, stronger pressures mask weaker pressures, and it is more difficult to discriminate when two events occur at the same time.

Shape Deformation Angle

The sharpness of the reconstructed image can be derived by considering the difference between its RES_{75} and its RES_{50} spatial resolution, where RES_{75} is similar

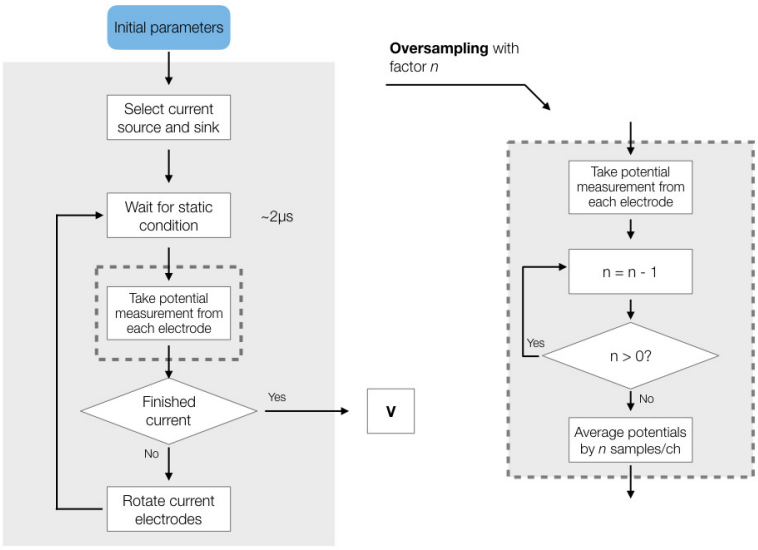

Fig. 4.5: Flow chart of the EIT data acquisition stage for a full set of potential measurements both with, and without, the over-sampling stage.

to the measure just introduced with the main difference in the threshold used. The angle β can be obtained as follows:

$$\beta = \tan^{-1}\left(\frac{25\% \text{ of max amplitude}}{(RES_{75} - RES_{50})/2}\right) \tag{4.2}$$

In a discontinuous reconstruction, RES_{75} is expected to be equal to RES_{50}, hence $\beta = 90\,\text{deg}$. This metric is based on the shape deformation metric presented by Adler et al. [3] in which the difference between two assumed circular areas is computed. Here the assumption of circular reconstructions is removed and only the absolute differences are computed. The metric is calculated as an angle since this provides additional information about the overall shape.

Distance Error at 75% of Maximum Image Amplitude

The distance error (ERR_{75}) was evaluated by computing the Euclidean distance between the centroid of the stimulus (x_1, y_1) and the centroid of the reconstructed image (x_2, y_2). Only those elements in the reconstructed image containing at least 75% of the maximum amplitude were considered

$$ERR_{75} = \sqrt{(x_1 - x_2)^2 + (y_1 - y_2)^2}. \tag{4.3}$$

A distance error value of zero ($\text{ERR}_{75} = 0$) would represent perfect performance by this measure. Similar to the spatial resolution metric, the distance error

accuracy varies depending on the drive pattern, reconstruction algorithm, total number, and location of electrodes.

4.4.2 Image Processing and Data Analysis

The just mentioned metrics can be used to extract the position and specific information of a single inhomogeneity that has been detected in the reconstructed image. In case more than one event occur over the sensitive surface, additional processing is needed to identify each event and the information retrieved from them. This processing does not affect the reconstructed image, it is only used to identify the position and area of the detected inhomogeneities.

Each of these can be described as a point spread function (PSF), such as the response of an imaging system to a point source or point object. In this context, due to the low resolution of the imaging technique, the PSF can be seen as the extended blob in an image that represents an unresolved object. As in the typical application, the degree of spreading (blurring) of the point object is a measure for the quality of an imaging system. These considerations allow to apply common image processing techniques to identify the position of the inhomogeneities and extract information from them. Figure 4.6 gives an overview of the applied method.

Each inhomogeneity is considered independently, but to process them it is fundamental to identify its location. In order to proceed in the identification, an initial thresholding with respect to the maximum amplitude is performed. The value of the threshold Γ_1 is set according to the case, but experimentally values ranging between 60% and 70% of the maximum pixel intensity have proven to be a good choice. In order to reduce the steepness of the FEM discrete approximation, a gaussian filter is applied to the thresholded image followed by a second thresholding Γ_2 in which only the pixel having more than 90% of Γ_1 are selected. Simple thresholding process, as the ones described so far, are not enough to clearly distinguish between inhomogeneities that are relatively close to each other. To better identify them an additional step is needed.

Once the thresholded image is returned, the peaks of each detected region are identified. There are two possible approaches to perform this task. The first consists in scanning all the detected pixels and select only the ones that have a value greater that the ones of the neighbouring pixels. The process is robust, fast—linear with the number of detected elements—and has the advantage of identifying with high probability the "true" PSF local maximum. The second approach is based on the use of weighted centroids. This approach uses the same image processing, with the difference that it just calculates the weighted centroid of each connected object that was obtained following the image processing. While this gives sub-pixel resolution, it can miss peaks that are very close to each other, and runs slightly slower.

4.5 Development of the Conductive Layer

In this section we describe the development of the conductive substrate used in the experiments performed in this research. In order to allow full adaptability of the system we decided to develop two different conductive domains. A first one, made

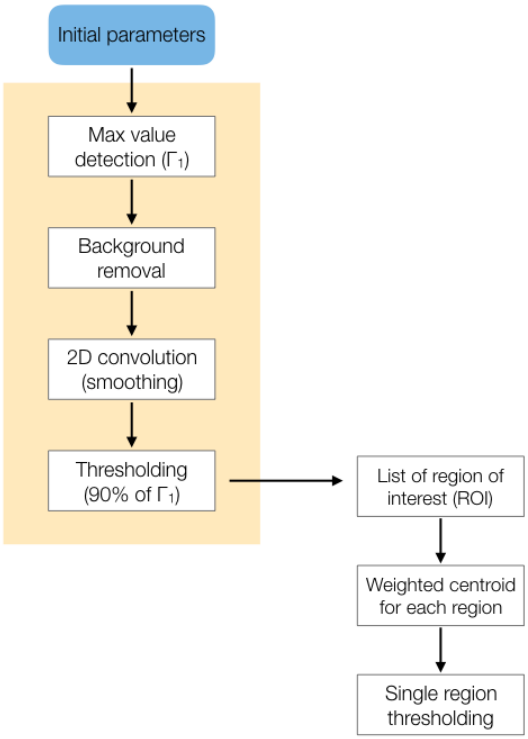

Fig. 4.6: Schematic overview of the process used to identify single inhomogeneities detected in the reconstructed image.

by layering a conductive textile over a thin foam substrate was used to evaluate the performance of the system in different scenarios. The second, a conductive silicone-based structure, was used to test the system capabilities in a soft robotic context. Details about the development and the properties of the materials used are discussed in the following sections.

4.5.1 Skin Fabrication

The properties of the material that is used to form the EIT-based skin are crucial to its performance. An ideal material would have continuous and homogeneous conductivity, give large, linear and local changes in conductivity in response to forces applied normal to the surface, and have no conductivity change as a result of stretch. Cost should also be low. A number of materials were investigated with the aim of finding the one with the best properties. To the writer's knowledge there are no suitable materials that are commercially available, so a custom-made material was necessary.

Initial experiments were performed with an inexpensive four-way knitted conductive fabric manufactured by Statex. This material is a highly conductive (sur-

face resistivity $\Omega < 1$ Ohm/sq), medical grade silver plated 78% Nylon 22% elastomer fabric with the ability to stretch in both directions (maximum stretch $\approx 100\%$ in length and $\approx 65\%$ in width). The surface conductivity of the material changes as it is stretched in-plane or compressed normal to the plane of the fabric. These conductivity changes are due to changes in the contact area between the conductive strings in the structure of the fabric. Then when the fabric is stretched, the increased separation between conductive strings causes a non-linear reduction in the contact area and—as a result—a non-linear decrease in conductivity. Compression of the fabric has the opposite effect, although greater conductivity changes were observed due to stretch.

Sheet resistance is used when measuring the resistance of thin films of conductive materials that are nominally uniform in thickness. Values are typically expressed as "Ohms per square" (Ohm/sq) to emphasise that the resistance is independent of the size of the sample. The term conductivity, as opposed to resistivity, will be used here for consistency with the EIT mathematical model and the literature. The terms conductivity and surface conductivity—in Siemens per square (S/sq)—will be used interchangeably when referring to thin conductive fabrics.

A prototype circular sensitive skin was made by positioning eight stainless steel bolts used as electrodes around a circular piece of the conductive textile of 200 mm diameter, as can be seen in Figure 4.7. As electrodes, eight stainless steel bolts were used and fixed near the edge of this layer. A constant DC current was injected across adjacent pairs of electrodes while potential measurements were taken at all remaining adjacent pairs using the adjacent drive pattern. Due to the high conductivity of the cloth, 100 mA of current was required to achieve acceptable potential levels at the boundary. Since greater changes were observed due to stretch in comparison to pressure, a non-conductive foam was used under the fabric to increase fabric stretch as a result of pressure. The complete electrode model and a Gaussian-type prior regularisation were used for the inverse solution.

4.5.2 Conductive Soft Body

The use of conductive textile is a good starting point for the development of a stretchable sensor based on EIT. This approach allows the development of a simple structure that can be placed around different geometries and easily conform to those. But, when soft robots are considered, the advantages brought from the use of conductive text are reduced or even nullified by the effect of the material used to build soft robots: silicon rubber.

Silicone rubber is an elastomer composed of silicone that is widely used in industry. It is also becoming more and more accessible to the robotic community. In general, silicone rubber is stable, and resistant to extreme environments and temperatures while still maintaining its useful properties such as:

- The ability to repeal water and form watertight seals.
- Durability, it can stand up to large impacts.
- Flexible and can adapt to an underlying structure, and can be stretched.
- Does not support microbiological growth, it is inert, and non-toxic making it usable in biomedical application.

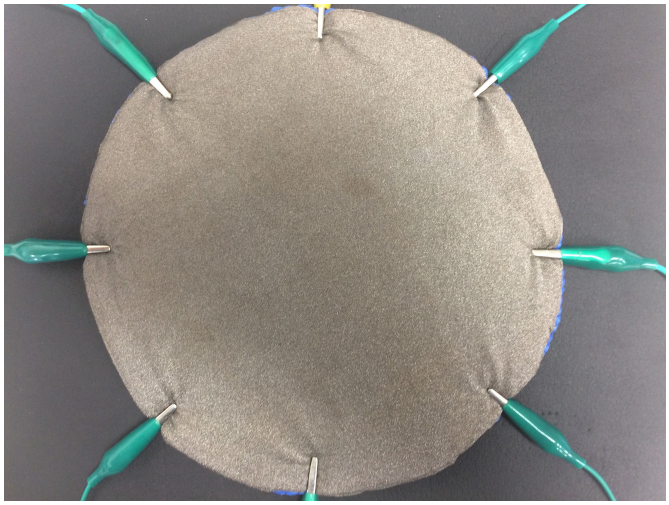

Fig. 4.7: Experimental conductive substrate (grey textile) made by layering a conductive textile over a thin foam material (blue material). The structure has been then attached to eight stainless alligator clip used as electrodes.

- Has low thermal and chemical conductivity.
- Can be moulded in unlimited number of shapes and textures.
- Shows electrical insulation properties, unless it is made conductive.

Due to these properties and its ease of manufacturing and shaping, silicon rubber can be found in a wide variety of products. In its uncured state, silicone rubber is a highly-adhesive gel or liquid. In order to convert to solid, it must be cured, vulcanised, or catalysed. This is normally carried out in a two-stage process while manufacturing the desired shape, and then during a prolongated post-cure process. This simple shaping process makes the use of silicon rubbers simple for developing robotic devices that are inherently flexible, safe for interaction, and adaptable. In addition, the possibility to easily reproduce any shape allows the design and embedding of pneumatic actuators within the soft structure [66, 118, 127].

Although these properties make silicone rubber a good candidate for developing novel robotic technologies, they also bring some limitations. One of these, as mentioned earlier, is the incompatibility with conductive textiles. This incompatibility is related to the fact that once the textile is embedded within the silicone, it looses the capability to conduct current. In fact, silicone fills the spaces between conductive strings and thus prevents the current to properly distribute over the surface. A different approach to overcome this issue consists in attaching the textile over the silicone rubber surface [28]. This can not be done by using of glue since silicone does not stick to many surfaces. Alternatives, such stitching the textile to the silicon rubber, may be advantageous for some applications but it is not trivial to keep a constant compliance wth the underlying structure.

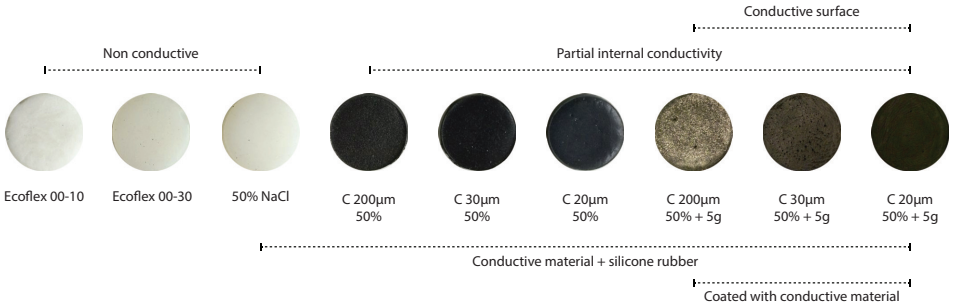

Fig. 4.8: A series of mixture made to create a conductive silicone. Two different conductive substances have been added to the silicone rubber: Sodium chloride (NaCl), and Graphite (C). Values in percentage indicate the quantity of conductive material added w.r.t. the amount of silicone used, while values in grams indicate the quantity of material spread over the surface before the silicone rubber was fully cured.

In order to fully exploit EIT as sensing technique to silicon rubber, it is necessary to make it conductive. The process of making silicone rubber conductive it is not new, but it has been generally only possible in large industrial process. The basic idea of conductive silicone is that, while silicone is totally insulating, it can be impregnated with conductive particles. Often this is done by adding small metal or carbon particles to the compound. Graphite, often in the form of carbon powder, is probably the most common choice because it is cheap, non-toxic, and does not corrode. Figure 4.8 shows some of the mixture initially used to create a conductive silicone.

Silicone is a instable material and adding different substances can lead to different problems. Some common problems are:

- Cure inhibition: the material added may prevent the silicone from curing into its solid state and thus keeping it in its semi-liquid form.
- Non-rubber property: the addition of the material can make the silicone rubber conductive but if it can also stiffen it. This is an unwanted property especially in the development of a complaint sensor.
- High impedance: most of the common techniques allow to create a rubber that is conductive, with high resistance ($> 100\text{M}\Omega$).
- Platinum interference: this problem emerges when platinum cure silicones are used. Adding Graphite to these compounds makes them conductive only in their semi-liquid state. Once the silicone cures, it completely looses the conductive properties of the added element. In fact, once mixed silicone surrounds all the individual particles and insulate them from each other inhibiting the current to be transferred.

Instead of using graphite, in this research chopped carbon fibres have been incorporated within a platinum cured silicon rubber from Smooth-On, Inc. (Ecoflex® 00-10, Ecoflex® 00-30). Carbon fibres are conductive bits of material used to increase the strengths of different materials. These, unlike graphite particles, have

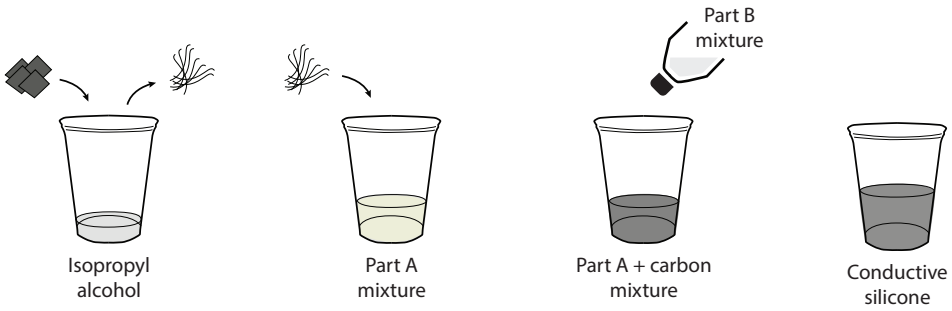

Fig. 4.9: Sequence of steps required for the development of a soft, conductive silicone rubber.

the advantages of being into thin fibres that once mixed to the platinum cured compound do not interfere with the curing process, and still maintain their conductive properties both in the silicone semi-liquid and cured form. In addition, using carbon fibres allows the following advantages in the final product:

- Rubber properties and conductivity.
- The mixture results are non-toxic.
- Low resistivity (40-150 Ω) when compared to other techniques. This means that the same compounds can also be used for capacitive sensing and not only for resistive sensing.
- Electrically stable: slight changes in pressure or bending do not greatly change the resistance of the material.
- Tight connection: the use of thin fibres increases the connectivity between the single elements.
- Fully mouldable: the resulting compound is more viscous w.r.t. the original silicone rubber, but it can still be moulded into any shape.

The steps needed for the development of the soft silicon-based conductive sensor are shown in Figure 4.9. The process begins with the cast of the conductive part. Carbon fibres are mixed with a small quantity of rubbing alcohol (isopropyl alcohol) in order to break apart the little hairs forming the carbon fibre structure. Some of the dispersed hairs are then mixed with Part A of the silicone mixture. In order not to interfere with the curing process, all the alcohol should be totally evaporated before mixing the fibres with the silicone. At the same time, the fibres should not be completely dry otherwise they will combine again forming bloks of conductive material that will stiffen the silicone rubber. Once the two material are completely blended, Part B is added to the mixture. After this process, the mixture is ready to be moulded into any shape. In the final step of the process, the entire sensor is sealed with the same silicone material to protect it, and to prove the embedded capability into a soft robot developed with this mixture.

In general, by adding 5% carbon fibres to the mix, the average resistivity is s about 500 Ω for a piece of conductive rubber of 5 cm length. This value varies from 40 Ω to 2-3 kΩ. In theory the property of this conductive rubber should vary with

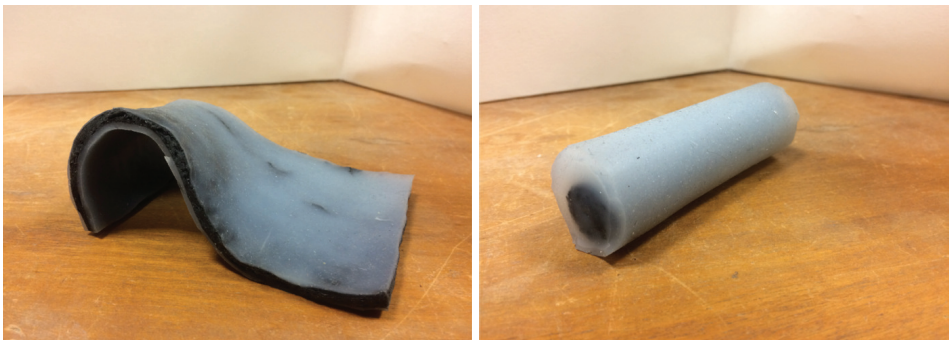

Fig. 4.10: Developed silicon rubber-based sensors. (Left) A two dimensional, stretchable, skin-like sensor. (Right) A cylindrical soft conductive structure.

the volume being measured across. Depending on the arrangement of the fibres within the compound, it is possible to measure smaller resistance across larger chunks than when probes are placed in closer proximity. However, the conductive silicon material changes its resistance when bent, compressed, or stretched. Figure 4.10 shows some of the conductive substrates developed during this thesis.

4.6 Summary and Conclusions

This chapter introduces the requirements and the implementation steps used in the development of the hardware and software used in this research to implement a deformable sensor based on EIT with multiple external electrodes. The requirements have been derived fro the mathematical formulation of the problem presented in the previous chapter. Using these, a series of simplifications have been considered to reduce the hardware requirements, to allow portability, and to facilitate battery-driven applications.

A key point in the development of a portable EIT system was the choice of using DC current—instead AC current—in conjunction with the application of bipolar patterns. These choices allow the use of a single current source that simplifies the hardware implementation and to reduce the cost and the power consumption, and to avoid synchronisation mechanism for data sampling. Detail of the components used in the development, and circuit diagrams are also provided in the chapter as reference. In addition to the details of the driving/read-out electronics, in this chapter we also introduced the functions implemented in the software used for the inverse solving, and the metrics used to evaluate the reconstructed images. These metrics also characterise the ability to differentiate between multiple stimuli that are applied simultaneously. In order to detect the applied stimuli, additional post-processing is performed over the returned conductivity map. The process is presented and discussed in the chapter.

In addition to the developed hardware, in this chapter we also presented the step used for the realisation of the conductive substrate used as sensing layer. Two different versions have been developed, for both the main properties are

presented and analysed. The first substate is based on the use of a conductive textile that changes its resistivity value when stretched in-plane or compressed by a normal force. In order to better discriminate normal forces with respect to in-plane stretches, we applied a soft, thin, deformable foam layer has been placed beneath the conductive textile. The sensing layer can take any two-dimensional geometry, and can also be wrapped around three-dimensional shapes. The second substrate, instead, has been realised in silicon rubber that has been made conductive by the use of a mixture of carbon fibres. Differently from the previous version of the conductive substrate, the resulting material can be shaped in any two–, three-dimensional geometry according to the needs. The use of silicon rubber allows to the substrate to be stretched, bended, and can absorb normal forces.

The following chapters will present the characterisation of the developed hardware and conducive substrates. Various experiments have been performed in order to capture the features and the limitations of the materials used. Initial tests have been conducted with the artificial skin fixed flat on a desk, while later ones demonstrate EIT applied to create sensitive skin that covers three-dimensionally contoured bodies.

5

System Performance Evaluation

5.1 Introduction

In this chapter the initial system performance evaluation will be presented. Performance will be determined based on experiments with the hardware described in previous chapter, and by using the textile-based conductive domain. The system has been tested with different configurations spanning from data acquisition to test the basic measurements protocols, to the application of the sensor around curved surfaces to prove the adaptability of the method. In the following sections, for each tested scenario we will present both the experimental setup and the related experimental protocol used to perform the test.

5.2 Experimental Evaluation

In this section, we will describe the experimental setup used to characterise the behaviour of the sensor under different conditions. In a first phase, electric potentials are acquired both in absence and in presence of different loads applied to the artificial skin. These initial measurements are fundamental to create a series of reference values for the conductivity reconstruction. In a second phase, we applied the reconstruction algorithm to prove the capability of the system to correctly identify the presence of the probe and its position. In the last phase, more complex interactions—as multi-touch contact, and application over curved surfaces—were addressed to test the artificial skin capabilities.

5.2.1 Experimental Setup

The experimental setup employed for the characterisation of the smart skin system consists of the components schematically illustrated in Figure 5.1. The artificial skin is connected to the driving/readout electronics previously described. This is controlled by an external ATmega2560 powered micro-controller that is used to both switch the status of the different channels, and as data acquisition board (DAQ). A laptop with Matlab installed is connected to the micro-controller, used to control the whole system, and to compute the inverse problem solution.

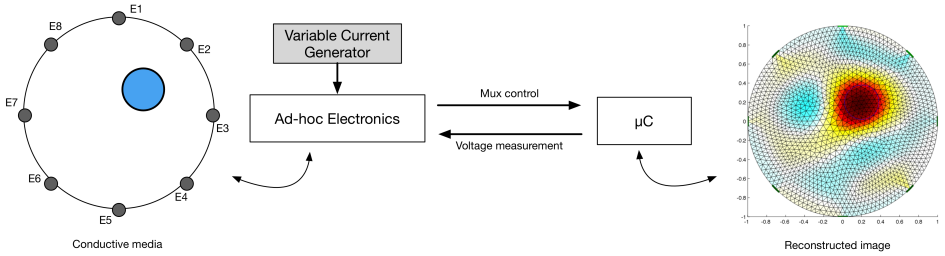

Fig. 5.1: Schematic view of the experimental setup. The artificial skin is connected by wire to the ad-hoc developed driving/read-out circuit. This is connected to a microcontroller that sets the status of each channel, and functions as a digital acquisition board. The whole system is then connected to a laptop on which the main program and the inverse solver are running.

To prove the adaptability of the system to react and detect various stimuli, we used different probes that vary in size and shape. For instance, we used 3 different circular probes with radius ranging from 15 mm to 25 mm, and a square probe with a side of 15 mm. In all experiments, in order to cope with possible fluctuations of the acquired value, a series of 10 measurements were made and then the mean value was used. In all experiments, unless differently stated, the artificial skin was placed on a flat surface.

For the reconstruction process, we used a dynamic imaging approach. A reference measurement was acquired and stored to be compared with voltage measurements takes at consecutive times. Although the EIT community is moving toward a unified approach to reconstruct 2D medical images [3], as inverse solving algorithm we used the Gauss-Newton EIT reconstruction approaches, which have been widely used in EIT since the late 1980s [21]. The approach allows to represent the solution as a linear reconstruction matrix, which can be pre-computed and thus allows rapid, real-time imaging. The parameters used for the inverse solver were derived empirically by measuring the error of the reconstruction using different probes and then by selecting the best solution. In order to provide consistency in the reconstruction, the parameter values remain the same during all experiments, unless otherwise stated.

5.2.2 Experimental Protocol

Different tests were performed to assess the overall performance of the sensors, according to the following protocols.

Preliminary Analysis on the Sensor Working Principle

A first series of experiments were performed in order to capture the output value of each electrode in absence of any force applied over the sensing area. At first, the output of an arbitrary chosen electrode was directly monitored and acquired with Matlab during a full driving cycle. In order to obtain valid measurements, we

waited the fixed amount of time of 2 μs (empirically found) to ensure electromagnetic stability before acquiring the data. The obtained value can be considered as the offset for the voltage potential measurements to be used in later phases where differences in the measured data correspond to the presence of inhomogeneity within the sensing layer due to external stimuli (i.e. touch or stretch).

Indentation Tests and Electrode Sensibility

Following the results obtained in the first series of experiments, we continued by evaluating the changes in conductivity as a function of size and position of different loads applied over the sensing area. In order to better understand this phenomenon, we applied the probe to the region directly facing each electrode. The test were performed using probes with different sizes and shapes while keeping the applied force constant. For each configuration, we acquired the data 10 times and then averaged them to obtain a more stable waveform. Two of the results are shown in Figure 5.5 and 5.6 respectively.

Pressure Map Reconstruction

The artificial skin functionality was validated by means of indentation tests with different probes as indenter. The acquired voltage potentials obtained in the previous experiments were then used to tune the inverse problem solver and then reconstruct the conductivity map associated with the artificial skin. This series of experiments was aimed at proving the capabilities of the inverse solver in detecting the position and size of the different probes used in the tests. Once the reconstruction was returned, to identify the position and the area associated to the inhomogeneity we performed first a peak detection to identify the point with maximum intensity, and then a thresholding according to the peak value. In this phase we only considered single events that occurred over the surface.

Multi-Pressure Test

To prove the capability of the artificial skin in detecting multiple contacts at the same time, the system was placed on a flat surface, and different contacts were made on its sensing area by means of hand-held probes with a circular section. Each loads was added sequentially, and then removed in the same order. During the experiment to provide uniform pressure, over each probe was applied a constant force. Additional test to improve object discrimination and pressure measurements will be left as future work.

Application over Curved and Deformable Surface

With the last series of experiments we wanted to prove the adaptability of the artificial skin to different substrates, in particular to curved and deformable surfaces. In order to proceed in this direction, we first placed the artificial skin over cylindrical surfaces with different radii. Afterwards, we placed the sensor over other objects such as a bendable mannequin arm, the back of a chair, and around a

deformable foam-made cylinder. Where the underlying object did not provide sufficient support for the artificial skin, we placed the object over a table. Once the artificial skin was applied over these geometries, we performed similar experiments as in the case of the flat surface. During these tests, we focused or attention on: i) the capability of the system to detect a change of shape, ii) and the robustness of the sensing technique even under large deformations. In the first case, we used the reference voltage taken on a flat surface and we compared these with the ones taken when the sensor was wrapped around the curved surface. In the second case, instead, both the reference and later measurements were taken directly when the artificial skin was placed over the curved surface.

5.3 Results

The results of each single experiments are reported in the following sections subdivided into their respective category.

5.3.1 Working Principle and Material Characterisation

Initial tests were performed to understand the behaviour of the conductive material—used as sensing layer—when an electrical current flows through it. Due to the high conductivity of the material (¡ 1 Ohm/sq.), 100 mA of current were required in order to achieve an acceptable voltage potential level at the boundary. During the characterisation process, no physical contact or force was applied over the sensing area of the smart artificial skin. Figures 5.2 and 5.3 show the voltage potential measurements, respectively at electrode 3 and 6 during a full cycle of excitations. The values were acquired using adjacent patter, thus each value in the graph represents the potential calculated between two adjoining electrodes. As the measurements suggest, the maximum and minimum variations can be found when the driving electrodes are close to the one where the measurements are taken. The voltage potentials acquired from all the electrodes represents a reference voltage, V_0, used to calculate differences in the electric potentials when an event occurs over the sensor surface. Figure 5.4 shows an example of the reference measurement.

5.3.2 Single Point Contact - Signal Indentation

Using the same electrode configuration as in the previous experiments, we evaluated the changes in the acquired electric potentials as a consequence of an applied load over the sensing area. To better notice the phenomenon, we chose the position of the probe 5-10 mm apart from to the electrode under test. For this specific test we used only one probe with a circular section (15 mm radius) over which we applied a constant force of 3 N. By simply comparing the measurements in presence and in absence of the applied load is not possible to clearly appreciate the difference between them. A more clear understanding is noticeable by considering the absolute variation ($V_{meas} - V_0$) between the two measurements. Figure 5.5 shows the absolute difference using the value acquired by electrode 2 (E2) when the probe was placed in the region facing the electrode. In the figure, the

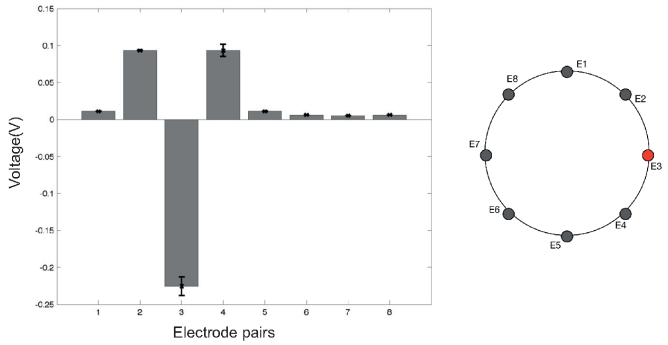

Fig. 5.2: Electric potentials measured at electrode 3 (E3) in an 8-channel configuration. Measurements are taken using an *adjacent pattern* both in excitation and acquisition phases. The positive peaks correspond to the electrode "closed" to ground nodes. Differently, the negative peak occurs when E3 is used as current sink. Error bars show the variability of measurements calculated over 10 samples.

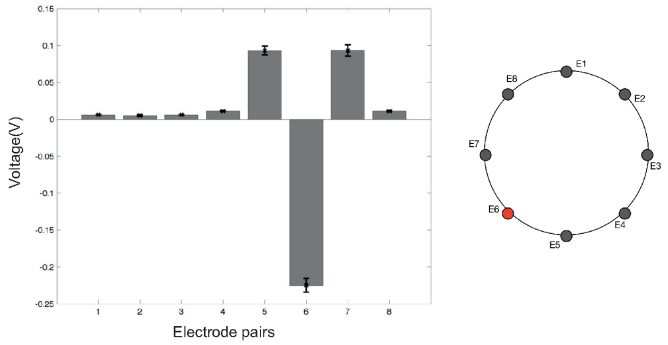

Fig. 5.3: Electric potentials measured at electrode 6 (E6) in an 8-channel configuration. Measurements are taken using an *adjacent pattern* both in excitation and acquisition phases. The positive peaks correspond to the electrode "closed" to ground nodes. Differently, the negative peak occurs when E6 is used as current sink. Error bars show the variability of measurements calculated over 10 samples.

different measurements are grouped according to the electrode acting as ground. Each bar represents a voltage difference computed over adjacent electrodes—e.g. the first bar refers to electrodes E1-E2, the second to E2-E3, and so on until all the electrode pairs are considered. Shaded regions present in the figure are not to be considered since the electrode under consideration was acting as current source or connected to ground. In the figure, major negative changes occur in the electrode pairs that involve E2 (i.e. first 3 bars in each group). The changes are a consequence of the presence of the probe that, acting on the conductive surface, changes the local conductivity of the layer. Is possible to notice a similar pattern when any of the other electrodes is considered. As reference, Figure 5.6 shows the

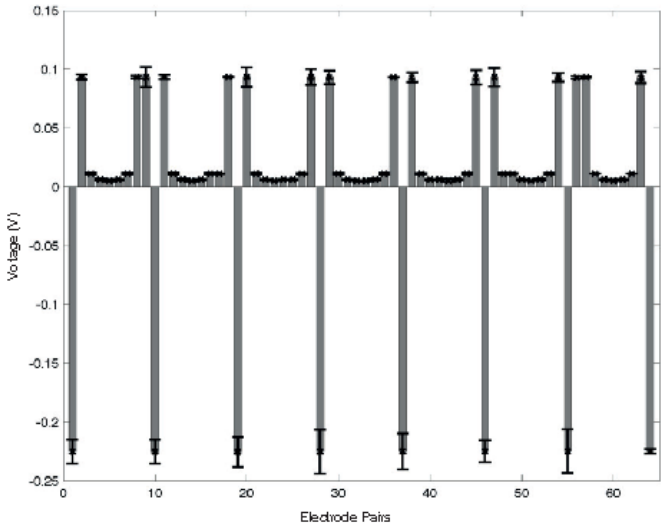

Fig. 5.4: Electric potentials measured at each electrode pair by using an adjacent pattern both in excitation and acquisition phases. The measurements were taken when no load was applied over the artificial skin.

absolute voltage potential when a load is acting in the region facing the electrode 7 (E7).

Considering the same electrode configuration, we evaluated the changes in the absolute voltage variation as a function of the probe size while applying a constant force (5 N) over them. Three different circular probes with radius of 15 mm, 18 mm, and 25 mm were placed independently in front of the region facing electrode 4 (E4). Figure 5.7 shows the results of the experiments. As the graph suggests, with the increase of the probe size, the variations of the voltage potential increase. The phenomenon was expected since a larger probe generates a wider inhomogeneity area that causes a consequent voltage drop. Even if the probe size is changed, it is still possible to notice a large negative change in the electric potentials when E4 is considered in the measure. Similar effects are expected in the case where the probe area remains constant and the applied force is increased. This consideration requires additional verification that is left as future work.

5.3.3 Conductivity Map Reconstruction

In this phase, we validate the capabilities of the inverse solver to reconstruct the pressure map of forces acting over the sensing area of the artificial skin. As previously introduced (section 5.2), in order to guarantee the solvability of the inverse problem, we precondition the solution using NOSER (Newton's one-step error reconstructor) Gauss-Newton normalised difference inverse. For the initial test, we used a single circular probes with a radius of 18 mm, and we placed it in different regions of the sensing area. Figures 6.3a-6.3c show the results obtained by the reconstruction algorithm. It is worth to say that no filtering of the data

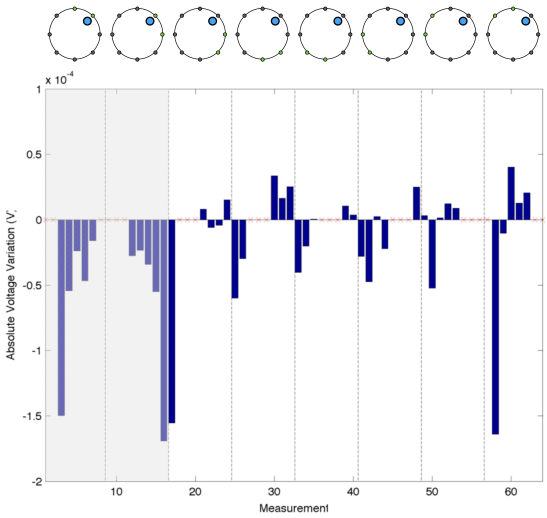

Fig. 5.5: Electric potential measurements acquired when a probe is placed in the region facing the electrode 2 (E2). The values are grouped by what electrode is used as ground following an adjacent pattern (highlighted in the top part of the figure). The shaded portion of the graph corresponds to the configuration when E2 is one of the driving electrodes. The major noticeable differences are the ones when E2 is involved in the measurements.

was performed during any phase of the process. In the image, the inhomogeneity is clearly distinguishable from the background but its shape is not well defined. As the images suggest, the closer the object is to the centre of the sensitive area, the lower is the interaction between the applied force and the constraint produced by the electrodes (Figure 6.3c). Differently, the closer the probe is placed to the boundaries, and thus closer to the electrodes, the reconstructed shape of the probe results to be less precise. This can be caused by the effect the pressure has in the applied point and the constraints due to the presence of the electrodes. To partially overcome this issue, we processed the reconstructed map by thresholding it and considering only the pixels having value up to 70% of the detected maximum value. Figures 6.3d-5.8f show the reconstructed conductivity map with superimpose its centre.

We also tested the inverse solver capabilities to distinguish different probe shapes when applied, independently, in the same position. In order to have less interaction with the boundaries, that have proven to suffer from a highest distortion due to the interaction of the probe with the electrode, we decided to use the central region for the tests. Figure 5.9 shows the results of the reconstruction using the 3 circular probes, and a square one to which was applied a constant force of 3 N. Due to the intrinsic low spatial resolution of the EIT method in this region it was not possible to clearly discriminate between the sharp-edged probe (Figure 5.9d) from the circular ones. Nevertheless the change in the probe size (Figures

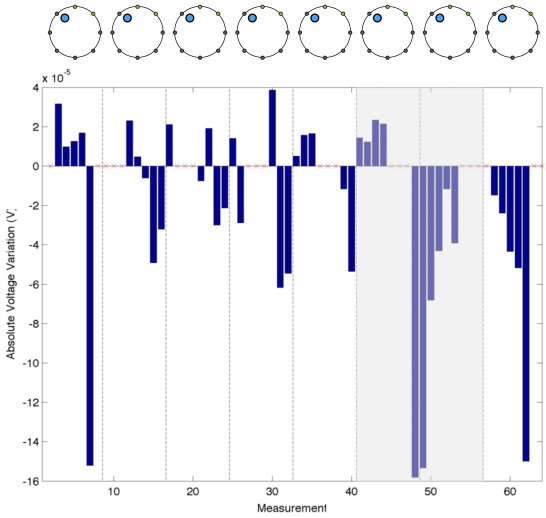

Fig. 5.6: Electric potential measurements acquired when a probe is acting in the region facing the electrode 7 (E7). The values are grouped by what electrode is used as ground following an adjacent pattern (highlighted in the top part of the figure). Not considering the region where E7 is acting as driving electrode (shaded area), the major noticeable differences are the ones when E7 is involved in the measurements (i.e. last two bar in each group).

5.9a-5.9c) can be clearly identified as the increase of the detected maximum value when a common colour scale is used.

5.3.4 Multi-Pressure Test

Following the experimental design described in the previous sections, we tested the capabilities of the artificial skin to detect multiple events that occur sequentially and simultaneously over the sensing area of the artificial skin. Three probes with the same size and shape (circular section with 15mm radius) were manually placed and then removed sequentially over the sensitive surface of the artificial skin. In order to ensure the equal applied forces, a mass of 400 g was placed over each probe. As in the previous case, no signal processing was performed prior or during the image reconstruction; the only operation that was performed was the precondition of the solver to ensure solvability. In Figure 5.10, selected frames obtained trough the reconstruction process are presented.

As in the previous cases, we processed the conductivity map to obtain the area where each probe was acting. We first applied the same methodology as in the precious cases, but we were unable to correctly identify the third probe when it was placed on the sensing area together with the other probes (Figure 5.10e). For this reason, we reduced the threshold value from 70% of the maximum value to its 60% value. As the images suggest, the shapes of the probes could not be correctly

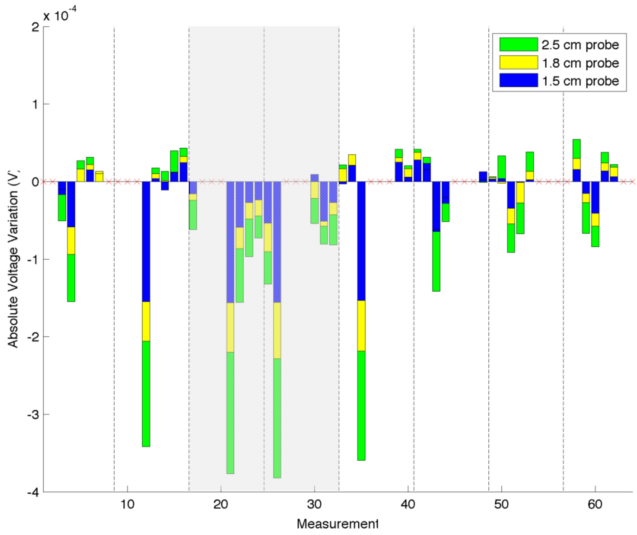

Fig. 5.7: Difference in electric potentials measured when different probes are placed in the region facing electrode 4 (E4). The probes have different size, while the applied force is kept constant. As in the previous image, the shaded regions correspond to E4 acting as driving electrode.

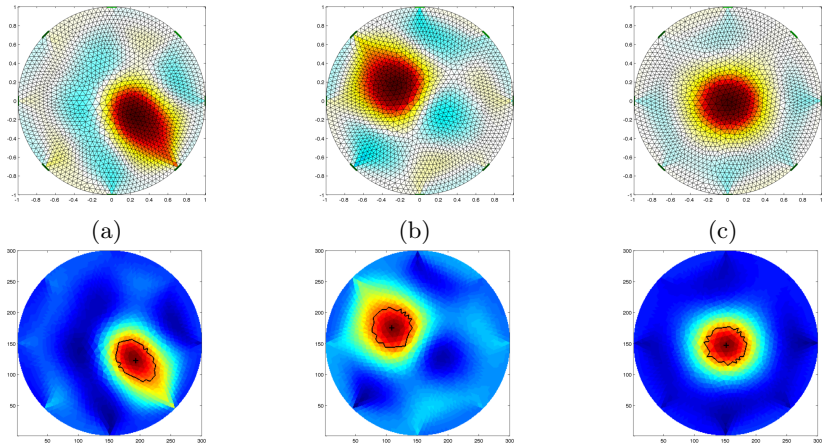

Fig. 5.8: Reconstructed conductivity map of different stimuli applied over the artificial skin by a circular head probe of 18mm radius. The probe was placed (a) between electrodes E3 and E4, (b) between electrodes E7 and E8, (c) in the centre of the sensing area. Figures (d), (e) and (f) show the processed data respectively of figures (a), (b), and (c). In each of the processed images, the centre and the computed boundary of the detected inhomogeneity are shown.

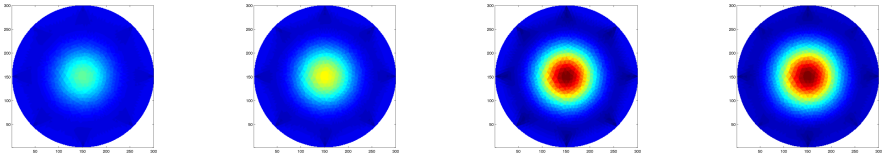

(a) (b) (c) (d)

Fig. 5.9: Reconstructed images as a function of different probes applied at the centre of the artificial skin. The results provided are respectively for: (a) a circular probe with 15 mm radius, (b) a circular probe with 18 mm radius, (c) a circular probe with 25 mm radius, and (d) a square probe with a side of 15 mm. Due to the low resolution of the system, it is not possible to clearly discriminate between the different shapes. Nevertheless the change in the probe size can be easily identified.

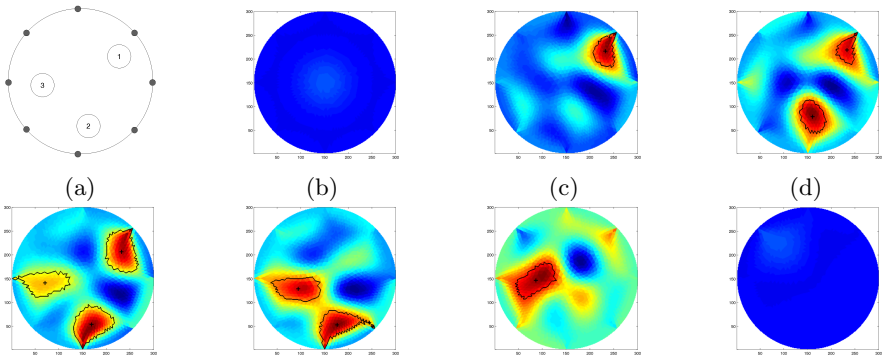

(a) (b) (c) (d)

(e) (f) (g) (h)

Fig. 5.10: Selected frames in the multi-pressure experiment. (a) Probes positions, (b) reference voltage, (c)-(e) sequential load and (f)-(h) unload of the different probes. In each frame, for each probe, its centroid and the computed boundaries are shown.

detected as a consequence of the position and the interaction of the electrodes. In addition, the artificial skin shows some hysteresis after the removal of all the probes. This can be caused by the partial detachment of the conductive textile from its substrate, and by the change of conductivity of the sensing layer as a consequence of the applied forces.

5.3.5 Application over Curved Surface

The last series of experiments was carried out to prove the adaptability of the artificial skin to conform to different geometries while maintaining its sensing property. Furthermore, is also possible to test the efficiency in determining changes in shape (e.g. bending) due to the application of the artificial skin over different geometries and comparing the acquired electric potentials with the ones acquired over a flat

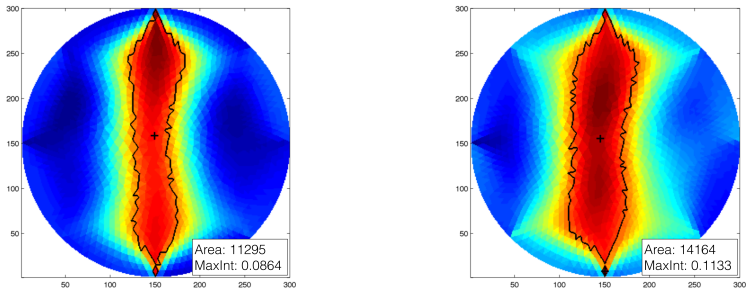

(a) (b)

Fig. 5.11:]
Results of the application of the artificial skin over a curved surface. The reconstructed conductivity map was generated by using as reference the measurements taken over a flat surface with no load acting over the artificial skin. In this experiment we used two polyethylene foam extruded cylinders with diameters of (a) 40 mm, and (b) 70 mm. As the results suggest, as the diameter of the underlying object increases, the maximum intensity and the area of the detected inhomogeneity increase.

surface. In this section we present the results obtained after the application of the artificial skin over different curved and deformable objects.

As initial test, we placed the artificial skin over a flat surface and then took a series of voltage potential measurements. With those values stored as a reference, we placed the artificial skin over different cylindrical objects—two polyethylene foam extruded cylinders—with a radius of 40 mm and 70 mm, respectively. The two cylinders were then placed over a flat surface in order to provide sufficient support, and avoid their bending. Due to the presence of the foam substrate, and the small size of the underlying object, the artificial skin could not conform perfectly to it. Thus, in order to fully cover the cylindrical object, we kept the two free sides of the artificial skin together by means of a plastic strip. In such configuration, we performed the electric potentials measurements. Figures 5.11a and 5.11b show the results for the two different cylinders respectively. The reconstructed conductivity maps presented in the two figures show a different behaviour compared to the one shown in the previous experiments. In fact, instead of having a ellipsoidal region, this type of deformation produces a more elongated shapes. By comparing the images in Figure 5.11, it is possible to notice a slight change both in the maximum value detected, and in the computed deformation area—obtained as in the previous cases by thresholding the reconstructed map. This information can be used as clue to discriminate between different type of deformations applied to the artificial skin.

Following the results obtained in the first part of the trials, we further tested the artificial skin capability to sense pressure when placed on curved geometries. We evaluate such property on the following objects: a 70 mm radius cylinder (deformable), the back of a chair (soft substrate), and a mannequin arms with circumference of 30 mm and a total length of 295 mm. Before proceeding with the measurements, we firmly attached the artificial skin to the underlying object to limit the error in the reconstruction due to changes in the electrode positioning.

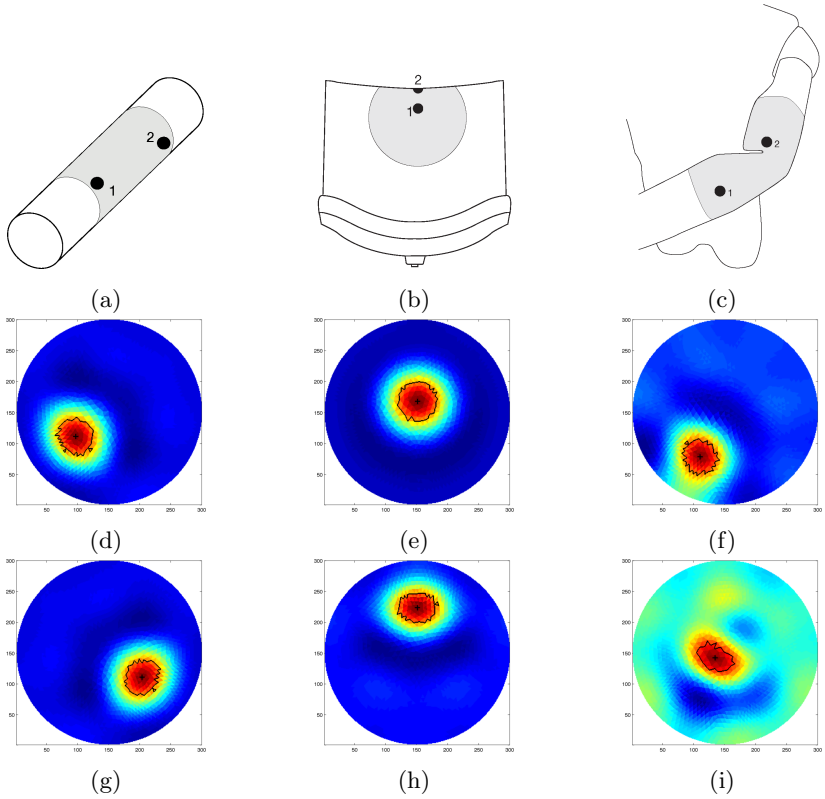

Fig. 5.12: Example of conductivity map reconstruction over different geometries, results are grouped by column. First column (a, d, g) experimental setup and results when applied to a 70 mm radius cylinder (deformable). Second column (b, e, h) experimental setup and results when applied to the back of a chair (soft substrate). Third column (c, e, i) experimental setup and results when applied to a mannequin arms with circumference of 30 mm (bendable). Results are ordered according to the number shown in their relative experiment setup. The last row of the Figure shows measurements performed when the probe was applied to the most curved area (g, h), and when the joint angle of the mannequin arm was changed (i). For each case, the results are obtained by applying a circular shape probe with 18 mm of radius.

Where the object was not able to support itself, i.e. in the polyethylene foam extruded cylinder case, we placed the object of a flat surface during the whole test. We limit the experiments to a single probe of circular section of 18 mm radius. Differently from the precious cases, reference measurements were taken after attaching the artificial skin on the curved surface. Results for each configuration are shown in Figure 5.12. As the images suggest, the artificial skin can provide similar results as the ones shown in previous cases even under large deformations.

5.4 Summary and Conclusions

This chapter presents the experimental setup, the experimental protocol, and the results obtained during the evaluation of the performance of the developed system. It has been tested in different configuration spanning from data acquisition to test the basic measurement protocols, to the application of the sensor on flat and curved surfaces to prove its adaptability, and the robustness of the method.

A first series of experiments was performed to characterise the behaviour of the system by using the conductive textile presented in the previous chapter. Eight electrodes have been attached to the conductive textile and current was injected sequentially at each electrode while the output of an arbitrary chosen electrode was directly monitored and acquired with Matlab. The value obtained were used to evaluate the variability of the measurements within readings, and as reference for later phases.

To evaluate the capabilities of the system to detect changes in the conductivity over the surface, we placed the textile-based conductive skin over a flat surface, and applied a constant force by the means of a single probe to the region directly facing each electrodes. The test were performed using different probe shape, and size while the applied force remained constant. The measured values showed a common behaviour when grouped by what electrode was used as current sink in a adjacent pattern stimulation. The maximum and minimum variation, in fact, can be found when the electrodes carrying electrical current are close to the one in which proximity the probe was acting.

Following the results provided in the previous tests, we further investigate the capabilities of the system in detecting single and multiple events that occur sequentially and simultaneously. In this series of experiments, the sensor has been placed on a flat surface and different probes were applied to different region of the sensor. For the single probe cases, the system was able to identify the location of the applied stimulus but the returned shape was not very precise, especially when the probe was placed closer to the edge of the sensor and to the attached electrodes. In these areas, the shape of the reconstructed inhomogeneity is elongated and not circular as expected. The reason of this result can be traced back to the fact that the applied forces did not deform only locally but also on the surroundings, and the electrodes used interact with these by additionally stretching the textile. A different limitation can be identified, instead, in the results obtained in the multi-probe tests. Despite the fact the system was able to detect all the probes when acting independently and simultaneously, in order to identify the third probe acting on the sensor we had to reduce the initial threshold used to identify the peaks of the inhomogeneities. The reason why the system did not perform correctly by the use of the common threshold was traced back to the low resolution of the technique and by the fact that most of the electrodes were covered by the other two. It was confirmed by the fact that by removing one of the probes, the third probe was correctly detected.

The last series of experiments had the aim to prove the adaptability of the sensor over different geometries and to detect changes in the underlying structure. To do this we investigate two different scenarios in which the experimental setup was kept identical as in the previous cases. In the first scenario, the reference mea-

surements were taken when the sensor was placed over a flat surface, and then it was wrapped around two different cylindrical structures. When compared to previous results, the ones obtained following this protocol showed a different structure. Instead of a well-localised circular structure, as in the case of single or multi-probe experiments, it is more elongated and cover the whole domain. With the increase of the bending angle, the area of the detected inhomogeneity and its maximum value change. This information can be used to identify between different events and the amount of deformation. In the second scenario, we placed the textile-based sensor over different geometries. For each of them, reference measurements were taken when the sensor was already in position. To prove the adaptability of the technique to different geometries, we repeated the indentation tests in each configuration. The results showed that by acquiring the reference measurements when the sensor already paced over the geometry allows to neglect the changes in the sensor configuration and thus maintain its functionalities.

In the next chapter, we will present possible application scenarios for the developed sensor. For each of them we will introduce the experimental setup, the protocol used, and the results obtained by applying the EIT technique on the textile-based sensor.

6

Applications for an Adaptable Soft Sensor

6.1 Introduction

In the previous chapter we presented a series of experiments and results that gave an insights of the developed EIT system and its application over the conductive textile substrate. In these experiments, the system's performance and its limitations were tested in different configurations designed to provide specific results on distinct situations, and were not focused on practical applications. In this chapter, instead, we will extend the investigation from simple scenarios to more complex ones by considering possible applications in which and EIT-based adaptable soft sensor can be used.

Two different scenarios will be considered in this chapter: i) the use of EIT in medical applications to detect inhomogeneities within a soft body, and ii) the use of EIT to detect and measure deformation. In the first case, the combination of the imaging technique applied to the conductive substrate allows to extend is functionalities also from functional monitoring—i.e. patient ventilation—and bio-impedance analysis—i.e. tissue discrimination—to mechanical imaging and remote palpation. In the second scenario, instead, we continued the experiments carried out on the deformable cylinder and on the bendable arm presented in the previous chapter. With these experiments we wanted to focus the attention on the detection and evaluation of the changes in the underlying structure, a feature that is needed for the development of a dedicated sensor for soft robots. For each case, the aim of the experiment, its experimental setup and protocol, results, and discussion will be provided.

6.2 Sensing within Soft Bodies

Manual palpation is still one of the most important screening process in the medical field. By its means, doctors can infer information of the examined area—such as resistance, resilience, roughness, temperature, moisture, texture, mobility—and thus identify possible pathologies. In fact, human tissues present a different range of movements when inhomogeneities, such as lesions or tumours, are present [57].

Different techniques for screening have been developed but in addition to the fact that they use sophisticated hardware such as superconductive magnets, expensive X-ray equipment and complex ultrasonic phased arrays, it is not always possible to retrieve the mechanical properties of the domain under study. For this reason, a different imaging modality has been developed to translates the sense of touch into a digital image; this is known as tactile imaging [40, 121]. Mechanical imaging is an imaging modality of medical diagnostics based on reconstruction of tissue structure and viscoelastic properties using mechanical sensors [121]. The tactile image is a function of the applied pressure on soft tissue surface, and the reaction force measured in a specific point. Tactile imaging closely mimics manual palpation, since the probe of the device acts similar to human fingers during clinical examination. By deforming the soft tissue it is possible to detect changes in the pressure pattern. The changes in the tissue stiffness provide a means for characterising it, and to detect tumours and other lesions.

EIT found its main application in the medical field since its early stage. Now it is an established technique to sample and recognise biological tissues by using the information such as conductivity and permittivity [122] which change according to tissue's state of health, and during the normal functioning of the organ. The property has been studied and now, it can be applied locally to detect the presence of tumours in the mammary glands and in the subcutaneous tissue [20, 70, 138]. Similarly to other tomographic techniques, EIT can not provide mechanical information per se. By applying a conductive layer that changes conductivity when a pressure is applied it is possible to extend the functionalities of the EIT system. In this configuration, and by using an approach similar to one used in elastography [150], it is possible to discriminate between stiff and hard substrates. The main idea is that whether the tissue is hard or soft will give diagnostic information about the presence or status of disease. For example, cancerous tumours will often be harder than the surrounding tissue, and diseased livers are stiffer than healthy ones.

With this aim in mind, a first series of experiments was carried out to provide an insight on the feasibility of using an EIT for mechanical imaging. In order to provide such capability, a conductive textile was places over a soft deformable domain within which stiffer elements have been placed. The imaging processing remains the same as in the previous experiments, but the detected elements are a function of the applied pressure on soft tissue surface, and the reaction forces measured over the domain.

6.2.1 Experimental Setup and Protocol

As previously mentioned, in order to allow an EIT system to provide mechanical imaging, the pressure map should be converted into changes of conductivity over the domain. The developed hardware and its application over the conductive textile layer already offer this capability. For this reason, during the experiments presented in this section the hardware configuration, the conductive material, and the injected current (100 mA) remain the same as in previous cases. However, in order to simulate the structure of a soft organ, we developed a simple phantom in which it is possible to place different elements that can be used to simulate the presence of tumours or lesions.

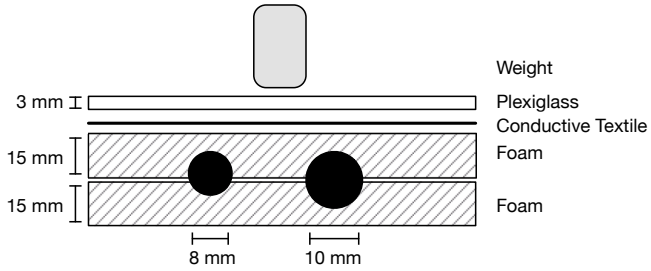

Fig. 6.1: A schematic representation of the experimental setup. Two rigid bodies were placed within the soft phantom to simulate the presence of tumours.

The phantom consisted of two distinct layers of foam (100x100x15 mm^3) within which two medium-size spheres made of stiff rubber have been placed. The top layer was then covered with a square-cut conductive textile (100x100 mm^2) that was then connected to the EIT system. To reconstruct the tactile image in a single measurement, a homogenous pressure over the whole domain was needed. This was achieved by positioning a rigid layer (90x90x3 mm^3) over the conductive textile, and then by applying a fixed weight over the rigid structure. Figure 6.1 shows the schematic representation of the described experimental setup.

Before attempting direct measurements over the experimental setup, various simulations were performed to select the optimal parameters to be used in the different phases of the data acquisition process. Once the parameters were set, the measuring system was connected to the conductive textile that covered the soft body. To reduce the possible effect of artefacts in the reconstructed images, the adjacent pattern was used in the current injection and voltage acquisition phases.

With this configuration, reference measurements were acquired when no force was applied over the rigid substrate, while later measurements were taken when the weight was positioned over it. A constant force of 2 N was applied and as a consequence, the underlying soft structure deformed. On the countrary, the stiff components did not deform and as a consequence they produced a measurable reaction force on the conductive textile that locally changed its resistance.

In the data processing phase, part of the boundary data was removed. It was necessary to remove the effects produced by the interaction of the stiff layer over the conductive textile. In fact, since it was not covering the while layer, its sharp edges interacted with the textile and produced changes in the conductivity. A part from this post-processing, the data was processed as in previous cases.

6.2.2 Results and Discussion

Initial tests were performed with the previously described setup to understand possible limitations. Two series of tests related to the spatial resolution were performed. In the first, we investigated the capability of the system to discriminate different size of inhomogeneity. In the second, the minimum distance between two elements was investigated. Results are presented in Figure 6.2 and Figure 6.3 respectively. As the results suggest, the system can correctly identify elements with

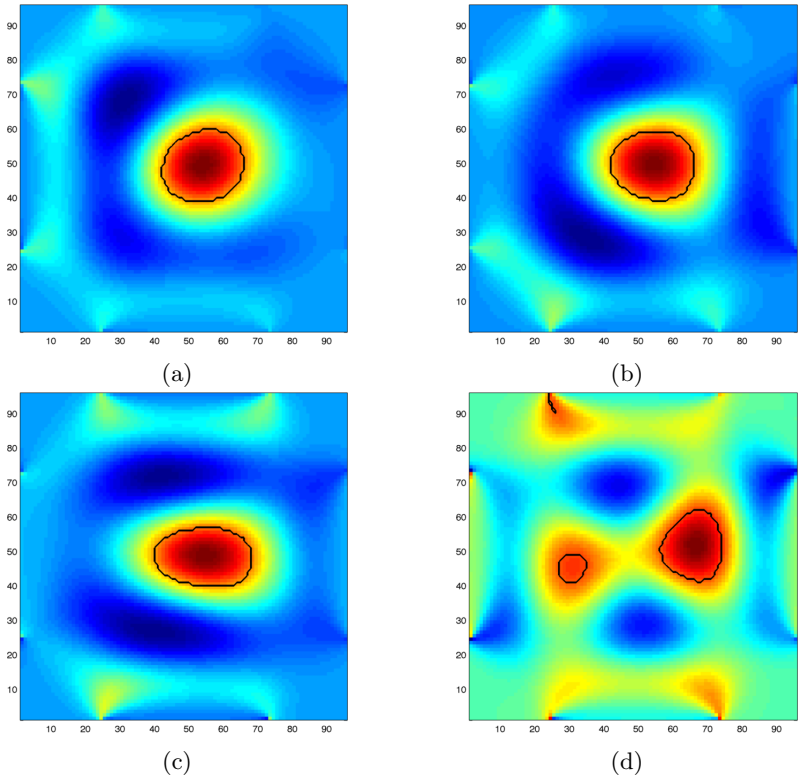

Fig. 6.2: Experimental results obtained by testing different size of inhomogeneity. (a-d) the reconstructed images of elements of 10 mm, 8 mm, 7 mm, and 6 mm radius respectively. By keeping fixed the parameters, the reconstructed image of elements with radii lower than 6 mm contains artefacts.

size larger than 8mm radius, and placed at least 20 mm apart. For lower sizes the system was not able to distinguish the element from the background noise, while if placed closer than the minimal distance the two elements were merged in a single structure.

With the system limits set, we proceeded with a series of tests in which two inhomogeneities of different sizes were placed within the soft structure. Figure 6.4(a) shows the results obtained in the case in which two stiff objects of 10 mm and 7 mm radii, respectively, are used to simulate the presence of tumours. A simplified representation is presented in Figure 6.4(b). The image was obtained by thresholding with respect to the maximum value detected over the single element. This can be used to provide a more clear portrayal of the situation, or as a tactile map for remote sensing.

Even if the system was able to correctly identify the location and the relative size of the elements used in the experiments, it shows some limitations. Among these, the spatial resolution is one of the most prominent. In most cases lesion and tumours have a size lower than the one that is currently detectable by the

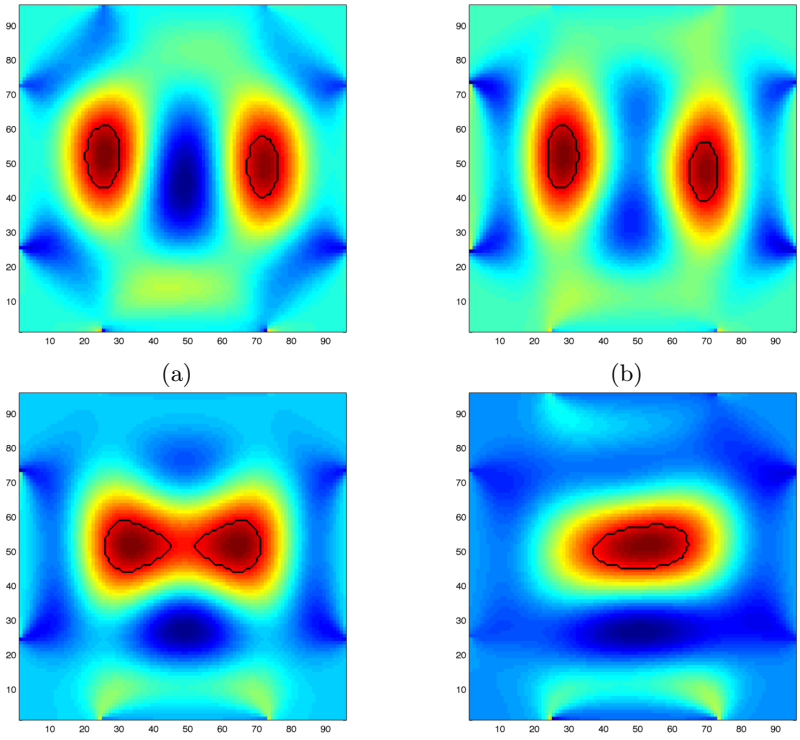

Fig. 6.3: Experimental results obtained by testing different distances between two elements of 10 mm radius. (a-d) the reconstructed images of inhomogeneities with relative distance of 50 mm, 40 mm, 30 mm, and 20 mm respectively. When the distance between elements reach the 20 mm, it is not possible to correctly distinguish them, and the system identify them as a single structure.

system, and an increase in the resolution is needed to clearly identify them. It is possible to combine the technique with other imaging modalities in order to overcome this limitation. Additional limitations can come when a more realistic scenario is considered since the presence of internal structures can interfere with the reconstruction process, or hide the presence of elements beneath them. This limitation is shared with other tactile imaging technique since these can perform only in the subcutaneous region. Some improvement should be considered in order to apply the technique to real scenarios. Electrical current should be reduced to ensure safety for the patient and a different material should be used as conductive substrate to enable the sterilisation process.

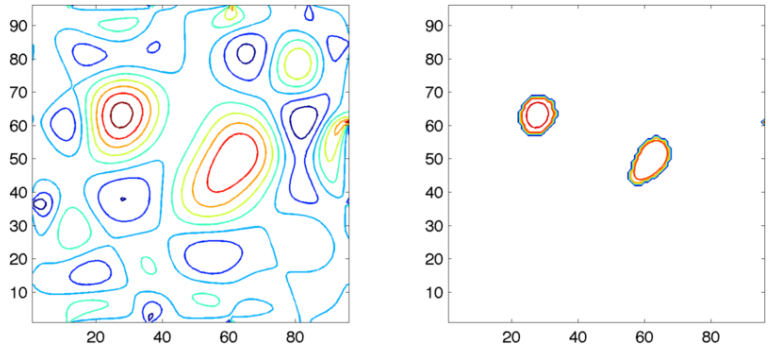

Fig. 6.4: Results of the proposed method presented as contour map. (a) Reconstructed image. (b) Region having intensity value more than 75% of the maximum value detected in each region. These regions represent the tumours inside the sensed object.

6.3 Sensing Structural Changes of a Deformable Body

EIT is not only an imaging modality used in the medical field but, as introduced in sections 2.4 and 3.2, it has also been used in other fields such as geophysical exploration, industrial applications, and most recently for robotic systems. In the latter case, EIT has been used as an adaptable sensitive skin able to detect forces applied over the rigid structure of the robot. As shown in the previous chapter, by properly selecting reference measurements, it is possible to detect changes in the underlying geometry (e.g. change in the bending radius), or neglect them and thus let the imaging technique adapt to different surfaces while maintaining its sensitivity.

The ability to detect and adapt to changes of the underlying structure is a property that makes EIT a suitable technique not only for traditional robotic applications, but also for the soft robotics domain. In fact, soft robots can deform under the effect of external forces, but at the same time these devices can absorb and distribute the forces over the whole body. With traditional sensors it is possible to measure forces applied directly on or in their proximity, and as a consequence it is not always possible to identify events that occur over the whole robotic structure. A possible solution is the use of matrix-based distributed sensing, but the main issue remains the stiffening of the robotic structure due to the sensor architecture. The use of EIT does not totally overcome the latter limitation, in fact, even if the sensing layer is deformable and can easily adapt according to the needs, the electrodes should be fixed in position, and the driving/readout electronics is made of rigid material. The issue can be overcome by the use of flexible material for the developing of the hardware, and by placing it in a specific location where it minimally effects the deformability of the robotic structure.

In order to prove the feasibility of using EIT in a soft robotic application, we extended the experiments presented in section 5.3.5. We designed a series of experiments with the aim to test the sensor capability to adapt to the structure over which it was placed. The sensor should follow the structure deformations,

and should detect and differentiate the events that occur independently over the sensorized surface. As support structure for the sensor, a continuos deformable foam-made cylinder was used. The size of the structure chosen is larger than the size of current soft robots, but it has been chosen accordingly to the resolution capabilities of the available EIT sensor.

6.3.1 Experimental Setup and Protocol

Experiments were carried out on a setup similar to the one used in the tests presented in section 5.3.5. The support structure for the sensing layer was a continuos deformable foam-made cylinder of 62 mm diameter and 865 mm in length. The cylinder was partially covered with a square-cut conductive textile (100x100 mm^2) that was then firmly fixed to it to avoid any movement of the electrodes during the measurements. This is an important factor since any change in the electrode position can create artefacts and errors in the reconstructed image. The system was then connected to the EIT electronics via rigid wires. As in all the experiments presented so far, the hardware configuration, the current injected, and the pattern used for the measurements remained unchanged.

With the experimental setup, we tested the capability of the system to detect multiple touching points over the surface and deformations such as bending. In this last test, we could evaluate the system only over a single bending location due to the material stiffness that limited local deformations, and due to limitations of the sensor size. As in the previous cases, before attempting direct measurements, various simulations were performed to select the optimal parameters to be used in the different phases of the data acquisition process. Once the parameters were set, the measuring system was connected to the conductive textile.

During all the experiments experimental setup was placed over a flat, rigid surface. In order to neglect the effects due to changes in the reference measurements, we acquired both the reference measurement and the later ones when the textile was already placed around the cylindrical structure. The choice allowed to detect applied forces, and to identify changes in the configuration of the experimental setup with respect to the initial one.

Once the experimental setup was put in place, a constant force of 2 N was applied over two locations of the sensing surface with a relative distance larger than the one needed to correctly identify two independent event (i.e. 20 mm). As indenter, we used two identical circular probes (30 mm diameter) over which the force was separately applied. The experiment then continued with the deformation tests. The setup was left over the flat surface and was manually bent while holding its extremes. The conductive textile, placed in the central part of the cylinder, consequentially stretched. In this case, potential measurements were acquired when the structure was in its reference position, and right after the bending was completed. In these experiments we were not directly interested in measuring the bending angle of the structure, but we were more focused in proving the capability of the system in discriminating between different events that may occur over the surface.

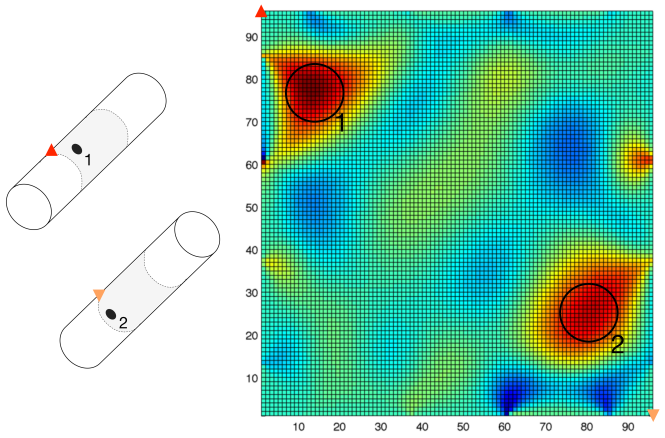

Fig. 6.5: Multi-touch detection. Left: contact points over the conductive textile. Right: reconstructed conductivity map according to the changes produced by the direct contact on the surface

6.3.2 Results and Discussion

This section presents the results obtained by applying, independently, normal forces and by deforming the experimental setup just introduced. In each configuration, reference measurements were taken when the sensor was placed and fixed over the deformable cylinder. To ensure repeatability of the results, for each scenario we acquired ten distinct measurements and processed them independently. Figures 6.5 and 6.6 show the results obtained in the two scenarios, respectively. As the results suggest all the events were correctly identified.

As in the previous cases, when the detection of normal forces was considered (Figure 6.5), the system was able to identify the presence and locations of each of the applied forces. More interesting results were obtained in the experiments related to the detection of applied deformations. Figure 6.6 presents the reconstructed image obtained after bending the foam-made cylinder into a u-shape by its extremes. As it is possible to notice, the structure of the detected inhomogeneity assumed a different shape when compared to the structure obtained when a normal force was applied to the surface. Instead of having a slightly elongated circular shape well localised around the pressure area, the inhomogeneity reconstructed as a consequence of the applied deformation has a more elongated shape that covers large portion of the sensing area. By analysing the properties of the extracted inhomogeneity it is possible to identify features that allow to discriminate between the different events.

Even if the results are promising, it is important to consider possible limitations related to this simple classification method. As shown in previous results, the method suffers from drawbacks when spatial resolution is taken into consideration. In fact, if two or more independent events—such as normal forces—are acting simultaneously over the sensitive area with relative distance lower than the one needed to clearly discriminate between events, the system cannot properly identify

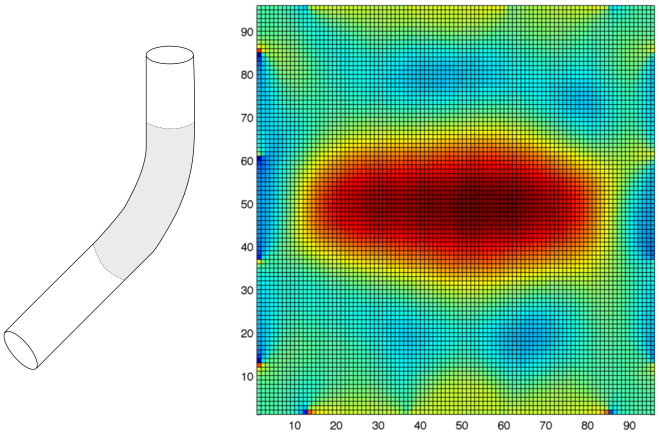

Fig. 6.6: Deformation identification. The red area indicates where the stretching of the textile occurred. During the experiments almost the whole area covered by the skin was subjected to the bending.

them. In fact, these events are detected as a single event that spreads across the area detected by the sensor. As a consequence, this reading will generate a misclassification of the inhomogeneity that will be identified as a deformation due to changes in the structure' shape and not as two separated events.

6.4 Angle Measurement Detection

In order to use the EIT-based sensor to measure deformation, it is fundamental to characterise the results with known values provided by external references. In this section, we will extend the results obtained in the previous section, and describe the system capability to detect and estimate the amount of specific types of deformation. In particular, we are interested in detecting the amount of internal forces produced as consequence of the bending of a joint. The combination of this feature, with the ones already presented can be beneficial when applied to rigid robotic links, and when soft deformable devices are considered.

The use of EIT as transduction method, when compared to other sensing mechanisms, allows the portability of the method without the need of a precise geometrical model, and to adapt the sensor architecture to the different structures. In addition, since the returned information is continuous and distributed over the whole sensing area, it is possible not only to obtain data about events that occur directly beneath or on the sensor, but also in its proximity. This feature is favourable especially in the soft robotic domain where a deformation that occurs in one part of the device can propagate along the whole body.

During this series of experiments, we used EIT imaging technique with a conductive textile that was wrapped around a semi-rigid mannequin arm that could bend and keep the position once set in place. The arm could bend around a single

Fig. 6.7: Experimental setup. The sensor was placed over a dummy arm that can bend and kept in position. We tested the capabilities of the sensing system to distinguish between different angles.

point (two link joint) over which we performed all the measurements. The choice in using a semi-rigid arm instead of a deformable one, like in the previous scenario, was motivated by the previous results related to the detection of the bending region. In those results, even if the area effected by the deformation was clearly identified, it did not have a uniform structure that made the results difficult to analyse and to understand. With the use of a more rigid structure, instead, the results were clearer and easier to be analysed.

6.4.1 Experimental Setup and Protocol

The experimental setup used in this series of measurements was similar to the one adopted in the previous tests. It consisted in a layer of conductive textile (250x150 mm^2) that was wrapped around a dummy arm (diameter 30 mm, total length 295 mm). The arm could be bent continuously between 0° and 90°, and once placed in position it could keep the desired angle. In order not to let the electrodes move during the experiments, the stretchable textile was firmly attached to the structure when the arm was fully extended. Figure 6.7 shows a close up of the sensor applied over the mannequin arm.

In this series of experiments, we were interested in detecting events that were directly applied over the sensitive layer from which EIT image was extracted. For this reason, as in previous cases, we applied directly the conductive textile over the semi-rigid supporting structure without the use of an additional layer. Previously, this layer was used to insulate the conductive substrate form the underlying structure, and to better distribute normal forces locally and to create smooth results in the reconstructed images. The use of the same layer in this situation might have

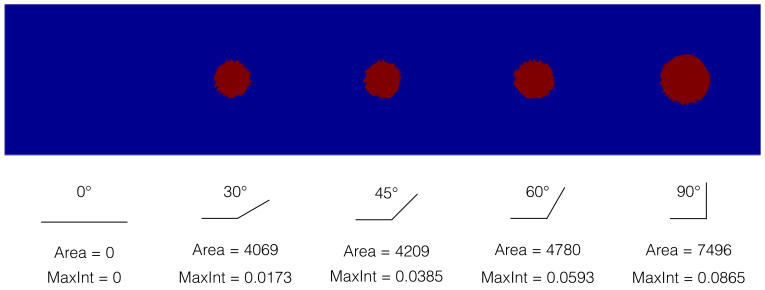

Fig. 6.8: Results obtained on a single bending area. For each angle the region of interest was extracted by considering the pixel having intensity greater or equal to 75% of the image maximum value. Area of the ROI, and the maximum intensity value of the image are also reported.

reduced the range of movement of the mannequin arm, and could have limited the detection of the applied forces.

The mannequin used in the experiment had two arms with two links each that could be bent around a single axis. Reference measurements were acquired when the arm was fully extended, then we tested the system by varying the bending angle from 0° to 90° with incremental steps of 15° each. For each of the measured angles, we performed a full cycle of EIT voltage acquisitions, and then the data was processed using Matlab. Processing consisted in reconstructing the conductivity map associated to the inverse EIT problem, and then the extraction of a region of interest (ROI) located around the elbow area of the mannequin. The ROI was identified by first cropping a circular region of the returned image around the area of interest, and then by thresholding the pixels value. As threshold value we used 75% of the maximum value identified on the conductivity map. The number of pixel contained inside the ROI (i.e. its area), and the maximum value detected over it were used to identify a specific angle.

6.4.2 Results and Discussion

The arm of the mannequin was bent following the experimental protocol described in the previous section, and post-processing was applied to the reconstructed conductivity map. For each configuration, the maximum value detected and the area of the ROI were extracted. To prove repeatability in the measurements, we did the data acquisition ten times. Figure 6.8 shows the results of this process for selected angles.

The area extracted from the processes ROI of each angle configuration was stored and used to fit a curve (5^{th} order polynomial) that was used to characterise the sensor readings. The curve is plotted in Figure 6.9. As the results suggest, with the increase of the bending angle, the area of region of interest increases. A similar trend can also be identified when the maximum intensity value is considered. These results can be explained with the fact that wider angles generate a stronger push of the underlying structure towards the conductive textile. As a consequence, the

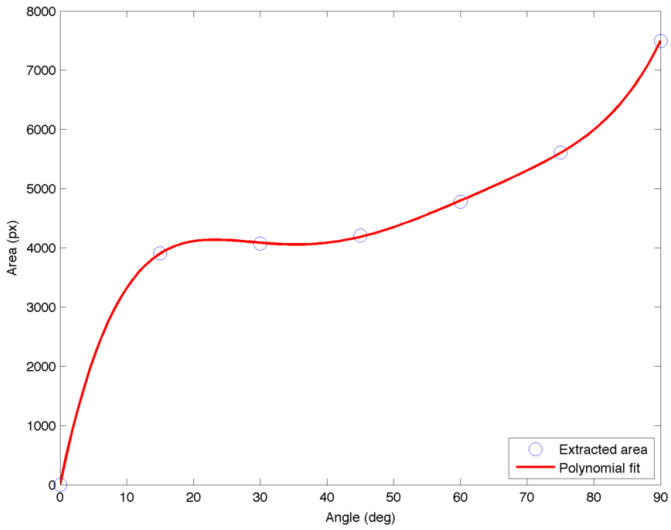

Fig. 6.9: A 5^{th} order polynomial fit of the data. Angles lower than 15° do not provide reliable values due to a limitation of the conductivity map reconstruction algorithm.

conductive textile stretches and thus changes its conductivity in the area where the force is applied by the arm joint.

The system was not able to detect deformation created by angles lower than 15°. The cause was found in the fact that the mannequin arm did not apply forces sufficient enough to stretch the textile, and create detectable changes in its conductivity. Additionally, between each steps, the variation between the maximum detected value and, as consequence, the extracted area had a non-linear trend. This was due to the property of the conductive textile used that from the early characterisation phase showed a non-linear change in the resistivity when stretched. Despite this, using the relationship between the area and the angle, it was possible to derive the simple calibration rule shown in Figure 6.9. To prove the robustness of the fitting, a second series of measurements was carried out and the results were compared with the model. Due to fluctuation in the numerical value of the reconstructed images, the approach was able to correctly identify the bending angle with an error of ±5°.

6.5 Summary and Conclusions

This chapter presented a series of experiments that extended the results obtained in the previous chapter to offer possible application scenarios in which EIT-based adaptable soft sensor can be used. Two situations were considered: i) the use of EIT as pressure imaging, and ii) the use of the textile-based system to detect deformations that occur over deformable continuum soft devices. With the second case, we further investigate the capabilities of the system in detecting and evaluating

the amount of deformation. For each considered configuration, the experimental scenario and protocol were presented together with the respective results.

The first series of experiments was carried out to provide an insight on the feasibility of using an EIT for mechanical imaging. In order to provide such capability, a conductive textile was placed over a soft deformable domain within which stiffer elements have been placed. To reconstruct the tactile image in a single measurement, a homogenous pressure over the whole domain was applied. This was achieved by positioning a rigid layer over the conductive textile, and then by applying a fixed weight over the rigid structure. To reduce the effect of the noise that was created in correspondence of the sharp edges of the stiff layer, part of the boundary data was removed. The system was then tested to identify its limits in spatial resolution, after which a series of additional tests were performed. Even if the system was able to correctly identify the location and the relative size of the elements used in the experiments, it showed some limitation when the objects used to simulate the presence of tumours were too small (size lower than 7 mm) or placed too close to each other (relative distance lower than 20 mm).

A second series of experiments was performed to prove the feasibility of using EIT in a soft robotic application as an extension of the experiment carried out in section 5.3.5. The experimental setup consisted of a continuos deformable foam-made cylinder that was partially covered with a square-cut conductive textile firmly attached to the structure to avoid any movement of the electrodes during the measurements. With the experimental setup, we tested the capability of the system to detect multiple touching points over the surface and deformations such as bending. The provided results show that all the different events were correctly identified both in the case of applied external forces, and when the the foam-made cylinder was bent into a u-shape by its extremes. The results suggested that it is possible to discriminate between these two events by simply comparing the structure and the area of the returned inhomogeneities. Despite this, the method suffers from drawbacks when spatial resolution is taken into consideration. In fact, if two or more independent events—such as normal forces—are acting simultaneously over the sensitive area with relative distance lower than the one needed to clearly discriminate between events, the system can not properly identify them.

The last series of experiments was carried out to characterise the measurements obtained with the proposed method with known value provided by external references. This feature is needed in case the system would be used to measure deformations. The use of EIT as transduction method, when compared to other sensing mechanisms, allows the portability of the method without the need of a precise geometrical model, and to adapt the sensor architecture to the different structures. To do this, we applied EIT imaging technique to a conductive textile that was wrapped around a semi-rigid mannequin arm that could bend and keep the position once set in place. The arm could bend around a single axis over which we performed all the measurements. We tested the system by varying the bending angle from 0° to 90° with incremental steps of 15° each. As the results show, with the increase of the bending angle, the area of region of interest increases. A similar trend can be also identified when the maximum intensity value is considered. By using such value it was possible to fit a calibration curve to the data, and used to calibrate the sensor readings. The fitting was further tested with an other series of

measurements that, due to fluctuation in the numerical values of the reconstructed images, could identify the bending angle with an error smaller than the resolution step.

7

Characterisation of a Flexible Sensor for Continuum Soft-Bodied Robot

7.1 Introduction

In this chapter, we will present the experimental results obtained by applying the EIT imaging method to a continuum soft-Bodied domain. This, as described in section 4.5.2, is structured as a layer of conductive stretchable material—a mixture of silicon and carbon fibres—incapsulated between two non conductive silicon layers. The use of such structure allows to develop conductive and stretchable domains of any desired shape, and thanks to the use of the same material of which soft-robotic devices are made, is an easy embedment into such devices.

During the development phase, different shapes and sizes have been investigated in order to prove the adaptability of the method to different situations. Despite this, in this chapter we will describe the experiments carried out with only one of them. We opted for a cylindrical shape for the three-dimensional domain since it offers a symmetric three-dimensional shape that is a direct extension of the shape used in the two-dimensional case (i.e. circle), and that can be easily generalised to different soft robotics applications (e.g. robot's link). The cylindrical conductive domain was then used in combination with the developed EIT imaging system and tested under different conditions. In the specific, we tested the system's adaptability in detecting events such as elongation and bending of the sensor, features that are fundamental for the development of a dedicated sensor for soft robotic devices. For each case, the experimental scenario and protocol will be provided together with the respective results. To prove the correctness of the experimental results, we will also provide FEM simulations.

7.2 Experimental Evaluation

In this section we will present the experimental setup and protocol used to evaluate the performance of the EIT system when applied to a continuum, deformable, three-dimensional domain. The use of such domain as conductive layer allowed evaluating the proposed method in situations where the sensor is not just a part of the robotic system—e.g. attached to the surface, or embedded in pre-defined sections of the robot—but it constitutes the body itself of the robot. This feature

can be beneficial in the soft robotics domain since it allows applying distributed sensing without the need of many localised sensor that may interfere with the robot motion.

Starting from this consideration, we tested the capability of the system in detecting two common events that can occur in a soft robotic application: i) elongation of the link, and ii) its bending. Both experiments were carried out using a soft cylinder made of conductive silicon covered by a thin insulation layer. Earlier tests showed that there was no need of an addition insulation since the conductive mixture was not subject to external electromagnetic noise. The choice of adding it to the final structure was to recreate a possible situation where the sensor is placed within the robot body.

Once the EIT system is connected to the three-dimensional domain, it is important to implement the correct strategy to capture the morphological information. Most of the work that has been done with EIT has used only a single band of electrodes to produce two-dimensional images. When applied to the three-dimensional case, this approach limits the versatility and the effectiveness of the technology since it is unable to observe changes in a volume, and also assumes that the path of the electric field is in a plane rather then a volume. It is possible to expand the use of EIT to three-dimensional application, however there are challenges to overcome before it is possible. The main drawback is the computational complexity, but the use of dedicated algorithm and fast processing speed overcame the issue [2]. An additional challenge consists in the proper evaluation of the various electrode placement and stimulation patterns. In fact, the selection of the stimulation and measurement pattern for 3D EIT imaging have a strong influence on the resulting image. In a two-dimensional measurement pattern, all stimulations and measurements are taken on a single plane. In a three-dimensional measurement pattern, instead, there can be a mix of horizontal, vertical, and diagonal measurements. There have been several studies involving the analysis of measurement protocols for 3D EIT. Undoubtedly, the approach highly depends on the application and the domain under study.

7.2.1 Array of Electrodes

The basic layout for electrode placement configurations in three-dimensional EIT consists of 2 concentric rings placed around the domain. The electrodes in the two rings can be lined up or offset around the whole external surface of the domain. Common patterns such as *planar*, *planar-offset*, *planar-opposite*, *zigzag*, *zigzag-offset*, *zigzag-opposite*, and *square* [53, 148] are specific to a 2 layers, 16 electrode EIT system having 8 electrodes per layer. The *offset* configuration has the electrodes of the second layer offset from the first layer by half of the horizontal electrode separation. Figure 7.1 shows an example for some of the cited pattern.

In [53] the patterns' results have been analysed based on a number of criteria and several conclusions have been made.

1. Either of the *opposite* pattern was highly susceptible to noise and thus not recommended.
2. The *zigzag* patterns performs poorly under noisy conditions.
3. *Zigzag-offset* is susceptible to offset error.

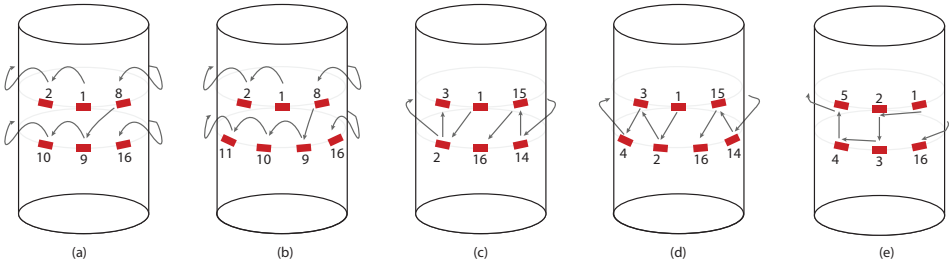

Fig. 7.1: Diagram of electrode placement and stimulation patterns. Each electrode (red) is numbered according to the sequence in which it is used to inject the electrical current. The pattern shown are: (a) planar, (b) planar-offset, (c) zigzag, (d) zigzag-offset, and (e) square. Images adapted from [54]

4. *Square* pattern performs poorly for vertical position error, noisy conditions, and artefacts.
5. *Planar* and *planar-offset patterns* are the most robust to noise and systematic electrode placement errors and perform equally or better than other patterns in the region of interest.
6. *Planar* pattern provides the largest image energy in the central regions, and is the most robust to noise.

Following these considerations, the final recommendation of this work was to use *planar* patterns.

Additional key point that effect the measurement strategy and the image quality are the number and position of the electrode arrays. To better understand this factor, we tested the system capabilities with two different electrode arrangements: i) a single array of eight electrodes, and ii) two arrays in two configuration having, respectively, four and eight arrays. To better capture the changes in the conductivity map, we further tested the two arrangements by considering arrays placed on a plane perpendicular to the cylinder axis, and on a plane inclined with respect to the same exes. Since there were numerous variables when considering the right amount of electrodes per array, its inclination, and the distance between two different array, we performed a series of simulations before attempting the real measurements. The results suggested that an inclination of 15° with respect to the main axis of the cylinder gives good results, in the considered scenario, even with a limited number of electrodes. For this reason, we decided to use 15° as tilt value when the "inclined plane" configuration was considered. Figure 7.2 presents each of the configurations for the electrodes arrays.

7.2.2 Experimental Setup

The experimental setup employed for the characterisation of the three-dimensional domain consists of the system presented in chapter 5, connected to the silicon-based soft conductive domain. Details of the domain under study are presented in in Table 7.1.

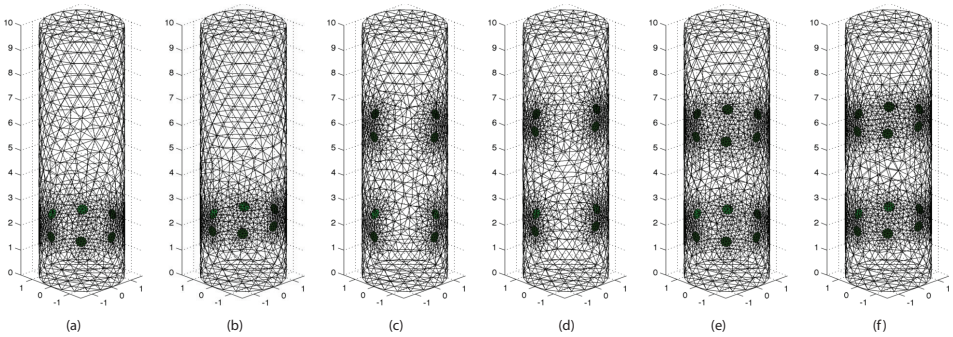

Fig. 7.2: Electrode configurations for the three-dimensional case. Electrodes are arranged in a (a-b) single array configuration both perpendicular and inclined with respect to the cylinder axis, and in a (c-f) two array configuration having four (c-d) and eight (e-f) electrodes each in both perpendicular and inclined configuration.

	Conductive core	**Outside shell**
Length (mm)	250	200
Diameter (mm)	16	32
Resistance (Ω/cm)	500	non conductive

Table 7.1: Parameters of the developed silicon-based cylindrical sensor.

Differently from the previous experiments, we changed the type of electrodes. In fact, the material chosen for the development of the conductive domain, and its size did not allow using alligator clips or snap button as in the case of the conductive textile. Here, instead, we used rigid steal wires that were inserted within the soft structure of the silicone body until they reached its conductive core. Before attempting any measurements, connections were tested and then the electrodes were fixed in position.

To prove the adaptability of the system to discriminate between events such as elongation and bending, we tested the system under different configurations. According to the experiment type, the soft cylinder was firmly attached at one, or both its ends before acquiring both the reference measurements and those of the cylinder deformation. Deformations were measured with respect to a checkerboard with a square size of 5 mm. For the reconstruction process, as in the previous experiments, we used a dynamic imaging approach. A reference measurement was acquired and stored, and then compared with later measures. The parameters used for the inverse solver were derived empirically by measuring the error of the reconstruction using different probes and then by selecting the best solution. In order to provide consistency in the reconstruction, the parameter values remain the same during all experiments, unless otherwise stated. In all experiments, in order to cope with possible fluctuations of the acquired value, a series of 10 measurements were made and then the mean value was used.

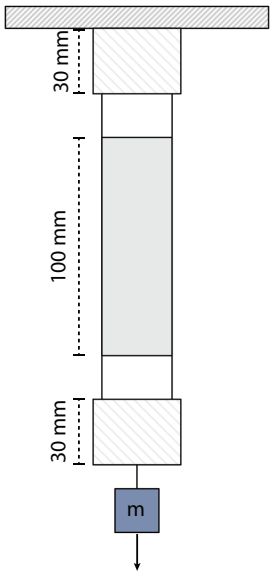

Fig. 7.3: Experimental setup for the elongation tests. The sensor was suspended from one side and pulled form the other by means of different weights. The highlighted area is the portion of the soft cylinder where the measurements were taken.

7.2.3 Experimental Protocol

Two main experiments were carried out to test the capability of the EIT system applied to the silicon-based sensor introduced in this chapter. In the next section, we will describe the experimental protocol used during the measurements. In each experiment, we tested the array configuration previously introduced in this chapter over which a *planar* stimulation pattern was applied. Results will be presented in section 7.3.

Elongation of the Soft Body

A first series of experiments was carried out to understand the behaviour of the sensor when subject to a force that elongates its body. The sensors, after having the electrode attached and fixed to its conductive body, has been firmly attached to one of its ends, and left hanging freely. While in this configuration, no external forces have been applied to the sensor, it was only subject to the gravitational force. The effect of which did not produce any visible elongation of the sensor. While in the initial configuration, reference measurements were acquired following the same procedure described in the previous chapters.

Later measurements were taken by applying to the soft cylinder a series of fixed weights spanning from 200 g to 700 g. These were attached and fixed at the free end of the cylinder with an inextensible wire connected to a plastic ring attached to the cylinder. Together with the measurements acquired with the EIT system,

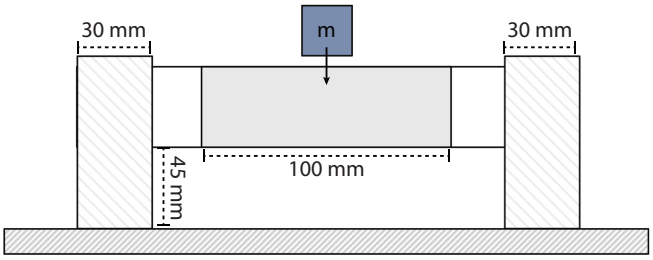

Fig. 7.4: Experimental setup for the bending tests. The highlighted area is the portion of the soft cylinder where the measurements were taken.. The sensor has been attached to two supports and placed parallel to the underlaying plane.

elongations were measured with respect to the checkerboard. The choice of using such experimental setup to evaluate elongation was made to minimise the effects of directional forces that can occur when the sensor is placed horizontally and pulled manually. In this case, in fact, the gravitational force acts perpendicularly to the elongation direction and thus may compromise the measurements. In the used method, instead, both the elongation and the gravitational forces act in the same direction. Figure 7.3 shows an overview of the experimental setup with one of the weight attached to the sensorized cylinder.

Bending of the Soft Body

In this series of experiments, we focus on the effect of bending on the measurements taken using the soft conductive cylinder. As in the previous case, we fixed the electrodes in place and then put the cylinder in its reference position. Differently from the previous case, the reference position had the cylinder with its long axis parallel to a table, and both ends fixed to rigid structures in correspondence to the electrodes. This configuration avoided the electrode movements between measurements while leaving the central part of the cylinder free to be deformed. In this configuration it is possible to notice a small deformation due to the gravitational force. In order not to let this alter the measurements, we moved the supports until no deformation was visible, and then fixed the support in position. The experimental setup is shown in Figure 7.4.

With the experimental setup just introduced, we acquired a first set of measurements used as reference. With the data stored we proceeded with the experimental evaluation. This was done by applying, at the centre of the sensor' structure, the same weights used in the previous experiment. For each deformation, data were acquired by the EIT system and the deformation was measured by comparing the position of the cylinder with respect to the checkerboard. Since the use of a single array of electrodes did not provide any distinguishable information when compared to the elongation case, we evaluate the system by using only two arrays of different number of electrodes in the configurations described before.

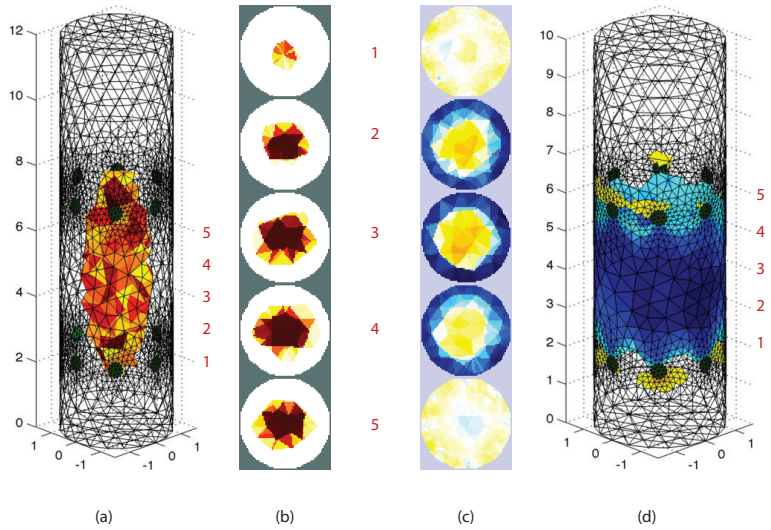

Fig. 7.5: Reconstructed volume using the FEM model (a-b) and the real measurements taken from the soft cylinder (c-d) after its elongation (units are in cm). Results are also shown as two-dimensional slices to better capture the differences between the methods used for the reconstruction. The slices presented in images (b) and (c) were taken on equally spaced planes relative to the volume contained between the two electrode arrays. Images (c) and (d) show a higher level of noise especially in the proximity of the boundary of the domain.

7.3 Results

Before attempting any real measurement, we performed a series of FEM simulations to first find the correct parameters for the inverse reconstruction, and then prove the effectiveness of the method used and the correctness of the results. During the reconstruction process of the elongation measurements we noticed an increase of noise and the presence of artefacts especially at the volume boundaries. These have been created as a consequence of the electrode movements during the measurements (i.e. reference vs. measurements taken at later time) that introduces an error in the model used for the inverse solving. Figure 7.5 shows a comparison between the expected and the obtained measurement.

Ideally, in situations where the electrodes move, it would be possible to calculate both the change of conductivity and the electrode locations. Different algorithms that iteratively fit the model have been proposed. In this thesis, however, we opted to use the Jacobian that allows a non-iterative approach for the inverse solving. By formulating the reconstruction problem in terms of a regularised inverse as proposed in [135], it is possible to overcome the problem of the electrode move, and compute the impedance changes. The method was then used to reconstruct the changes in conductivity measured in the elongation tests, while for the bending case there was no need of extending the Jacobian since the electrodes were fixed and their position did not change during the measurements.

The remaining of the chapter reports the results of each experiment subdivided in their respective categories.

7.3.1 Performance of the Elongation Tests

With the soft cylinder positioned as described in the previous section, we tested the developed EIT system in detecting changes of conductivity when the conductive domain (i.e. the soft cylinder) was subject to elongation. This was achieved by applying different weights to the soft structure that provided constant force along the main axis of the cylinder. For each configuration, the reconstructed conductivity map was computer and thresholded in order to highlight the volume which change its conductivity. As early introduced, initial results were not compatible with the ones obtained using FEM simulations. The use of an augmented Jacobian that took into consideration electrode movements was needed in order to obtain valid results.

Two different electrode arrangements were used during this test: i) a single array positioned in correspondence of the location where the soft cylinder was suspended, and ii) two arrays with a gap of 40 mm between them. For both arrangements, two additional configurations were tested: i) arrays perpendicular to the main axis, and ii) arrays tilted of 15° with respect to the same axis. Figures 7.6 and 7.7 show, respectively, the results of these measurements. As it is possible to notice from the results, the different number of electrodes array provides a different type of information.

The use of a single array (Figure 7.6), either placed perpendicular or inclined with respect to the main axis of the cylinder, provided only information of the voxel in the direct proximity of the array. Differently, from the FEM simulation it is possible to infer the propagation of the electrical current over the whole domain and thus obtain data from any point of the boundary. In the case of two arrays, on the contrary, it is possible to obtain information about the change in conductivity in the volume contained between the two arrays of electrodes (Figure 7.7). By properly adjusting the distance between the two arrays it is possible to extend this volume and thus cover a wider volume. In this case, the change of orientation did not effected significantly the reconstructed image. A real improvement was introduced by increasing the number of electrodes at each array. In this case, in fact, the noise was reduced and the structure representing the change of conductivity narrowed.

7.3.2 Identification of the Bending Region

With a similar methodology we further investigated the capabilities of the EIT system in detecting changes in conductivity due to an applied deformation that caused the bending of the structure. The applied force was directed perpendicularly to the main axis of the soft cylinder and was acting around its middle point. As in previous experiments, for each configuration, the reconstructed conductivity map was computed and thresholded in order to highlight the volume which changed its conductivity. Differently from the elongation experiments, the results obtained with the FEM model and the ones reconstructed using the acquired data matched.

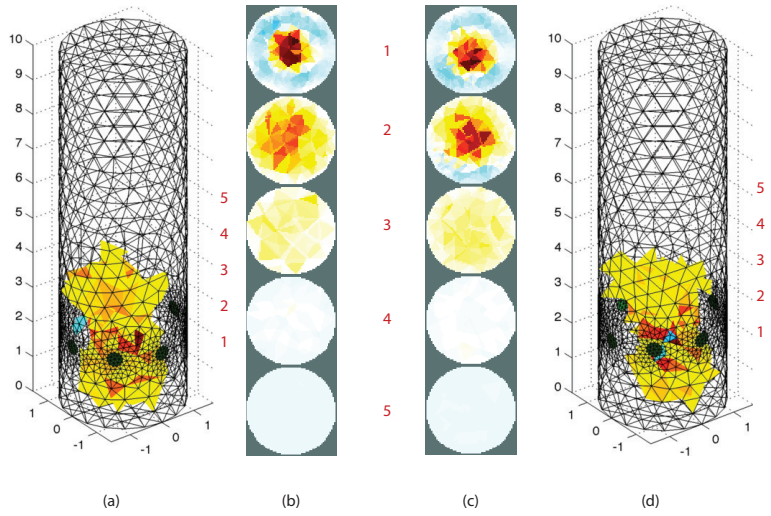

Fig. 7.6: Result of elongation test by using a single array of electrodes (units are in cm). (a-b) Show the results obtained with the array of electrodes oriented perpendicular w.r.t. the main axis of the cylinder. (c-d) Present the case when the array was inclined by 15°. For both cases, two-dimensional slices (indicated with red numbers in all the images) have been used to better capture the reconstructed volume.

As a consequence there was no need to use the extended Jacobian formulation as in the previous case. The main reason why the two experiments differ consists of the fact that during the bending tests, the electrodes were fixed and did not move between measurements.

Initial tests were performed by using a single array of electrodes, but no difference from the results presented in Figure 7.6 have been noticed. This was expected due to the limited volume that could be considered if a single array is used. For this reason, only the case with two arrays will be discussed in this section.

Experimental results are presented in Figures 7.8 and 7.9. If compared to the results previously presented, it is possible to notice some resemblance, however these show some distinct features. As in the previous case, the detected region extends along the main axis, but is more compact, and it is restricted between the two arrays of electrodes. This is clearly noticeable in Figure 7.8. Improvements in the image resolution in term of noise reduction, can be provided by changing the array configuration from the planar to the tilted, and by increasing the number of electrodes.

With the increase of the bending angle (Figure 7.9), the volume in which the conductivity changed extends and assumes a more elongated structure similar to the one obtained when the soft cylinder was subject to elongation (Figure 7.7). However, it is still possible to distinguish the two different events by considering the position of the detected volume within the cylindrical structure. In fact, while an elongation produced a structure that is located in the middle of the cylinder,

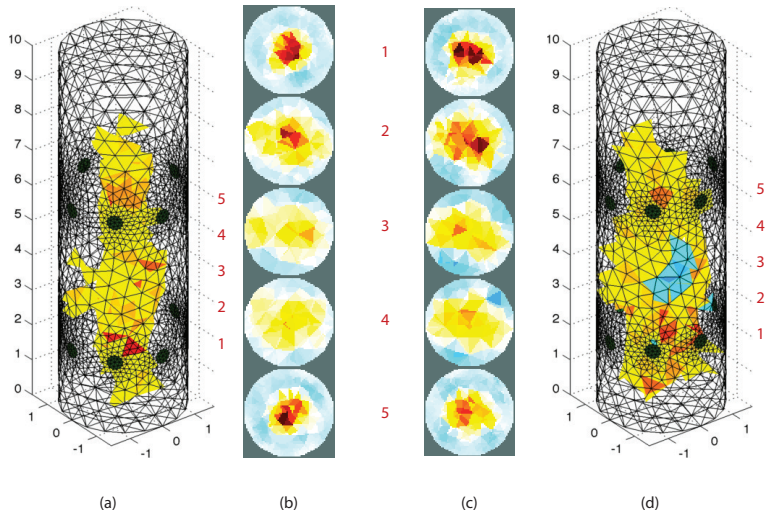

Fig. 7.7: Results (real data) for the two arrays configuration in the elongation test (units are in cm). (a-b) Present the array configuration perpendicular to the cylinder axis, while (c-d) the configuration inclined by 15°. When compared to the results obtained with a single array, it is possible to notice differences in the reconstructed volume. In fact, as a consequence of the elongation of the soft structure, the change of conductivity extends to the whole volume and it is not only localised around the electrode array as in the previous case.

in the bending case the volume tends to be positioned close to the boundary of the domain. This can be explained by considering that during an elongation—that acts along the main axis of the structure—the whole body is subject to it and thus it deforms "uniformly". On the countray, if the structure is bent only the region effected by the deformation changes its structure. As a consequence, by properly tuning a classification algorithm, and after characterising the sensor by applying known forces, it is possible to use the proposed method to reconstruct the configuration of the cylinder.

7.4 Summary and Conclusions

This chapter presented a series of experiments performed by applying the EIT imaging method to a three-dimensional soft structure. The soft domain was structured as a layer of conductive stretchable material incapsulated between two non conductive silicon layers. During the development phase, different shapes and sizes were investigated to prove the adaptability of the method. However, the results presented in this chapter were related to a cylindrical shape chosen since it allowed a direct extension of the shape used in the two-dimensional case, and for the fact that could be generalised for different soft robotics applications (e.g. robot's link).

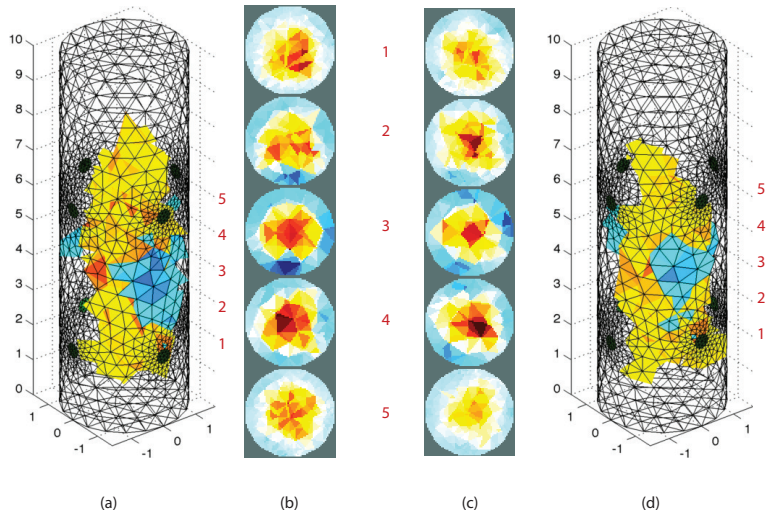

Fig. 7.8: Results (real data) of bending tests considering two arrays of four electrodes each (units are in cm). (a-b) Present the array configuration perpendicular to the cylinder axis, while (c-d) the configuration inclined of 15°. The use of only 4 electrodes per array does not provide enough independent readings to clearly distinguish elongation from bending. In fact, when compared with previous results, the reconstructed volume is similar in shape, but has a slighter smaller extension along the central axis. In addition, the extension along the X-Y plane is wider than the elongation case.

The cylindrical conductive domain was then used in combination with the developed EIT imaging system and tested under different configurations. We tested the capability of the system in detecting two common events that can occur in a soft robotics application: i) elongation of the link, and ii) its bending. For each case, the experimental scenario and protocol were provided together with the respective results. In order to obtain correct morphological information, it is important to implement the correct measurement strategy. We based it on common patterns used in 3D medical application, and applied them in our case. The stimulation patterns were injected using either a single array or multiple array approach, both with the arrays oriented perpendicular or inclined with respect to the main exes of the cylinder. To prove the correctness of the experimental results, we also performed FEM simulations and compared them with the results obtained with the reconstruction method.

After comparing the FEM results to the reconstructed images, we noticed some discrepancy between them especially in the case of elongation. The cause was the incorrect model due to of the electrode movement during the measurements. By using an extended version of the Jacobian matrix and by formulating the reconstruction problem in terms of a regularised inverse as proposed by other authors, it was possible to overcome the problem and compute the impedance changes.

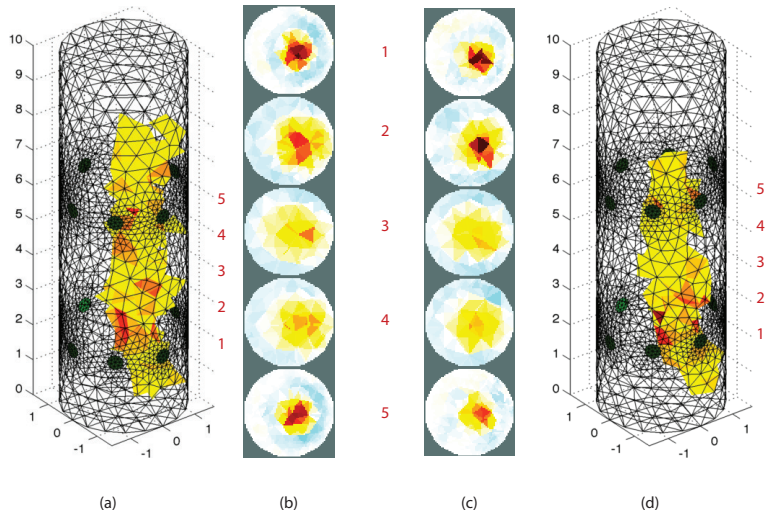

Fig. 7.9: Results (real data) of bending tests considering two arrays of eight electrodes each. (a-b) Show the results obtained with the array of electrodes oriented perpendicular w.r.t. the main axis of the cylinder. (c-d) Present the case when the array was inclined of 15°. The use of 8 electrodes improves the resolution of the volume and allow a clearer visualisation of the reconstructed volume. Here, as additional feature that can be used to distinguish bending from elongation, there is the position of the volume w.r.t. the central axis.

With the correct mathematical model, we then performed the inverse problem solving for all the considered cases. Regarding the results obtained by elongating the soft cylinder, the system was able to detect the volume where the conductivity changed as a consequence of the applied force that resulted in the elongation. By changing the electrode arrangement we were able to obtain information of different volumes of the cylinder. The use of a single array, either in the case it was placed perpendicular or inclined with respect to the main axis of the cylinder, provided only information of the voxel in the direct proximity of the array. On the contrary, the use of two arrays gave information on the volume contained between the two arrays. The change of orientation did not effected the reconstructed image in a significant way. A real improvement was introduced by increasing the number of electrodes in each array.

Regarding the experiments where the soft cylinder was bent, the results had some similarities with those related to the elongation but also showed some distinct feature. In fact, the detected region extends along the main axis, but it is more compact, and it is restricted between the two arrays of electrodes. Improvements in the image resolution in term of noise reduction, can be provided by changing the array configuration from the planar to the tilted, and by increasing the number of electrodes. With the increase of the bending angle, the two volumes tended to be similar, but it was still possible to distinguish between them by considering the location where they were detected.

In the next chapter we will collect all the conclusions and discuss them more generally trying to point out limitation and features of the developed system.

8

Discussion

In this chapter we will present a summary of the conclusions discussed in the previous chapters, especially the ones presented from chapter 5 to chapter 7. The experiments performed were designed to demonstrated the feasibility and the capabilities of the proposed EIT based deformable sensor. A summary of the whole results is presented in Table 8.1, while a more detailed discussion of each experiments, their implications, justifications, and limitations will be further discussed in the rest of the chapter.

8.1 Indentation Test

A first series of experiments was performed to characterise the behaviour of the EIT sensor in a planar configuration similar to an artificial skin. The specific results obtained in the indentation tests were presented in chapter 5. In these tests, it is possible to notice a common pattern in the variation of the acquired signal as a consequence of the presence of a weight (in this specific case a weight with 15 mm circular section) that applies a force in the region directly facing one of the electrodes under test. In order to understand the measurements we computed the absolute variation of the electric potential with respect to a reference voltage ($V_{meas} - V_0$) that was acquired when no weight was on the conductive surface. By analysing these variations, the presence of the inhomogeneity can be noticed as a drop in the electric potentials measured at the electrode under test. The variation is caused by the change in conductivity of the conductive layer used for sensing as a consequence of the normal force applied to it.

Considering the same electrode configuration, we evaluate the changes in the absolute voltage variation as a function of the weight size while applying a constant force (5 N) over them. Three different circular weights with radius of 15 mm, 18 mm, and 25 mm were placed independently in front of the region facing one of the electrode. As the results suggest, with the size increase, the variations of the voltage potential increase. This phenomenon was expected since a larger size generates a wider inhomogeneity area that is the cause a consequent voltage drop. Even though it is possible to make a correspondence between the size and the change of

Experiment	Results	Limitations
Single probe indentation	Inhomogeneity identified with an error in the cm-scale (max error $\approx$ 50mm). The system could identify the change of size of the indenter when the same force was applied on them	The indenter shape is not possible to be discriminates (round vs. square). Inhomogeneity identified is less precise at the boundaries
Multi-pressure on hard substrate	The system could identify the presence of each of the 3 probes places and removed sequentially, even when they were placed simultaneously on the conductive surface	The low number of electrodes limited the resolution of the identification
Curved and deformable surfaces	By taking the reference readings when the sensor is on a flat surface allows to detect changes of curvature. On the countrary, if the reference measurements are taken already when the sensor is deformed allows to overcome the change of the underlying structure.	Displacement of the electrodes could create artifacts.
Sensing within a soft bodies	Results confirmed the resolution in the identification of one or more inhomogeneities	The spatial resolution of the method limits the discrimination capabilities in identifying more than one inhomogeneity.
Sensing a continuum soft deformable structure	Some features are clearly distinguishable when the results of the bending and elongation are compared.	Electrode positioning and number influence the results and the capability to discriminate between different events (e.g. bending vs. elongation).

Table 8.1: A summary of the different results obtained during the experimental phase.

the electric potential, the same results can be generated by using different weights to the sensor area.

8.2 Pressure Map Reconstruction

Following these results, we moved towards the evaluation of the conductivity map reconstruction algorithm. To prove its effectiveness, we tested the sensor under different configurations, in which we applied different weights independently or simultaneously over the artificial skin. The reconstructed pressure map (which is equivalent to the conductive map of the domain under study) was obtained by

solving the associated inverse problem using a dynamic imaging approach. This consists of comparing a reference reading taken when no load was applied over the surface with a later one where a force was applied. Due to the ill-posed and ill-conditioned nature of the EIT inverse problem, in order to ensure uniqueness of the solution, we needed to regularise the model during the inverse problem solution. Parameters to correctly tune the solver were selected after a series of trial and error experiments, and have been proved to be appropriate by evaluating them under different sensor configurations. It is worth noting that we kept the parameters constant in all experiments. Because of the low number of emitters and detectors used to build the electronic skin tested in this thesis, we did not expect a good spatial resolution for the contacts applied over the sensing area. Despite this, results show that the inverse solver can correctly identify the position of the applied force, but could not clearly identify its shape. To have a sharper identification of the area, we further process the data by thresholding it, identifying the pixels having value grater or equal to 70% of the maximum value present in the map. Considering the limitations due to the low resolution, we further tested the system capabilities to discriminate between different weight sizes and shapes. As the reconstructed images suggest, the system is not able to correctly discriminate between different weight shapes (i.e., circular and square head), but is able to correctly capture the differences in size (i.e., 15 mm, 18 mm, 25 mm for the circular probe, and 15 mm side for the square-headed probe).

8.3 Multi-Pressure Test on Hard Substrate

As a last test for this series of experiments, we evaluated the capability of the system to determine the presence and position of multiple weights that act sequentially and simultaneously over the sensing area of the artificial skin. For this series of experiments, we used three identical weights (circular section with radius of 15 mm) that were loaded and unloaded in the same order. In the results presented chapter 5, it is possible to clearly distinguish the area where the weights are placed, but due to the low spatial resolution, it is not possible to correctly identify their shapes. In addition, when all the weights were placed on the surface, in order to detect their positions, we had to change the value of the thresholding parameter used in the image segmentation. In the future, the use of a larger number of components, along with the introduction of more advanced coupling schemes for emitter–detector pairs can improve the spatial performance and thus overcome some of the problems that the system is currently facing.

8.4 Application over Curved and Deformable Surfaces

We further tested the capabilities of the artificial skin by evaluating its ability to adapt to different geometries while maintaining its sensing performance. In the first phase, we tested the system's ability to detect a change in the underlying geometry caused by a significant change in the potential measurements. We first acquired a series of electric potentials with the artificial skin placed over a flat

surface, and then manually placed it over a curved one. As curved surfaces, we used two different cylindrical objects with radii 40 mm and 70 mm, respectively. As the results indicate, when compared to the reconstructed images from the flat cases, the reconstructed images show a different "shape". These results, together with the fact that the maximum detected value and the size of the "deformation area" increased with respect to the radius of the underlaying cylinder, can be used as a clue to discriminate between different events (i.e., bending vs. touch) and their intensity (e.g., bending angles). Additionally, we tested the sensing capabilities to provide reliable pressure readings when subject to large deformations. In order to prove this, we tightly attached the artificial skin to objects having different shapes, and then performed pressure sensing. Contrary to the precious case, we acquired both the reference measurements and the later ones when the artificial skin was already placed over each object. Doing so, all of the deformations that occur as a consequence of the underlying geometries are negligible, since they are already taken into consideration in the reference measurements. As the results suggest, the system maintains its sensing capabilities and can identify the position where the weight was applied. Some issues were noticed when the sensor was applied over the mannequin, especially in the joint area. If the joint is moved after acquiring the initial reference measurements, the measurements acquired later are affected by a planar force applied by the joint—i.e., the joint stretching the material. The sensor can be still used in this situation by taking new reference measurements according to the information provided by the joint encoder. For all the other cases, results remain valid, even when the weight was applied over the most bent area.

8.5 Sensing within Soft Bodies

We further stress the idea of detecting different stimuli by using the EIT based sensor by applying it to a soft deformable structure. The conductive textile has been placed over an in-house developed medical phantom consisting of two layers of foam (100x100x15 mm^2) within which a more rigid material—a medium-size stiff material—was placed to simulate the presence of a tumour. The top layer was then been covered with a highly conductive textile (100x100 mm^2) connected to the EIT system. To provide a homogenous pressure over the whole domain, we added an additional rigid layer (90x90x3 mm^3) and a weight that is used to apply a constant force over the whole structure. A constant pressure was applied to the structure and the response force from the internal stiff material was acquired. As the results suggest, the system was able to correctly identify the presence of the inhomogeneities and their positions. The experiment offers an insight on possible applications in the medical field especially related to palpation of soft tissue. The technique can be used in combination to others, and if miniaturised can be possible included within generic medical tools or into those used for minimal invasive surgery.

8.6 Sensing Structural Changes of a Deformable Body

We further stress the idea of detecting different stimuli by using the EIT based sensor by applying it to a soft deformable structure. The conductive textile was placed and fixed around a foam-made cylindrical structure and different test were performed while in this configuration. The system was tested in the task of detecting touch events, as already discussed earlier, and bending of the underlying structure. Here we will discuss only the second case since the touch either on soft or hard substrate has been already discussed in the previous sections. The foam-made cylinder was bent in a u-shape ten times and for each of the configuration a set of measurements was acquired. The results suggest that when compared with other type of applied stimuli the returned conductivity map shows a different detected inhomogeneity. This has a more elongated shape and fills most of the domain in length. By properly classifying the shape and values of the detected inhomogeneities it is possible to identify what is acting on the sensor surface or beneath it in the underlying structure. One of the main limitations of the method is related to the proximity of applied pressure points. In fact, if too close they can be merged together due to the low resolution of the technique. If this is the case, it is possible to misinterpret the applied stimuli as a bending point of the structure.

8.7 Single Point Deflection and Angle Estimation

A last series of experiments with the two-dimensional sensor was carried out to prove the capability of the system to detect and measure a single specific event (i.e. bending of a two link rigid arm). The textile-based sensor was wrapped around the elbow area of a two link arm that was bent from 0° to 90° with steps of 15°. After acquiring the measurements at the initial configuration, we acquired and reconstructed the changes in the conductivity map for all the others. In each of the returned images only the central region was considered since the elbow was acting there. The detected inhomogeneity was analysed and its maximum value, and its area (i.e. number of pixel having 75% or more of the maximum value detected) have been stored. These data were used to fit a calibration curve that can be used to identify the angle value accordingly to the returned maximum value or area from the data analysis. The method has shown to be effective, but has some limitation related to the low resolution of the sensor and the repeatability of the measurements. This can be caused by using only eight electrodes, and by the smoothing coefficient used in the regularisation step of the inverse solving. Additionally, since the textile changes its conductivity over time if stretched continuously, it is necessary to calibrate again the sensor when a large discrepancy in the measurements are detected.

8.8 Sensing a Continuum Soft Deformable Structure

The last series of experiments were made to prove the feasibility of using the proposed EIT based method in the soft robotics three-dimensional domain. In order

to prove this, a volume of conductive silicone-based sensor that change conductivity when stretched or bent was developed. The method was used to retrieve information about structural changes of the sensor, to obtain information about elongation and bending point. The use of a single array of electrode, as in all the previously two-dimensional cases, has shown not to be effective mainly because the structure under study is a complex three-dimensional volume. For this reason, we implemented two arrays of electrodes that were tested in different configurations to identify which of them returns the best information and thus better discriminates between different events applied to the body.

The results for each situation showed a similar but distinguishable behaviour that helped discriminating the two events when compared. In both cases, the reconstructed conductivity map had the form of a volume contained between the two arrays of electrodes. In the elongation case, since the body was hanging from one side and a fixed weight was attached to the other end, the volume indicating changes in the conductivity is collinear to the main axis of the cylinder With the increase of the weight, the returned volume became wider. By changing the number of the electrodes for each arrays the results became more clear, but no noticeable changes could be observed when the array was placed with a different orientation (i.e. 15° with respect to the main axis). Regarding the results of the bending experiments, the reconstructed structure had a more compact shape and it was not positioned on the main axis, but slightly moved on one of its sides. This is due to the different orientation of the sensor and the direction of the applied force and the consequences of its application to the body. As before, if the number of electrodes increased there was a sharpening in the results and no noticeable effect due the change of orientation of the array. It is interesting to notice that when a higher force acts on the sensor, the reconstructed volume assumes a shape that is similar to the one returned for the elongation case. The reason can be attributed to the fact that the whole structure is deformed as a consequence of the applied force.

9

Conclusions & Future Works

In this research we addressed the problem of providing dedicated sensing technology for the emerging field of soft robotics. After an in depth analysis of the current state of the art, we proposed a different approach compared to the most common transduction methods such as resistive or capacitive "matrix". In this work, we explored and realised an Electrical Impedance Tomography (EIT) sensor that has been used to detect deformations on soft and flexible materials. The use of such a technique allows removing most of the rigid components from the sensing area that can, theoretically, be made as wide as the device' surface. To test this approach, two sensors were developed: i) a conductive textile-based one, and ii) a silicone-based sensor.

Since the early stages of this research, we decided to develop all the components needed. This was motivated by the lack of off-the-shelf technologies (if medical-grade systems are not considered), and also to have the full control of the each phase of the data acquisition and image processing. In addition, this choice allowed us to develop a more compact system than the one currently available on the marker, that can be applied to different situations by properly tuning its parameters.

We verified the proposed method and developed sensors by a series of experiments that considered different configurations and application scenarios. In all of these, the sensor performed correctly not only in the identification of the single stimuli applied by providing the correct location (in the cm-range), but also in the discrimination between stimuli. The system was further tested to prove the adaptability to different rigid, semi-rigid, and soft substrates. In the latter case we also tested the capability of the system to detect changes of the underlying structure (i.e. bending), and the presence of stiff components placed within the soft substrate. A last series of experiments, focused on using EIT on a silicone-based continuum soft-bodied device. Here, we exploited the principle that the robot's body is the sensor. In fact, the sensor has been made conductive by using carbon fibres in the mixture and EIT was applied on it. The system (body and sensor), even with the intrinsic limitations due to the low spatial resolution of the technique, proved to be effective under different situations.

Contribution of This Work

The main contribution of the work is to introduce the Electrical Impedance Tomography to the field of deformable structures. This approach can be used in future applications such those involving *soft robotic* where there are strong requirements on the deformability and adaptability of the technology used in these robotic devices. The use of the EIT technique allows continuous distributed sensing without the need of active components directly embedded within or beneath the sensing area. A direct consequence of the use of this approach is the simplification of the fabrication process (the sensing area can be any conductive material) and a smooth extension to higher resolution. In addition, the absence of cables in the sensing area allows the developed of smart skins with a wider surface that can easily adapt to different substrates and shapes. These are features that are not always achievable with the classical transduction methods. Moreover, an important advantage of EIT is related to the architecture of the evaluation system. In fact, in order to increase the spatial resolution, the number of active components increases linearly with the length of the sensing area boundary, rather than with its area. This can be advantageous in terms of both cost and power consumption, and reduces the computation time during the voltage acquisition.

While the concept of EIT based sensing has been already exploited to create sensing structure in the past, the main applications were limited to touch detection over stiff substrate. Here, the developed sensor presents additional simplifications and hardware modularity that allows its use in situations where not only the sensor should adapt to different geometries, but also when the underlying structure can change its shape.

Future Directions

This research provided positive results, but still several improvements can be made in order to achieve even better results. These include the development of a larger electronic skin with higher density of active components, while keeping the focus on fast processing for real-time applications by exploring different coupling schemes. Additional work should also be done on the hardware, by adding a signal conditioning stage to ensure more precise measurements. Furthermore, coupling the current sensing methodology with capacitive measurements may provide additional information, and increase the performance in the detection of conductive an non-conductive objects applied on the sensor surface [7]. Finally, to boost the performance of the sensor for the specific application of the robot and its geometry, it is possible to customise the electrode placements, and the current injection and measurement patterns.

Application to the Soft Robotic Domain

The use of the proposed approach opens a new path in the research related to soft robotics. Either the use of the conductive silicone alone, or its combination with the EIT method can produce interesting applications for this new generation of robots.

Among these, fabrication of self-sensing fingers for anthropomorphic hands can be one of the possible applications. Together with this, the development of artificial conductive skins that can be used to cover artificial limbs—either soft or hard—and provide information on the position where a contact occurs. The technique can also be used in combination with "classical" actuation mechanism for soft robots such as pneumatic muscles. In fact, instead of being made as a simple chamber in the robot' structure, can be covered by the conductive silicone that can be used as a pressure-change sensitive layer.

Application to Other Domains

Looking to other possible future applications, the developed sensors provide some essential functionalities not only for the field mentioned above, but the sensing capability can also be applied in other fields where it is important to understand the changes in the morphology of the underlying structure without effecting it. Among these, the most straightforward to implement are those related to human-robot interaction. The use of EIT based sensing can support the development of interfaces that deform under the user action and thus provide a more natural feeling. An additional field that can take advantages of EIT based sensing is the one related to the development of medical tools. Among these, remote tactile displays, or sensors for deformable endoscope are the ones in which this technology can have a beneficial impact.

References

1. A. Adler and R. Guardo. Electrical impedance tomography: regularized imaging and contrast detection. *IEEE Transactions on Medical Imaging*, 15(2):170–179, Apr 1996.
2. A. Adler, R. Guardo, and Y. Berthiaume. Impedance imaging of lung ventilation: do we need to account for chest expansion? *IEEE Transactions on Biomedical Engineering*, 43(4):414–420, April 1996.
3. Andy Adler, John H Arnold, Richard Bayford, Andrea Borsic, Brian Brown, Paul Dixon, Theo J C Faes, Inéz Frerichs, Hervé Gagnon, Yvo Gärber, Bartłomiej Grychtol, Günter Hahn, William R B Lionheart, Anjum Malik, Robert P Patterson, Janet Stocks, Andrew Tizzard, Norbert Weiler, and Gerhard K Wolf. Greit: a unified approach to 2d linear eit reconstruction of lung images. *Physiological Measurement*, 30(6):S35, 2009.
4. Andy Adler and William R B Lionheart. Uses and abuses of eidors: an extensible software base for eit. *Physiological Measurement*, 27(5):S25, 2006.
5. H. Alirezaei, A. Nagakubo, and Y. Kuniyoshi. A tactile distribution sensor which enables stable measurement under high and dynamic stretch. In *3D User Interfaces, 2009. 3DUI 2009. IEEE Symposium on*, pages 87–93, March 2009.
6. N J Avis and D C Barber. Image reconstruction using non-adjacent drive configurations (electric impedance tomography). *Physiological Measurement*, 15(2A):A153, 1994.
7. Yang Bai, Izaak D Neveln, Michael Peshkin, and Malcolm A MacIver. Enhanced detection performance in electrosense through capacitive sensing. *Bioinspiration & Biomimetics*, 11(5):055001, 2016.
8. Y. Bar-Cohen. *Electroactive Polymers as Artificial Muscles: Capabilities, Potentials and Challenges*, chapter 23, pages 188–196.
9. Yoseph Bar-Cohen. Biomimetics–using nature to inspire human innovation. *Bioinspiration & Biomimetics*, 1(1):P1, 2006.
10. D C Barber and B H Brown. Applied potential tomography. *Journal of Physics E: Scientific Instruments*, 17(9):723, 1984.
11. D C Barber and A D Seagar. Fast reconstruction of resistance images. *Clinical Physics and Physiological Measurement*, 8(4A):47, 1987.
12. Richard H Bayford and Bill R B Lionheart. Biomedical applications of electrical impedance tomography. *Physiological Measurement*, 25(1), 2004.
13. J. Becker, M. S. Trotter, and J. D. Griffin. Passive displacement sensing using backscatter rfid with multiple loads. In *SENSORS, 2013 IEEE*, pages 1–4, Nov 2013.

14. T. Bhattacharjee, A. Jain, S. Vaish, M. D. Killpack, and C. C. Kemp. Tactile sensing over articulated joints with stretchable sensors. In *World Haptics Conference (WHC), 2013*, pages 103–108, April 2013.
15. D. Biermann, A. Zabel, T. Brüggemann, and A. Barthelmey. A comparison of low cost structure-borne sound measurement and acceleration measurement for detection of workpiece vibrations in 5-axis simultaneous machining. *Procedia CIRP*, 12:91 – 96, 2013.
16. C. Bonomo, L. Fortuna, P. Giannone, and S. Graziani. A sensor-actuator integrated system based on ipmcs [ionic polymer metal composites]. In *Sensors, 2004. Proceedings of IEEE*, pages 489–492 vol.1, Oct 2004.
17. A. Borsic, B. M. Graham, A. Adler, and W. R. B. Lionheart. In vivo impedance imaging with total variation regularization. *IEEE Transactions on Medical Imaging*, 29(1):44–54, Jan 2010.
18. B H Brown and A D Seagar. The sheffield data collection system. *Clinical Physics and Physiological Measurement*, 8(4A):91, 1987.
19. Eric Brown, Nicholas Rodenberg, John Amend, Annan Mozeika, Erik Steltz, Mitchell R. Zakin, Hod Lipson, and Heinrich M. Jaeger. Universal robotic gripper based on the jamming of granular material. *Proceedings of the National Academy of Sciences*, 107(44):18809–18814, 2010.
20. M. S. Campisi, C. Barbre, A. Chola, G. Cunningham, V. Woods, and J. Viventi. Breast cancer detection using high-density flexible electrode arrays and electrical impedance tomography. In *2014 36th Annual International Conference of the IEEE Engineering in Medicine and Biology Society*, pages 1131–1134, Aug 2014.
21. M. Cheney, D. Isaacson, J. C. Newell, S. Simske, and J. Goble. Noser: An algorithm for solving the inverse conductivity problem. *International Journal of Imaging Systems and Technology*, 2(2):66–75, 1990.
22. Margaret Cheney, David Isaacson, and Jonathan C. Newell. Electrical impedance tomography. *SIAM Review*, 41:85–101, 1999.
23. M.-Y. Cheng, C.-M. Tsao, Y.-Z. Lai, and Y.-J. Yang. The development of a highly twistable tactile sensing array with stretchable helical electrodes. *Sensors and Actuators A: Physical*, 166(2):226 – 233, 2011. 22 nd {IEEE} International Conference on Micro Electro Mechanical Systems,Sorrento, Italy, 25-29 January 2009MEMS 2009.
24. X. J. Chew, A. Van den Hurk, and K. C. Aw. Characterisation of ionic polymer metallic composites as sensors in robotic finger joints. *International Journal of Biomechatronics and Biomedical Robotics*, 1(1):37–43, 01 2009.
25. Chin-yu Chien, Rong-Hao Liang, Long-Fei Lin, Liwei Chan, and Bing-Yu Chen. Flexibend: Enabling interactivity of multi-part, deformable fabrications using single shape-sensing strip. In *Proceedings of the 28th Annual ACM Symposium on User Interface Software & Technology*, UIST '15, pages 659–663, New York, NY, USA, 2015. ACM.
26. Kyu-Jin Cho, Je-Sung Koh, Sangwoo Kim, Won-Shik Chu, Yongtaek Hong, and Sung-Hoon Ahn. Review of manufacturing processes for soft biomimetic robots. *International Journal of Precision Engineering and Manufacturing*, 10(3):171–181, 2009.
27. M. Y. Chuah and S. Kim. Improved normal and shear tactile force sensor performance via least squares artificial neural network (lsann). In *2016 IEEE International Conference on Robotics and Automation (ICRA)*, pages 116–122, May 2016.
28. M. Cianchetti, F. Renda, A. Licofonte, and C. Laschi. Sensorization of continuum soft robots for reconstructing their spatial configuration. In *2012 4th IEEE RAS EMBS International Conference on Biomedical Robotics and Biomechatronics (BioRob)*, pages 634–639, June 2012.

29. J J Cilliers, W Xie, S J Neethling, E W Randall, and A J Wilkinson. Electrical resistance tomography using a bi-directional current pulse technique. *Measurement Science and Technology*, 12(8):997, 2001.
30. A. Cirillo, F. Ficuciello, C. Natale, S. Pirozzi, and L. Villani. A conformable force/tactile skin for physical human robot interaction. *IEEE Robotics and Automation Letters*, 1(1):41–48, Jan 2016.
31. R. D. Cook, G. J. Saulnier, D. G. Gisser, J. C. Goble, J. C. Newell, and D. Isaacson. Act3: a high-speed, high-precision electrical impedance tomograph. *IEEE Transactions on Biomedical Engineering*, 41(8):713–722, Aug 1994.
32. M. D. Cooney, S. Nishio, and H. Ishiguro. Recognizing affection for a touch-based interaction with a humanoid robot. In *2012 IEEE/RSJ International Conference on Intelligent Robots and Systems*, pages 1420–1427, Oct 2012.
33. L. Cramphorn, B. Ward-Cherrier, and N. F. Lepora. Tactile manipulation with biomimetic active touch. In *2016 IEEE International Conference on Robotics and Automation (ICRA)*, pages 123–129, May 2016.
34. Artem Dementyev, Hsin-Liu (Cindy) Kao, and Joseph A. Paradiso. Sensortape: Modular and programmable 3d-aware dense sensor network on a tape. In *Proceedings of the 28th Annual ACM Symposium on User Interface Software & Technology*, UIST '15, pages 649–658, New York, NY, USA, 2015. ACM.
35. E. Demidenko, A. Hartov, N. Soni, and K. D. Paulsen. On optimal current patterns for electrical impedance tomography. *IEEE Transactions on Biomedical Engineering*, 52(2):238–248, Feb 2005.
36. M. K. Dobrzynski, R. Pericet-Camara, and D. Floreano. Contactless deflection sensor for soft robots. In *2011 IEEE/RSJ International Conference on Intelligent Robots and Systems*, pages 1913–1918, Sept 2011.
37. Joseph C. Doll, Sung-Jin Park, and Beth L. Pruitt. Design optimization of piezoresistive cantilevers for force sensing in air and water. *Journal of Applied Physics*, 106(6):064310, 2009.
38. A.M. Dollar, C.R. Wagner, and R.D. Howe. Embedded sensors for biomimetic robotics via shape deposition manufacturing. In *Biomedical Robotics and Biomechatronics, 2006. BioRob 2006. The First IEEE/RAS-EMBS International Conference on*, pages 763–768, 2006.
39. A.M. Dollar, C.R. Wagner, and R.D. Howe. Embedded sensors for biomimetic robotics via shape deposition manufacturing. In *Biomedical Robotics and Biomechatronics, 2006. BioRob 2006. The First IEEE/RAS-EMBS International Conference on*, pages 763–768, 2006.
40. Vladimir Egorov and Armen P Sarvazyan. Mechanical imaging of the breast. *IEEE transactions on medical imaging*, 27(9):1275–1287, 09 2008.
41. M. T. Erwati and N. Farrukh. Application of electrical impedance tomography for imaging in bio-medical and material technology. In *Research and Development (SCOReD), 2009 IEEE Student Conference on*, pages 168–171, Nov 2009.
42. Nicholas Fellion, Alexander Keith Eady, and Audrey Girouard. Flexstylus: A deformable stylus for digital art. In *Proceedings of the 2016 CHI Conference Extended Abstracts on Human Factors in Computing Systems*, CHI EA '16, pages 2482–2489, New York, NY, USA, 2016. ACM.
43. Sean Follmer, Daniel Leithinger, Alex Olwal, Nadia Cheng, and Hiroshi Ishii. Jamming user interfaces: Programmable particle stiffness and sensing for malleable and shape-changing devices. In *Proceedings of the 25th Annual ACM Symposium on User Interface Software and Technology*, UIST '12, pages 519–528, New York, NY, USA, 2012. ACM.
44. I. Frerichs, G. Hahn, and G. Hellige. Thoracic electrical impedance tomographic measurements during volume controlled ventilation-effects of tidal volume and pos-

itive end-expiratory pressure. *IEEE Transactions on Medical Imaging*, 18(9):764–773, Sept 1999.
45. Andreas Frutiger, Joseph T. Muth, Daniel M. Vogt, Yiğit Mengüç, Alexandre Campo, Alexander D. Valentine, Conor J. Walsh, and Jennifer A. Lewis. Capacitive soft strain sensors via multicore–shell fiber printing. *Advanced Materials*, 27(15):2440–2446, 2015.
46. W. S. Fulton and R. T. Lipczynski. Body-support pressure measurement using electrical impedance tomography. In *Proceedings of the 15th Annual International Conference of the IEEE Engineering in Medicine and Biology Societ*, pages 98–99, 1993.
47. David B. Geselowitz. An Application of Electrocardiographic Lead Theory to Impedance Plethysmography. *Biomedical Engineering, IEEE Transactions on*, BME-18(1):38–41, 1971.
48. H. H. Gharib and W. A. Moussa. On the feasibility of a new approach for developing a piezoresistive 3d stress sensing rosette. *IEEE Sensors Journal*, 11(9):1861–1871, Sept 2011.
49. D G Gisser, D Isaacson, and J C Newell. Current topics in impedance imaging. *Clinical Physics and Physiological Measurement*, 8(4A):39, 1987.
50. Camille Gómez-Laberge and Andy Adler. Direct eit jacobian calculations for conductivity change and electrode movement. *Physiological Measurement*, 29(6):S89, 2008.
51. B. M. Graham and A. Adler. A nodal jacobian algorithm for reduced complexity eit reconstructions. *International Journal of Systems Science*, 2:453–456, 2006.
52. B M Graham and A Adler. Objective selection of hyperparameter for eit. *Physiological Measurement*, 27(5):S65, 2006.
53. B M Graham and A Adler. Electrode placement configurations for 3d eit. *Physiological Measurement*, 28(7):S29, 2007.
54. Brad Graham and A. Adler. *Electrode Placement Strategies for 3D EIT*, pages 3866–3869. Springer Berlin Heidelberg, Berlin, Heidelberg, 2007.
55. J. Grosinger and J. D. Griffin. A bend transducer for backscatter rfid sensors. In *Proceedings of the 2012 IEEE International Symposium on Antennas and Propagation*, pages 1–2, July 2012.
56. J. Hadamard. *Lectures on Cauchy's Problem in Linear Partial Differential Equations*. Dover Books on Science. Yale University Press, 1923.
57. W. Hammer. *Functional Soft Tissue Examination and Treatment by Manual Methods: New Perspectives*. Jones and Bartlett Publishers, 2005.
58. J Han, F Dong, and Y Y Xu. Entropy feature extraction on flow pattern of gas/liquid two-phase flow based on cross-section measurement. *Journal of Physics: Conference Series*, 147(1):012041, 2009.
59. M. Hannan and I. Walker. Vision based shape estimation for continuum robots. In *Robotics and Automation, 2003. Proceedings. ICRA '03. IEEE International Conference on*, volume 3, pages 3449–3454 vol.3, Sept 2003.
60. R. P. Henderson and J. G. Webster. An impedance camera for spatially specific measurements of the thorax. *IEEE Transactions on Biomedical Engineering*, BME-25(3):250–254, May 1978.
61. S. Hirose. *Biologically inspired robots: snake-like locomotors and manipulators*. Oxford science publications. Oxford University Press, 1993.
62. T. Hoshi and H. Shinoda. Robot skin based on touch-area-sensitive tactile element. In *Proceedings 2006 IEEE International Conference on Robotics and Automation, 2006. ICRA 2006.*, pages 3463–3468, May 2006.
63. D. Hristu, N. Ferrier, and R. W. Brockett. The performance of a deformable-membrane tactile sensor: basic results on geometrically-defined tasks. In *Robotics*

and Automation, 2000. Proceedings. ICRA '00. IEEE International Conference on, volume 1, pages 508–513 vol.1, 2000.
64. Ying Huang, Xiaohui Ming, Bei Xiang, and Yunjian Ge. Two types of flexible tactile sensor arrays of robot for three-dimension force based on piezoresistive effects. In *2008 IEEE International Conference on Robotics and Biomimetics*, pages 1032–1037, Feb 2009.
65. Filip Ilievski, Aaron D. Mazzeo, Robert F. Shepherd, Xin Chen, and George M. Whitesides. Soft robotics for chemists. *Angewandte Chemie International Edition*, 50(8):1890–1895, 2011.
66. Filip Ilievski, Aaron D. Mazzeo, Robert F. Shepherd, Xin Chen, and George M. Whitesides. Soft robotics for chemists. *Angewandte Chemie International Edition*, 50(8):1890–1895, 2011.
67. D. Isaacson. Distinguishability of conductivities by electric current computed tomography. *IEEE Transactions on Medical Imaging*, 5(2):91–95, June 1986.
68. Yuji Ito, Youngwoo Kim, and Goro Obinata. Contact region estimation based on a vision-based tactile sensor using a deformable touchpad. *Sensors*, 14(4):5805, 2014.
69. Jiabin Jia, Mi Wang, and Yousef Faraj. Evaluation of eit systems and algorithms for handling full void fraction range in two-phase flow measurement. *Measurement Science and Technology*, 26(1):015305, 2015.
70. J. Jossinet. Variability of impedivity in normal and pathological breast tissue. *Medical and Biological Engineering and Computing*, 34(5):346–350, 1996.
71. Jari P Kaipio, Aku Seppänen, Arto Voutilainen, and Heikki Haario. Optimal current patterns in dynamical electrical impedance tomography imaging. *Inverse Problems*, 23(3):1201, 2007.
72. N. Kamamichi, M. Yamakita, K. Asaka, and Zhi-Wei Luo. A snake-like swimming robot using ipmc actuator/sensor. In *Robotics and Automation, 2006. ICRA 2006. Proceedings 2006 IEEE International Conference on*, pages 1812–1817, 2006.
73. N. Kamamichi, M. Yamakita, K. Asaka, and Zhi-Wei Luo. A snake-like swimming robot using ipmc actuator/sensor. In *Proceedings 2006 IEEE International Conference on Robotics and Automation, 2006. ICRA 2006.*, pages 1812–1817, May 2006.
74. Y. Kato, T. Mukai, T. Hayakawa, and T. Shibata. Tactile sensor without wire and sensing element in the tactile region based on eit method. In *Sensors, 2007 IEEE*, pages 792–795, Oct 2007.
75. Hitoshi KIMURA, Mokutaro KATAOKA, Shotaro SUZUKI, Daisuke AKIMOTO, and Norio INOU. A flexible robotic arm with hydraulic skeleton. *Journal of Advanced Mechanical Design, Systems, and Manufacturing*, 6(7):1107–1120, 2012.
76. Chang Seop Koh, Min-Kyu Kim, Hyun-Kyo Jung, Song yop Hahn, and Baek soo Suh. Electric resistivity tomography for geophysical inverse problems. *IEEE Transactions on Magnetics*, 33(2):1852–1855, Mar 1997.
77. V Kolehmainen, M Vauhkonen, P A Karjalainen, and J P Kaipio. Assessment of errors in static electrical impedance tomography with adjacent and trigonometric current patterns. *Physiological Measurement*, 18(4):289, 1997.
78. R. K. Kramer, C. Majidi, R. Sahai, and R. J. Wood. Soft curvature sensors for joint angle proprioception. In *2011 IEEE/RSJ International Conference on Intelligent Robots and Systems*, pages 1919–1926, Sept 2011.
79. R. K. Kramer, C. Majidi, and R. J. Wood. Wearable tactile keypad with stretchable artificial skin. In *Robotics and Automation (ICRA), 2011 IEEE International Conference on*, pages 1103–1107, May 2011.
80. M. A. Lacasse, V. Duchaine, and C. Gosselin. Characterization of the electrical resistance of carbon-black-filled silicone: Application to a flexible and stretchable robot skin. In *Robotics and Automation (ICRA), 2010 IEEE International Conference on*, pages 4842–4848, May 2010.

81. Cecilia Laschi and Matteo Cianchetti. Soft robotics: New perspectives for robot bodyware and control. *Frontiers in Bioengineering and Biotechnology*, 2:3, 2014.
82. H. Lee, J. Cho, and J. Kim. Printable skin adhesive stretch sensor for measuring multi-axis human joint angles. In *2016 IEEE International Conference on Robotics and Automation (ICRA)*, pages 4975–4980, May 2016.
83. H. K. Lee, S. I. Chang, and E. Yoon. A flexible polymer tactile sensor: Fabrication and modular expandability for large area deployment. *Journal of Microelectromechanical Systems*, 15(6):1681–1686, Dec 2006.
84. Darren Leigh, Clifton Forlines, Ricardo Jota, Steven Sanders, and Daniel Wigdor. High rate, low-latency multi-touch sensing with simultaneous orthogonal multiplexing. In *Proceedings of the 27th Annual ACM Symposium on User Interface Software and Technology*, UIST '14, pages 355–364, New York, NY, USA, 2014. ACM.
85. Alessandro Levi, Matteo Piovanelli, Silvano Furlan, Barbara Mazzolai, and Lucia Beccai. Soft, transparent, electronic skin for distributed and multiple pressure sensing. *Sensors*, 13(5):6578, 2013.
86. Bin Li, Adam K. Fontecchio, and Yon Visell. Mutual capacitance of liquid conductors in deformable tactile sensing arrays. *Applied Physics Letters*, 108(1), 2016.
87. Jessica Lo and Audrey Girouard. Fabricating bendy: Design and development of deformable prototypes. *IEEE Pervasive Computing*, 13(3):40–46, 2014.
88. Chiara Lucarotti, Massimo Totaro, Ali Sadeghi, Barbara Mazzolai, and Lucia Beccai. Revealing bending and force in a soft body through a plant root inspired approach. *Scientific Reports*, 5:8788 EP –, 03 2015.
89. R. Lytle and K. Dines. An impedance camera: A system for determining the spatial variation of electrical conductivity. Technical report, Lawrence Livermore Laboratory, University of California, Livermore California, 1978.
90. B. Vanderborgh R. Van Ham I. Vanderniepen A. Matthys P. Cherelle D. Lefeber M. Van Damme, P. Beyl. The role of compliance in robot safety. *Seventh IARP Workshop on Technical Challenges for Dependable Robots in Human Environments*, pages 65–71, 2010.
91. S. Maeda, Y. Hara, T. Sakai, R. Yoshida, and S. Hashimoto. Self-walking gel. *Advanced Materials*, 19(21):3480–3484, 2007.
92. P. Maiolino, M. Maggiali, G. Cannata, G. Metta, and L. Natale. A flexible and robust large scale capacitive tactile system for robots. *IEEE Sensors Journal*, 13(10):3910–3917, Oct 2013.
93. C Majidi, R Kramer, and R J Wood. A non-differential elastomer curvature sensor for softer-than-skin electronics. *Smart Materials and Structures*, 20(10):105017, 2011.
94. A. D. Marchese, K. Komorowski, C. D. Onal, and D. Rus. Design and control of a soft and continuously deformable 2d robotic manipulation system. In *2014 IEEE International Conference on Robotics and Automation (ICRA)*, pages 2189–2196, May 2014.
95. Kenneth Meijer, Marc S. Rosenthal, and Robert J. Full. Muscle-like actuators: A comparison between three electroactive polymers, 2001.
96. J. Missinne, E. Bosman, B. Van Hoe, G. Van Steenberge, P. Van Daele, and J. Vanfleteren. Embedded flexible optical shear sensor. In *Sensors, 2010 IEEE*, pages 987–990, Nov 2010.
97. H. Mochiyama and T. Suzuki. Kinematics and dynamics of a cable-like hyperflexible manipulator. In *Robotics and Automation, 2003. Proceedings. ICRA '03. IEEE International Conference on*, volume 3, pages 3672–3677 vol.3, 2003.
98. J E Molyneux and A Witten. Impedance tomography: imaging algorithms for geophysical applications. *Inverse Problems*, 10(3):655, 1994.

99. Stephen A. Morin, Robert F. Shepherd, Sen Wai Kwok, Adam A. Stokes, Alex Nemiroski, and George M. Whitesides. Camouflage and display for soft machines. *Science*, 337(6096):828–832, 2012.
100. A. Nagakubo, H. Alirezaei, and Y. Kuniyoshi. A deformable and deformation sensitive tactile distribution sensor. In *Robotics and Biomimetics, 2007. ROBIO 2007. IEEE International Conference on*, pages 1301–1308, Dec 2007.
101. Y. Noh, E. L. Secco, S. Sareh, H. Würdemann, A. Faragasso, J. Back, H. Liu, E. Sklar, and K. Althoefer. A continuum body force sensor designed for flexible surgical robotics devices. In *2014 36th Annual International Conference of the IEEE Engineering in Medicine and Biology Society*, pages 3711–3714, Aug 2014.
102. Y. Ohmura, Y. Kuniyoshi, and A. Nagakubo. Conformable and scalable tactile sensor skin for curved surfaces. In *Proceedings 2006 IEEE International Conference on Robotics and Automation, 2006. ICRA 2006.*, pages 1348–1353, May 2006.
103. Mihoko Otake, Yoshiharu Kagami, Masayuki Inaba, and Hirochika Inoue. Motion design of a starfish-shaped gel robot made of electro-active polymer gel. *Robotics and Autonomous Systems*, 40(2–3):185 – 191, 2002.
104. Y. L. Park, B. R. Chen, and R. J. Wood. Design and fabrication of soft artificial skin using embedded microchannels and liquid conductors. *IEEE Sensors Journal*, 12(8):2711–2718, Aug 2012.
105. Y. L. Park, B. r. Chen, C. Majidi, R. J. Wood, R. Nagpal, and E. Goldfield. Active modular elastomer sleeve for soft wearable assistance robots. In *2012 IEEE/RSJ International Conference on Intelligent Robots and Systems*, pages 1595–1602, Oct 2012.
106. Y. L. Park, B. r. Chen, and R. J. Wood. Soft artificial skin with multi-modal sensing capability using embedded liquid conductors. In *Sensors, 2011 IEEE*, pages 81–84, Oct 2011.
107. Y. L. Park, B. r. Chen, D. Young, L. Stirling, R. J. Wood, E. Goldfield, and R. Nagpal. Bio-inspired active soft orthotic device for ankle foot pathologies. In *2011 IEEE/RSJ International Conference on Intelligent Robots and Systems*, pages 4488–4495, Sept 2011.
108. Yong-Lae Park, Carmel Majidi, Rebecca Kramer, Phillipe Bérard, and Robert J Wood. Hyperelastic pressure sensing with a liquid-embedded elastomer. *Journal of Micromechanics and Microengineering*, 20(12):125029, 2010.
109. R P Patterson. Electrical impedance tomography: Methods, history, and applications. *Physics in Medicine and Biology*, 50(10):2427, 2005.
110. Linda Dailey Paulson. Biomimetic robots. *Computer*, 37(9):48–53, 2004.
111. Rolf Pfeifer, Max Lungarella, and Fumiya Iida. The challenges ahead for bio-inspired 'soft' robotics. *Commun. ACM*, 55(11):76–87, November 2012.
112. Nick Polydorides and William R B Lionheart. A matlab toolkit for three-dimensional electrical impedance tomography: a contribution to the electrical impedance and diffuse optical reconstruction software project. *Measurement Science and Technology*, 13(12):1871, 2002.
113. Roshin Raveendra, Pramod Sreedharan, and Ganesha Udupa. Innovative micro-walking robot using flexible microactuator.
114. Christian Rendl, Patrick Greindl, Michael Haller, Martin Zirkl, Barbara Stadlober, and Paul Hartmann. Pyzoflex: Printed piezoelectric pressure sensing foil. In *Proceedings of the 25th Annual ACM Symposium on User Interface Software and Technology*, UIST '12, pages 509–518, New York, NY, USA, 2012. ACM.
115. Christian Rendl, David Kim, Sean Fanello, Patrick Parzer, Christoph Rhemann, Jonathan Taylor, Martin Zirkl, Gregor Scheipl, Thomas Rothländer, Michael Haller, and Shahram Izadi. Flexsense: A transparent self-sensing deformable surface. In *Proceedings of the 27th Annual ACM Symposium on User Interface Software and Technology*, UIST '14, pages 129–138, New York, NY, USA, 2014. ACM.

116. P. Roberts, D. D. Damian, W. Shan, T. Lu, and C. Majidi. Soft-matter capacitive sensor for measuring shear and pressure deformation. In *Robotics and Automation (ICRA), 2013 IEEE International Conference on*, pages 3529–3534, May 2013.
117. Markus Rothmaier, Minh Phi Luong, and Frank Clemens. Textile pressure sensor made of flexible plastic optical fibers. *Sensors*, 8(7):4318, 2008.
118. Daniela Rus and Michael T. Tolley. Design, fabrication and control of soft robots. *Nature*, 521(7553):467–475, 05 2015.
119. Stefania Russo, Tommaso Ranzani, Hongbin Liu, Samia Nefti-Meziani, Kaspar Althoefer, and Arianna Menciassi. Soft and stretchable sensor using biocompatible electrodes and liquid for medical applications. *Soft Robotics*, 2(4):146–154, 12 2015.
120. S. Sanan, M.H. Ornstein, and C.G. Atkeson. Physical human interaction for an inflatable manipulator. In *Engineering in Medicine and Biology Society,EMBC, 2011 Annual International Conference of the IEEE*, pages 7401–7404, 2011.
121. Armen Sarvazyan. Mechanical imaging:: A new technology for medical diagnostics. *International Journal of Medical Informatics*, 49(2):195 – 216, 1998.
122. H. P. Schwan. Electrical properties of tissues and cell suspensions: mechanisms and models. In *Proceedings of 16th Annual International Conference of the IEEE Engineering in Medicine and Biology Society*, pages A70–A71 vol.1, Nov 1994.
123. T. C. Searle, K. Althoefer, L. Seneviratne, and H. Liu. An optical curvature sensor for flexible manipulators. In *2013 IEEE International Conference on Robotics and Automation*, pages 4415–4420, May 2013.
124. Metin Sitti Sehyuk Yim. Softcubes: Towards a soft modular matter. *2013 IEEE International Conference on Robotics and Automation (ICRA)*, pages 530–536, 2013.
125. Sangok Seok, C.D. Onal, Robert Wood, D. Rus, and S. Kim. Peristaltic locomotion with antagonistic actuators in soft robotics. In *Robotics and Automation (ICRA), 2010 IEEE International Conference on*, pages 1228–1233, 2010.
126. Robert F. Shepherd, Filip Ilievski, Wonjae Choi, Stephen A. Morin, Adam A. Stokes, Aaron D. Mazzeo, Xin Chen, Michael Wang, and George M. Whitesides. Multigait soft robot. *Proceedings of the National Academy of Sciences*, 108(51):20400–20403, 2011.
127. Robert F. Shepherd, Filip Ilievski, Wonjae Choi, Stephen A. Morin, Adam A. Stokes, Aaron D. Mazzeo, Xin Chen, Michael Wang, and George M. Whitesides. Multigait soft robot. *Proceedings of the National Academy of Sciences*, 108(51):20400–20403, 2011.
128. Robert F. Shepherd, Adam A. Stokes, Jacob Freake, Jabulani Barber, Phillip W. Snyder, Aaron D. Mazzeo, Ludovico Cademartiri, Stephen A. Morin, and George M. Whitesides. Using explosions to power a soft robot. *Angewandte Chemie International Edition*, 52(10):2892–2896, 2013.
129. Xuetao Shi, Xiuzhen Dong, Wanjun Shuai, Fusheng You, Feng Fu, and Ruigang Liu. Pseudo-polar drive patterns for brain electrical impedance tomography. *Physiological Measurement*, 27(11):1071, 2006.
130. David Silvera Tawil, David Rye, and Mari Velonaki. Interpretation of the modality of touch on an artificial arm covered with an eit-based sensitive skin. *The International Journal of Robotics Research*, 2012.
131. David Silvera-Tawil, David Rye, and Mari Velonaki. Interpretation of social touch on an artificial arm covered with an eit-based sensitive skin. *International Journal of Social Robotics*, 6(4):489–505, 2014.
132. P.P. Silvester and R.L. Ferrari. *Finite Elements for Electrical Engineers*. Cambridge University Press, 1983.
133. M. Sitti, A. Menciassi, A.J. Ijspeert, Kin Huat Low, and Sangbae Kim. Survey and introduction to the focused section on bio-inspired mechatronics. *Mechatronics, IEEE/ASME Transactions on*, 18(2):409–418, 2013.

134. Ronit Slyper, Ivan Poupyrev, and Jessica Hodgins. Sensing through structure: Designing soft silicone sensors. In *Proceedings of the Fifth International Conference on Tangible, Embedded, and Embodied Interaction*, TEI '11, pages 213–220, New York, NY, USA, 2011. ACM.
135. Manuchehr Soleimani, Camille Gómez-Laberge, and Andy Adler. Imaging of conductivity changes and electrode movement in eit. *Physiological Measurement*, 27(5):S103, 2006.
136. A. A. Stanley, K. Hata, and A. M. Okamura. Closed-loop shape control of a haptic jamming deformable surface. In *2016 IEEE International Conference on Robotics and Automation (ICRA)*, pages 2718–2724, May 2016.
137. Y. Sugiyama, A. Shiotsu, M. Yamanaka, and S. Hirai. Circular/spherical robots for crawling and jumping. In *Robotics and Automation, 2005. ICRA 2005. Proceedings of the 2005 IEEE International Conference on*, pages 3595–3600, 2005.
138. A. J. Surowiec, S. S. Stuchly, J. R. Barr, and A. Swarup. Dielectric properties of breast carcinoma and the surrounding tissues. *IEEE Transactions on Biomedical Engineering*, 35(4):257–263, April 1988.
139. K. Suzumori, S. Endo, T. Kanda, N. Kato, and H. Suzuki. A bending pneumatic rubber actuator realizing soft-bodied manta swimming robot. In *Robotics and Automation, 2007 IEEE International Conference on*, pages 4975–4980, 2007.
140. Barry A. Trimmer. New challenges in biorobotics: Incorporating soft tissue into control systems. *Applied Bionics and Biomechanics*, 5(3):119–126, 2008.
141. D. Trivedi, A. Lotfi, and C.D. Rahn. Geometrically exact dynamic models for soft robotic manipulators. In *Intelligent Robots and Systems, 2007. IROS 2007. IEEE/RSJ International Conference on*, pages 1497–1502, 2007.
142. Wei-Yu Tseng, J. S. Fisher, K. Rinaldi, and A. P. Lee. A slow-adapting microfluidic based tactile sensor. In *Micro Electro Mechanical Systems, 2008. MEMS 2008. IEEE 21st International Conference on*, pages 912–915, Jan 2008.
143. A. Ueno, Y. Akabane, T. Kato, H. Hoshino, S. Kataoka, and Y. Ishiyama. Capacitive sensing of electrocardiographic potential through cloth from the dorsal surface of the body in a supine position: A preliminary study. *IEEE Transactions on Biomedical Engineering*, 54(4):759–766, April 2007.
144. J. Ulmen and M. Cutkosky. A robust, low-cost and low-noise artificial skin for human-friendly robots. In *Robotics and Automation (ICRA), 2010 IEEE International Conference on*, pages 4836–4841, May 2010.
145. Marko Vauhkonen. Electrical impedance tomography and prior information, 1997.
146. L. Ventrelli, L. Beccai, V. Mattoli, A. Menciassi, and P. Dario. Development of a stretchable skin-like tactile sensor based on polymeric composites. In *Robotics and Biomimetics (ROBIO), 2009 IEEE International Conference on*, pages 123–128, Dec 2009.
147. D. M. Vogt, Y. L. Park, and R. J. Wood. Design and characterization of a soft multi-axis force sensor using embedded microfluidic channels. *IEEE Sensors Journal*, 13(10):4056–4064, Oct 2013.
148. Justin Wagenaar and Andy Adler. Electrical impedance tomography in 3d using two electrode planes: characterization and evaluation. *Physiological Measurement*, 37(6):922, 2016.
149. Robert J. Webster and Bryan A. Jones. Design and kinematic modeling of constant curvature continuum robots: A review. *The International Journal of Robotics Research*, 29(13):1661–1683, 2010.
150. Peter N. T. Wells and Hai-Dong Liang. Medical ultrasound: imaging of soft tissue strain and elasticity. *Journal of The Royal Society Interface*, 2011.
151. James L Wheeler, Wei Wang, and Mengxing Tang. A comparison of methods for measurement of spatial resolution in two-dimensional circular eit images. *Physiological Measurement*, 23(1):169, 2002.

152. R. Wijesiriwardana, K. Mitcham, W. Hurley, and T. Dias. Capacitive fiber-meshed transducers for touch and proximity-sensing applications. *IEEE Sensors Journal*, 5(5):989–994, Oct 2005.
153. Raphael Wimmer and Patrick Baudisch. Modular and deformable touch-sensitive surfaces based on time domain reflectometry. In *Proceedings of the 24th Annual ACM Symposium on User Interface Software and Technology*, UIST '11, pages 517–526, New York, NY, USA, 2011. ACM.
154. E. J. Woo, P. Hua, J. G. Webster, and W. J. Tompkins. A robust image reconstruction algorithm and its parallel implementation in electrical impedance tomography. *IEEE Transactions on Medical Imaging*, 12(2):137–146, Jun 1993.
155. M. Yamakita, A. Sera, N. Kamamichi, K. Asaka, and Zhi-Wei Luo. Integrated design of ipmc actuator/sensor. In *Proceedings 2006 IEEE International Conference on Robotics and Automation, 2006. ICRA 2006.*, pages 1834–1839, May 2006.
156. Y. Yamamoto, K. Kure, T. Iwai, T. Kanda, and K. Suzumori. Flexible displacement sensor using piezoelectric polymer for intelligent fma. In *2007 IEEE/RSJ International Conference on Intelligent Robots and Systems*, pages 765–770, Oct 2007.
157. A. Yao and M. Soleimani. A pressure mapping imaging device based on electrical impedance tomography of conductive fabrics. *Sensor Review*, 32(4):310–317, 2012.
158. A. Yao, C. L. Yang, J. K. Seo, and M. Soleimani. Eit-based fabric pressure sensing. *Computational and Mathematical Methods in Medicine*, 2013:9, 2013.
159. Tomoaki Yoshikai, Marika Hayashi, Yui Ishizaka, Hiroko Fukushima, Asuka Kadowaki, Takashi Sagisaka, Kazuya Kobayashi, Iori Kumagai, and Masayuki Inaba. Development of robots with soft sensor flesh for achieving close interaction behavior. *Advances in Artificial Intelligence*, 2012:27, 2012.
160. Ping Yu, Weiting Liu, Chunxin Gu, Xiaoying Cheng, and Xin Fu. Flexible piezoelectric tactile sensor array for dynamic three-axis force measurement. *Sensors*, 16(6):819, 2016.
161. Z. Zhu, V.G. Dhokia, A. Nassehi, and S.T. Newman. A review of hybrid manufacturing processes – state of the art and future perspectives. *International Journal of Computer Integrated Manufacturing*, 26(7):596–615, 2013.

My greatest gratitude is for my supervisor Prof. Paolo Fiorini for giving me the opportunity to be part of his laboratory during all these years, for his valuable support, inspiring vision, and unlimited support and patience. His vision and values are to remain with me for the rest of my career.

I would also like to thanks all the member at the Altair Laboratory and BBZ, present and past, for their friendship, the nice memory we shared, and for their support and encouragement during the challenges of graduate school.

Finally, I would like to thanks my family and my beloved Laura for all the love and support without which it would have been impossible accomplish this work.